CEN-203-NP
REVISION 1-NP

RESPONSE TO NRC ACTION PLAN ITEM II.K.3.30 JUSTIFICATION OF SMALL BREAK LOCA METHODS

Prepared for the C-E OWNERS GROUP

NUCLEAR POWER SYSTEMS DIVISION
MARCH, 1982

POWER SYSTEMS
COMBUSTION ENGINEERING, INC.

LEGAL NOTICE

THIS REPORT WAS PREPARED AS AN ACCOUNT OF WORK SPONSORED BY COMBUSTION ENGINEERING, INC. NEITHER COMBUSTION ENGINEERING NOR ANY PERSON ACTING ON ITS BEHALF:

A. MAKES ANY WARRANTY OR REPRESENTATION, EXPRESS OR IMPLIED INCLUDING THE WARRANTIES OF FITNESS FOR A PARTICULAR PURPOSE OR MERCHANTABILITY, WITH RESPECT TO THE ACCURACY, COMPLETENESS, OR USEFULNESS OF THE INFORMATION CONTAINED IN THIS REPORT, OR THAT THE USE OF ANY INFORMATION, APPARATUS, METHOD, OR PROCESS DISCLOSED IN THIS REPORT MAY NOT INFRINGE PRIVATELY OWNED RIGHTS; OR

B. ASSUMES ANY LIABILITIES WITH RESPECT TO THE USE OF, OR FOR DAMAGES RESULTING FROM THE USE OF, ANY INFORMATION, APPARATUS, METHOD OR PROCESS DISCLOSED IN THIS REPORT.

RESPONSE TO NRC ACTION PLAN ITEM II.K.3.30 - JUSTIFICATION OF SMALL BREAK LOCA METHODS

PREPARED FOR THE C-E OWNERS GROUP

NUCLEAR POWER SYSTEMS DIVISION

MARCH, 1982

ABSTRACT

In fulfillment of NRC Action Plan Item II.K.3.30 - Justification of Small Break LOCA Methods, this report responds to seven NRC questions concerning the C-E Small Break LOCA Evaluation Model. The majority of the questions address component models of the Evaluation Model, while one question deals with verification of the system response against experimental data from integral tests. Three of the seven questions had been addressed previously by C-E in report CEN-114-P and in test analyses for LOFT Small Break Tests L3-1 and L3-6. For the remaining questions, additional technical information was developed. In summary, the responses for the seven questions show that using the C-E Small Break LOCA Evaluation Model results in conservatively high cladding temperatures.

TABLE OF CONTENTS

Section	Title	Page
	ABSTRACT	i
	TABLE OF CONTENTS	ii
1.0	INTRODUCTION	1-1
2.0	SUMMARY AND CONCLUSIONS	2-1
3.0	RESPONSE TO NRC ACTION ITEM II.K.3.30-JUSTIFICATION OF SMALL BREAK LOCA METHODS	3.1-1
	3.1 Response to Question 1 (Condensation Heat Transfer)	3.1-1
	3.1.1 Statement of Question 1	3.1-1
	3.1.2 Detailed Response to Question 1	3.1-1
	3.1.3 Summary and Conclusions for Question 1	3.1-6
	3.1.4 References for Question 1	3.1-7
	3.2 Response to Question 2 (Modeling of ECCS Injection)	3.2-1
	3.2.1 Statement of Question 2	3.2-1
	3.2.2 Detailed Response to Question 2	3.2-1
	3.2.3 Summary and Conclusions for Question 2	3.2-9
	3.2.4 Nonequilibrium Component Model Description	3.2-9
	3.2.5 References for Question 2	3.2-15
	3.3 Response to Question 3 (Model Verification)	3.3-1
	3.3.1 Statement of Question 3	3.3-1
	3.3.2 Detailed Response to Question 3	3.3-1
	3.3.3 Summary and Conclusions for Question 3	3.3-6
	3.3.4 References for Question 3	3.3-8

TABLE OF CONTENTS, Continued

Section	Title	Page
3.4	Response to Question 4 (Flow Regime Effect on Pressure Drop)	3.4-1
3.4.1	Statement of Question 4	3.4-1
3.4.2	Detailed Response for Question 4	3.4-1
3.4.3	Summary and Conclusions for Question 4	3.4-7
3.4.4	References for Question 4	3.4-8
3.5	Response to Question 5 (Core Heat Transfer)	3.5-1
3.5.1	Statement of Question 5	3.5-1
3.5.2	Detailed Response to Question 5	3.5-1
3.5.3	Summary and Conclusions for Question 5	3.5-13
3.5.4	References for Question 5	3.5-14
3.5.5	Nomenclature of Question 5	3.5-16
3.6	Response to Question 6 (Metal Heat Transfer)	3.6-1
3.6.1	Statement of Question 6	3.6-1
3.6.2	Detailed Response to Question 6	3.6-1
3.6.3	Summary and Conclusions for Question 6	3.6-3
3.6.4	References for Question 6	3.6-4
3.7	Response to Question 7 (Break Flow Multiplier)	3.7-1
3.7.1	Statement of Question 7	3.7-1
3.7.2	Detailed Response to Question 7	3.7-1
3.7.3	Summary and Conclusions for Question 7	3.7-4
3.7.4	References for Question 7	3.7-5

1.0 INTRODUCTION

In the summer of 1979, C-E submitted two reports to the NRC, CEN-114-P (Reference 1-1) and CEN-115-P (Reference 1-2), which describe C-E's Small Break LOCA Evaluation Model. These submittals were prepared in response to NRC requests following the TMI-2 accident. After review of these documents, the NRC identified a number of questions with some portions of the small break model. The NRC requested a response to these questions in the NRC TMI Action Plan, NUREG 0737, Item II.K.3.30 (Reference 1-3). At a meeting held on January 26, 1981 (Reference 1-4) with members of the NRC staff and representatives of the C-E Owners Group and C-E, the NRC staff described seven technical items which form the basis for the seven specific questions relative to the C-E Small Break LOCA Evaluation Model. The NRC staff also indicated that responding to these seven questions would fulfill the response to Item II.K.3.30 of the NRC TMI Action Plan.

Six of the NRC questions pertain to component models within the Small Break LOCA Evaluation Model. The remaining question pertains to the verification of the system response of the Evaluation Model against test data from integral Small Break Tests. Responses to all seven questions are provided in this report.

REFERENCES

1-1 CEN-114-P (Amendment 1-P), "Review of Small Break Transients in Combustion Engineering Nuclear Steam Supply Systems," July 1979 (Proprietary).

1-2 CEN-115-P, "Response to NRC IE Bulletin 79-06C, Items 2 and 3 for C-E Nuclear Steam Supply Systems," August 1979 (Proprietary).

1-3 NUREG-0737, "Post TMI Action Plan Requirements," October 1980.

1-4 Letter, K. P. Baskin (CEOG) to P. S. Check (NRC), "Planned Response to NRC TMI Action Plan Requirement II.K.3.30," July 14, 1981.

2.0 SUMMARY AND CONCLUSIONS

This report provides responses to seven NRC questions relative to the C-E Small Break LOCA Evaluation Model. In a letter of July 14, 1981 (Reference 2-1) from the C-E Owners Group to the NRC, the C-E Owners Group stated their understanding that the responses to these seven questions fulfill the requirement of NRC Action Plan Item II.K.3.30. This understanding results from a meeting on January 26, 1981, between the C-E Owners Group, C-E and the NRC.

Two of the NRC questions were addressed in CEN-114-P (Reference 2-2) which was submitted to the NRC in 1979. A third question was addressed by test analyses for small break LOFT Tests L3-1 (Reference 2-3) and L3-6 (Reference 2-4), which were submitted to the NRC in 1980 and in the spring of 1981, respectively. For the remaining questions new or additional technical information was developed. This report provides responses for all seven questions, with the responses for the previously addressed questions presenting summary-type information from the earlier submittals.

The conclusions from the responses to the individual questions are summarized in the following:

1. Condensation Heat Transfer in the Steam Generators and Treatment of Noncondensible Gases.

   A condensation heat transfer correlation developed by Akers, Deans and Crosser is used. Comparison with other correlations and experimental data show that this correlation yields conservatively low heat transfer coefficients.

   Although not treated explicitly in the heat transfer calculations, the amount of noncondensible gases expected in the steam generators is shown to have a negligible effect on heat transfer.

2. Modeling of ECC Injection

In the C-E Small Break Evaluation Model the analytical treatment of the ECC water injection is based on thermal equilibrium conditions with the ECC water injected[ ]

An investigation of the effect of treating the ECC water discharged from the Safety Injection Tanks (SITs) assuming thermal nonequilibrium shows that the "worst" break size remains unchanged with thermal nonequilibrium treatment. The "worst" break size, having the highest cladding temperature, remains the largest break for which the system pressure does not decrease far enough to cause ECC discharge from the SITs.

This investigation also addresses modeling the injection of ECC[ ](as actually occurs in the reactor) for the "worst" break. Although the effect of nonequilibrium[ ]ECC injection is to increase cladding temperatures, when this effect is combined with a more realistic core heat transfer model, which is discussed under the response to Question 5, the cladding temperatures are more than 180°F lower than the temperatures calculated with the Evaluation Model.

3. Model Verification Against Integral Tests

References 2-3 and 2-4 provide best estimate blind pretest as well as post-test analyses of the two small break LOFT tests, L3-1 and L3-6. After accounting for unexpected and unforseen irregularities in the conduct of the test in the post-test analyses, the results show very good agreement between experimental data and calculated values for systems parameters of major significance (e.g. system pressure, break flow, system inventory).

4. Flow Regime Effect on Pressure Drop in Steam Generators

Section 3.4 of this report compares several applicable correlations to describe the flow regimes in the steam generators to the one used in the Small Break LOCA Evaluation Model. The results show that the various correlations have little effect on the calculated two-phase mixture level

in the core. The correlation used in the Evaluation Model does, however, result in the lowest two-phase mixture level which, in turn, would cause the highest cladding temperatures.

5. Core Heat Transfer

Section 3.5 of this report compares the component models for level swell of the two-phase mixture in the core as well as for heat transfer during core uncovery which are used in the Evaluation Model with experimental data from recent small break-type heat transfer tests at Oak Ridge National Laboratory. The comparison shows that the Evaluation Model predictsless level swell (more core uncovery) and poorer heat transfer than observed in the tests. Calculations also show that use of more realistic heat transfer models would reduce the cladding temperature of the worst small break (as calculated with the Evaluation Model) by at least $400^{o}F$.

6. Metal Heat Transfer

The Evaluation Model for heat transfer from metal surfaces (e.g. piping, reactor vessel walls, etc.) to the fluid in the primary system uses a lumped parameter approach together with a correction factor. This correction factor maximizes the wall heat input over the small break spectrum.

Results presented in Section 3.6 show that the impact of heat input from the walls is small because, for the primary system of a commerical nuclear plant, this heat input is small compared to the decay heat of the core.

7. Break Flow Multiplier

For the calculation of break flow, the choice of break flow multiplier, or discharge coefficient, during two-phase discharge is important. Results of sensitivity studies for the worst (highest clad temperature) small break show that the depth and duration of core uncovery are insensitive to variations of the subcooled discharge coefficient. However, a variation of the two-phase discharge coefficient does

affect the timing of core uncovery. A two-phase discharge coefficient of 0.6 results in less break flow, later core uncovery and, due to reduced decay heat, in lower cladding temperatures than a coefficient of 1.0.

In the C-E Small Break LOCA Evaluation Model a discharge coefficient of 1.0 is used for subcooled and two-phase break flow. As mentioned above, the choice of the numerical value of the discharge coefficient for the subcooled break flow is of little consequence for the cladding temperature. The choice of a discharge coefficient of 1.0 for two-phase flow, however, results in early core unocvery. Therefore, the discharge coefficient used in the C-E Evaluation Model maximizes the calculated cladding temperature.

Seven questions related to the C-E Small Break Evaluation Model were raised by the NRC and are addressed in this report. Six of the questions are directed at component models of the Evaluation Model, while one question deals with verification of the calculated system response against data from systems tests. The responses to the questions on component models show that the component models of the Evaluation Model maximize cladding temperatures. The verification against systems test data by post-test analyses of LOFT tests L3-1 and L3-6 show very good agreement between experimental data and calculated values. Thus, the overall conclusion from the work described in this report is that the C-E Small Break LOCA Evaluation Model yields analyses which result in conservatively high cladding temperatures.

REFERENCES

2-1 Letter, K. P. Baskin (CEOG) to P. S. Check (NRC), "Planned Response to NRC TMI Action Plan Requirement II.K.3.30," July 14, 1981.

2-2 CEN-114-P (Amendment 1-P), "Review of Small Break Transients in Combustion Engineering Nuclear Steam Supply Systems," July 1979 (Proprietary).

2-3 "Combustion Engineering Analysis of LOFT Test L3-1," February 1980.

2-4 "Analysis of LOFT Test L3-6 Performed by Combustion Engineering, Inc.," April 1981.

3.0 RESPONSE TO NRC ACTION ITEM II.K.3.30 - JUSTIFICATION OF SMALL BREAK LOCA METHODS

3.1 RESPONSE TO QUESTION 1 (CONDENSATION HEAT TRANSFER)

3.1.1 Statement of Question 1

Demonstration of the applicability of the condensation heat transfer coefficients used by C-E for the steam generator is requested. Their appropriateness for the geometry of a U-tube steam generator and to all modes of condensation experienced during a small break LOCA are to be shown. In addition, the effects of non-condensibles on the condensation heat transfer process is to be addressed.

3.1.2 Detailed Response to Question 1

C-E has submitted a response to this question in Reference 3.1-1. That response is summarized below.

Condensation Heat Transfer

The CEFLASH-4AS Steam Generator Model consists of [

] Heat is transferred from the primary to secondary side, or vice versa, based on an overall heat transfer coefficient. The overall heat transfer coefficient includes dynamically calculated heat transfer coefficients on both the primary and secondary sides.

The physical conditions on the steam generator primary side during a small break transient may be divided into four periods. They are:

1. Subcooled forced convection
2. Two-phase forward flow with condensation
3. Two-phase countercurrent flow with condensation and steam generator draining
4. Steam condensation

The heat transfer correlations used for the different heat transfer regimes are shown in Table 3.1-1.

When condensation fluid conditions exist in the primary side of the steam generator, the heat transfer coefficient is calculated using the high-flow correlation of Akers, Deans and Crosser (Reference 3.1-2),

$$h = .026 \frac{k_\ell}{D_{hy}} Re_e^{0.8} Pr^{1/3} \qquad (3.1\text{-}1)$$

where

$$Re_e = \frac{D_{hy}}{\mu_\ell} \left(G_\ell + G_v \left(\frac{\rho_\ell}{\rho_v}\right)^{1/2}\right) \qquad (3.1\text{-}2)$$

Equation (3.1-1) is based on an analogy between heat transfer across the condensate film and the heat transfer in turbulent single-phase flow. The Reynolds number, given in equation (3.1-2), defines the "equivalent" single-phase (liquid) flow, which would produce the same sheer force at the liquid film surface as does the flowing vapor in the true two-phase flow case. Reference 3.1-2 shows favorable comparisons between equation 3.1-1 and several sources of test data.

Shah (Reference 3.1-3) developed a more empirical correlation of the condensation heat transfer coefficient under a wide variety of conditions. His analysis considered 474 data points from 21 data sets for vertical and horizontal tubes. The ranges of parameters covered by his data analysis are given in Table 3.1-2. This data includes condensation of water.

Figure 3.1-1 compares the heat transfer coefficient of equation (3.1-1) with Shah's empirical correlation of test data for a broad range of flow rates and two values of fluid quality. The correlation of Akers, Deans, and Crosser is observed to be virtually identical to the correlation of Shah at low quality, while at high quality, it underpredicts the Shah correlation values. Use of equation (3.1-1) would therefore tend to be slightly conservative, since it would tend to produce higher values of the primary-to-secondary temperature differential for a given steam generator heat load.

The data used in Shah's analysis were primarily high flow rate data. At low flow rates, one may anticipate falling film condensation in the steam generator with little interaction between the liquid film and the vapor core at the film surface. The most widely known analysis of this heat transfer mode is the analysis of Nusselt (Reference 3.1-4). Figure 3.1-2 compares the Nusselt condensation heat transfer coefficient for a falling film with the correlation of equation (3.1-1). The Reynolds number in this figure is the Reynolds number of the liquid film. Figure 3.1-2 shows that equation (3.1-1) underpredicts the condensation heat transfer coefficient of the Nusselt model for film Reynolds numbers less than 850. The figure also shows opposite trends in the two models. Nusselt assumed laminar film flow which produced an increase in film thickness (decrease in heat transfer coefficient) with increasing condensate flow. The model of Akers, Deans and Crosser is based on an analogy to turbulent flow in which the film coefficient increases as the turbulence and flow increase.

Dukler (Reference 3.1-5) presents a unified theory of heat transfer across a falling liquid film considering laminar flow and turbulence in the film, as well as interaction between the flowing vapor and the film at the film surface. Results of this analysis are also shown in Figure 3.1-2. The Dukler analysis tends to agree with the Nusselt model at low Reynolds numbers when the film is predominantly laminar. At high Reynolds numbers, his model agrees well with equation (3.1-1). At intermediate Reynolds numbers, Dukler's analysis produces condensation heat transfer coefficients which do not exhibit a sharp boundary between laminar and turbulent flow. The water data of Carpenter (Reference 3.1-6) include points in this intermediate region and, as shown in Figure 3.1-2, they agree very well with Dukler's analysis. Also shown in Figure 3.1-2 is a low-flow correlation of Akers, Deans and Crosser. Their low-flow model also agrees well with Dukler's analysis in the intermediate Reynolds number region.

The conclusion from Figure 3.1-2, is that for falling film heat transfer, equation (3.1-1) underpredicts (i) the Nusselt theory in the laminar

flow region and (ii) the Dukler model, the low-flow correlation of Akers, Deans and Crosser, and the data of Carpenter in the intermediate Reynolds number region. Equation (3.1-1) will therefore overpredict the primary system temperature and pressure during periods of falling film condensation heat transfer in the steam generators. The extent of this overprediction of pressure is estimated to be no greater than 30 psi, however.

Non-Condensibles

The most likely place for non-condensibles to collect is in the upper head. The discussion below considers the highly unlikely event tnat all of the non-condensibles will collect in the steam generators.

As the steam or two-phase fluid condenses and flows back to the hot leg, any entrained non-condensible gas would be left in the steam generator. As the non-condensible gas collects in the steam generator tubes, it would reduce the condensation rate for a given temperature difference between the primary and secondary sides of the steam generators. As a result, the primary system pressure increases (as well as the primary side steam temperature) until a new equilibrium condition is found. This effect would tend to increase the leakage rate and decrease the ECC injection rate leading to higher cladding temperatures.

There are a number of non-condensible gas sources, as shown in Table 3.1-3. The core would have to undergo transients that are not predicted to occur, for applicable small breaks, in order for many of these sources to be important (present Appendix K Small Break Analyses show that clad temperatures remain low and no cladding rupture is predicted). In addition, the system pressure does not reduce to the safety injection tank pressure (of 200 or 600 psi) for the applicable breaks. The only sources that might be introduced are a) air dissolved in the refueling water, b) hydrogen dissolved in the primary coolant, and c) hydrogen contained in the pressurizer vapor space. As a conservative scoping analysis, the total quantity of non-condensible gas produced by these three sources is combined, and all of it is placed in the steam generators.

C-E has determined the effect of non-condensibles on the condensation processes that occur in the steam generators during the refluxing mode of a small break LOCA using the method of References 3.1-7 and 3.1-8. During the condensation process, the non-condensibles may accumulate forming a gas layer as shown in Figure 3.1-3. Since the concentration of the non-condensibles is higher at the liquid interface, its partial pressure (Pa) increases near the surface as shown. Since the static pressure is nearly uniform, the partial pressure of the steam must decrease near the surface. C-E conservatively assumes that the bulk mixture is stagnant which means that the only mechanism for getting the steam to the condensing surface is by diffusion across the gas layer. The driving force causing diffusion across the layer of non-condensibles is the concentration gradient of the steam. This is reflected in the difference in partial pressures of the vapor across the layer (P_{GO}-P_{GI}).

The overall heat conduction through the liquid film when equated to the sensible heat transfer in the diffusion layer plus the latent heat liberated at the film interface results in the equation:

$$h_c\ (T_{GI}-T_W) = h_s\ (T_{GO}-T_{GI}) + K_g\ M_g\ h_{LV}\ (P_{GO}-P_{GI})$$

where

h_c = heat transfer coefficient in liquid film BTU/hr ft^2 ^oF
h_s = sensible heat transfer coefficient, BTU/hr ft^2 ^oF
K_g = mass transfer coefficient, lb-mole/hr-ft^2-psia
M_g = molecular weight of vapor, lb/lb-mole
h_{LV} = latent heat, BTU/lb
Other terms are defined in Figure 3.1-3.

For conservatism, C-E assumes that h_s equals zero. This assumption minimizes the calculated values of overall heat transfer coefficient. K_g, the mass transfer coefficient is defined in Reference 3.1-7. The film heat transfer coefficient, h_c, was evaluated using the Nusselt film condensation model, Reference 3.1-4.

As non-condensibles are added to the steam generator, the heat transfer coefficient will decrease. Since the heat load to the steam generator is fixed by core decay power, the primary system pressure increases so that the increased driving force, $(P_{GO}-P_{GI})$, compensates for the reduction in the heat transfer coefficient due to the presence of the diffusion layer.

Figure 3.1-4 presents the calculated percent degradation in heat transfer coefficient, and the percent increase in primary side pressure as a function of the mass fraction of air. Similar curves result when other gases are assumed to be present. If all the air dissolved in the refueling water supplied were contained in the steam generators, the mass fraction of air to steam would be $\sim$.03. Figure 3.1-4 shows that the degradation in the overall heat transfer coefficient would be only $\sim$3% and the increase in primary side pressure is only $\sim$2%. This negligible rise in system pressure does not affect the inner vessel two-phase level or ECCS system performance during the transient.

3.1.3 Summary and Conclusions for Question 1

The C-E model for condensation heat transfer has been compared to data and correlations for condensation conditions. The correlations and data cover the range of conditions found in U-tube steam generators - vertical tubes, cocurrent and countercurrent flow, laminar to turbulent flow, and fluid quality from saturation to steam conditions. The C-E model predicts lower heat transfer coefficients than the comparison base. Consequently, the C-E model overpredicts system temperature and pressure during periods of condensation heat transfer in the steam generator leading conservative core temperature predictions. Therefore, the C-E model for condensation heat transfer is appropriate for a U-tube steam generator.

The effect of non-condensibles on condensation heat transfer in the steam generator is important only for break sizes small enough to require the steam generators as a heat sink. For the non-condensibles which are available for breaks requiring the steam generator as a heat sink, a conservative analysis shows a 3% reduction of the condensation heat transfer coefficient with a consequent 2% increase of system pressure. This pressure increase does not affect the inner vessel two-phase level or ECCS flow rate during the transient.

3.1.4 References for Question 1

3.1-1 CEN-114-P (Amendment 1-P), "Review of Small Break Transients in Combustion Engineering Nuclear Steam Supply Systems", Sections 3.2.3.4, 3.3.3.3 and 3.5.3.2, July 1979 (Proprietary).

3.1-2 Akers, W. W., Deans, H. A. and Crosser, O. K., "Condensing Heat Transfer Within Horizontal Tubes", Proc. 2nd Nat. Heat Transfer Conf., ASME/AIChE, August, 1958.

3.1-3 Shah, M. M., "A General Correlation for Heat Transfer During Film Condensation Inside Pipes", Int. J. Heat & Mass Transfer, Vol. 22, pp. 547-556, 1979.

3.1-4 Nusselt, W., Z. Ver. Deut. Ingen., 60, 541 and 569, 1916.

3.1-5 Dukler, A. E., "Fluid Mechanics and Heat Transfer in Vertical Falling-Film Systems", Chem. Eng. Prog. Sym. Series, No. 30, Vol. 56, 1960.

3.1-6 Carpenter, F. G., Ph. D. Thesis, U. of Delaware, 1948.

3.1-7 Collier, J. G., Convective Boiling and Condensation, McGraw-Hill New York (1972).

3.1-8 Akers, W. W., Davis, S. H. Jr., and Crawford, J. E., "Condensation of a Vapor in the Presence of a Non-Condensing Gas", Chem. Eng. Prog. Sym. Series, No. 30, Vol. 56, pp. 139-144, 1960.

Table 3.1-1

Steam Generator Heat Transfer

Forward HTF

HTF Period	Primary Side Assumed HTF Regime	Correlation	Secondary Side HTF Regime	Correlation
Subcooled Forced Convection	Subcooled Forced Convection	Dittus-Boelter	Pool Boiling	Modified Rohsenow
Two-Phase Forward Flow with Condensation	Two-Phase Flow with Condensation	Akers, Deans Crosser		
Two-Phase Counter Current Flow with Condensation (SG Draining)				
Steam Condensation				

Table 3.1-2

Range of Conditions for
Shah Correlation

Flow Channel	Tubes, annulus
Flow Direction	Horizontal, vertical, inclined
Tube I.D. in.	0.3 - 1.6
Tube length, ft	4 - 40
Pressure, psia	10 - 1400
Temperature, ^{o}F	70 - 590
Quality	0.0 - 1.0
Mass Flux, lbm/ft^2-hr	8000 - 155,000
Prandtl Number	1 - 13

Table 3.1-3

Sources of Non-Condensibles

Source	Volume	Mass
1. Dissolved in Primary Coolant (Hydrogen)	384 ft^3	2.2 lbs.
2. Pressurizer Vapor Space (Hydrogen)	793 ft^3	4.5 lbs.
3. Dissolved in Refueling Water Tank (Air)	1360 ft^3	109.7 lbs.[A]
4. Complete Oxidation of Clad (Hydrogen)	448000 ft^3	2514.8 lbs.[B]
5. Fuel Rod Fill Gas (Helium)	1140 ft^3	12.7 lbs.[B]
6. Fission Gases (Xe, Kr, I_2)	26 ft^3	~9.0 lbs.[B]
7. Safety Injection Tanks (Nitrogen)		
A. Cover Gas	51820 ft^3	4042.2 lbs.[C]
B. Dissolved Gas	690 ft^3	53.8 lbs.[C]

NOTES:

A. The largest amount of liquid injected from the refueling water tank (RWT) during the boiling phase for breaks that return to natural circulation is ~40% of the RWT volume.

B. For breaks requiring the return to natural circulation no fuel rod rupture or oxidation is predicted. Numbers are based on 36924 fuel rods.

C. For breaks requiring the return to natural circulation the SIT's do not inject water.

Figure 3.1-1

Comparison of Condensation Heat Transfer Coefficients at High Flow Rates

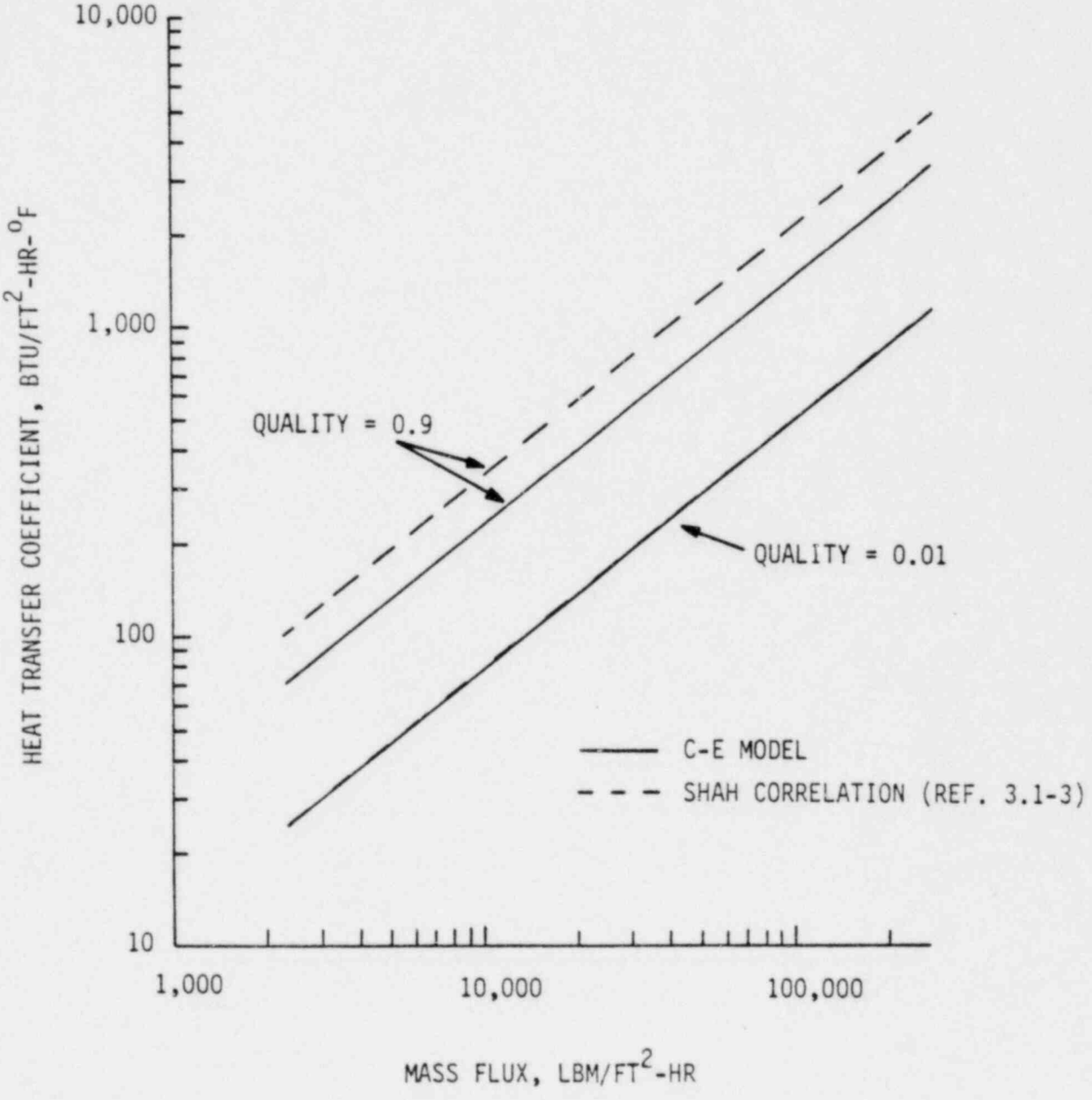

Figure 3.1-2

Comparison of Condensation Heat Transfer Coefficients for Falling Films

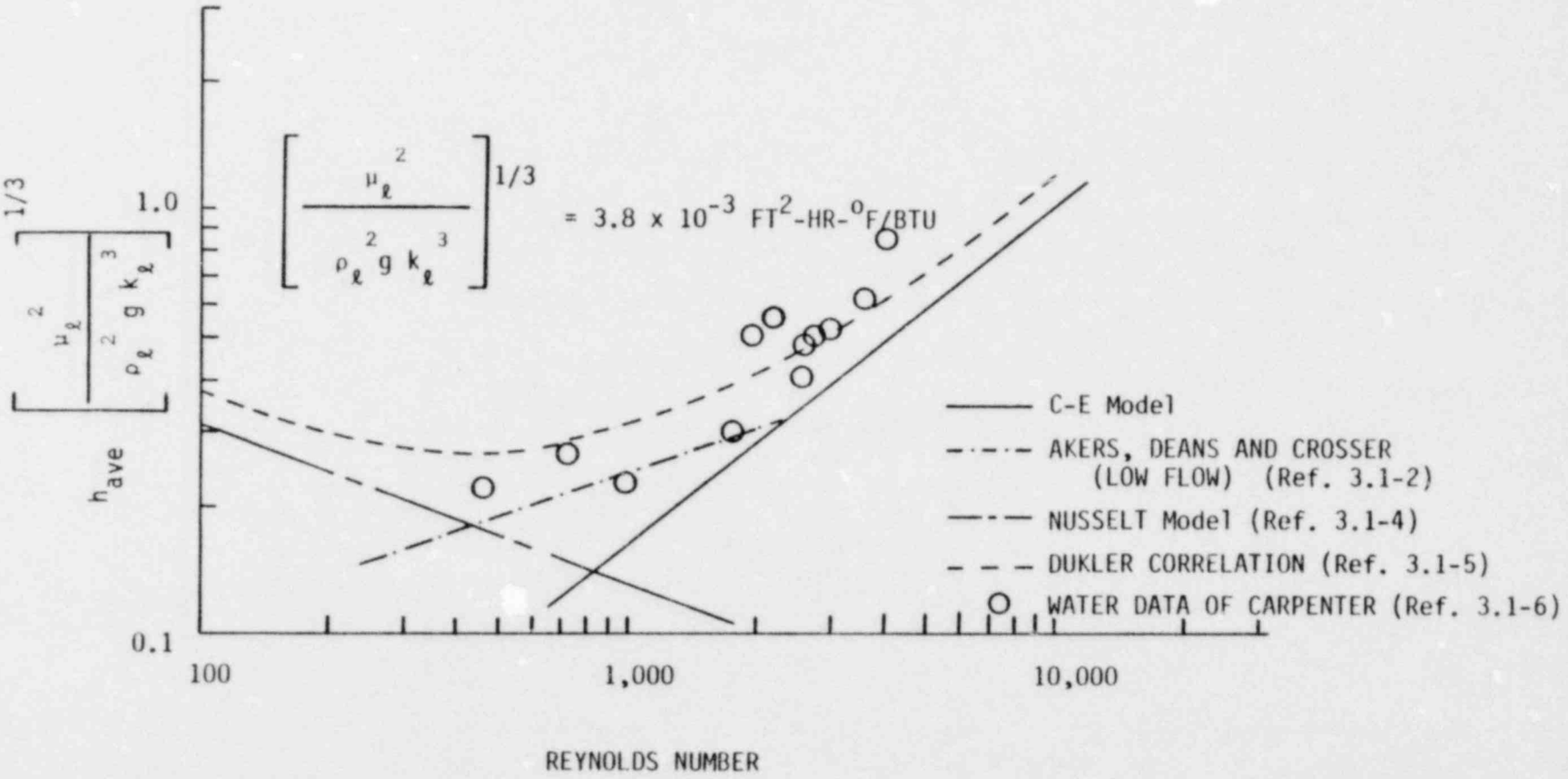

Figure 3.1-3

The Influence of Non-Condensibles on Interfacial Resistance

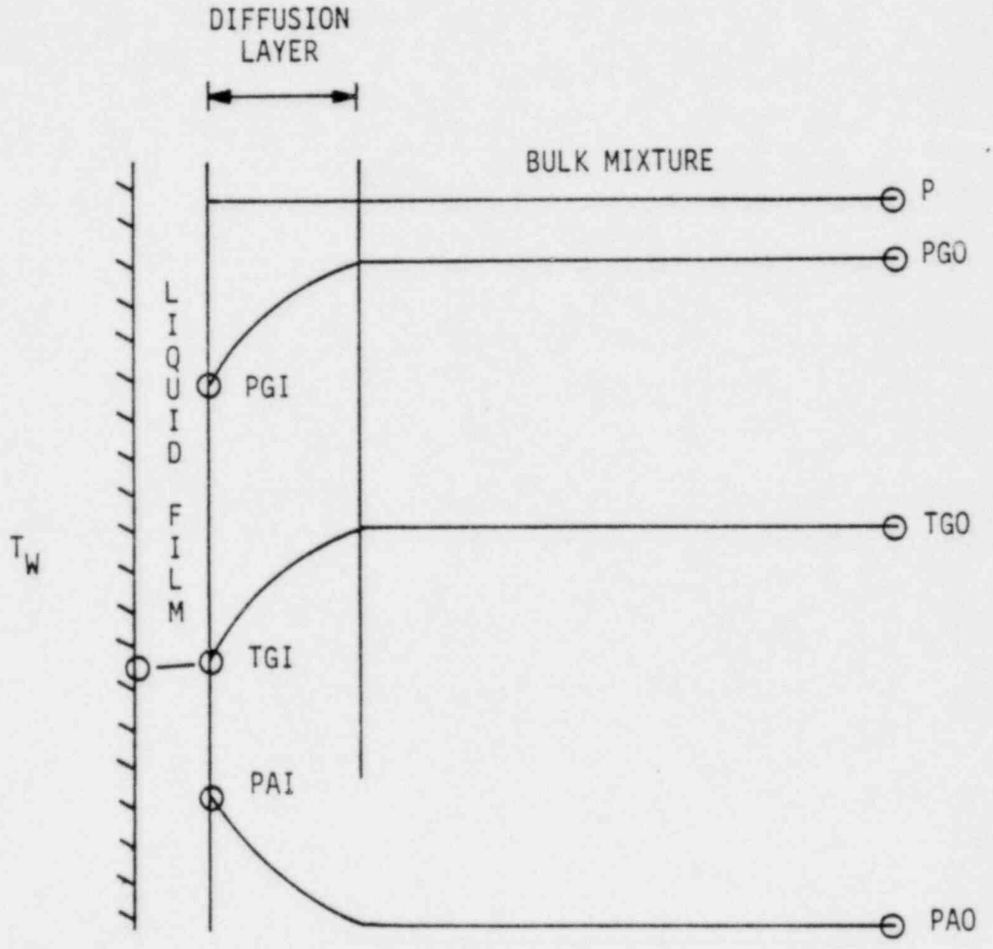

P = TOTAL SYSTEM PRESSURE
PGO = STEAM PARTIAL PRESSURE IN BULK MIXTURE
PGI = STEAM PARTIAL PRESSURE AT INTERFACE
PAO = NON-CONDENSIBLE PARTIAL PRESSURE IN BULK MIXTURE
PAI = NON-CONDENSIBLE PARTIAL PRESSURE AT INTERFACE
TW = WALL TEMPERATURE
TGO = BULK MIXTURE TEMPERATURE
TGI = INTERFACE TEMPERATURE

Figure 3.1-4

Effect of Non-Condensibles on Condensation

Heat Transfer Coefficient and Primary Side Pressure

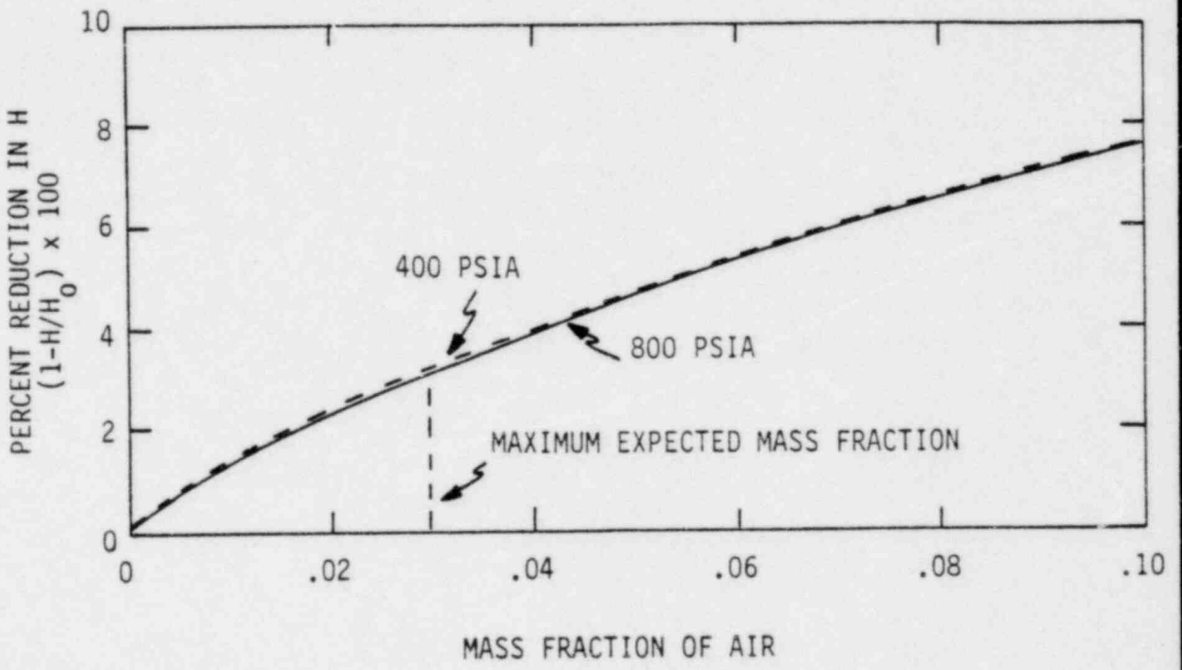

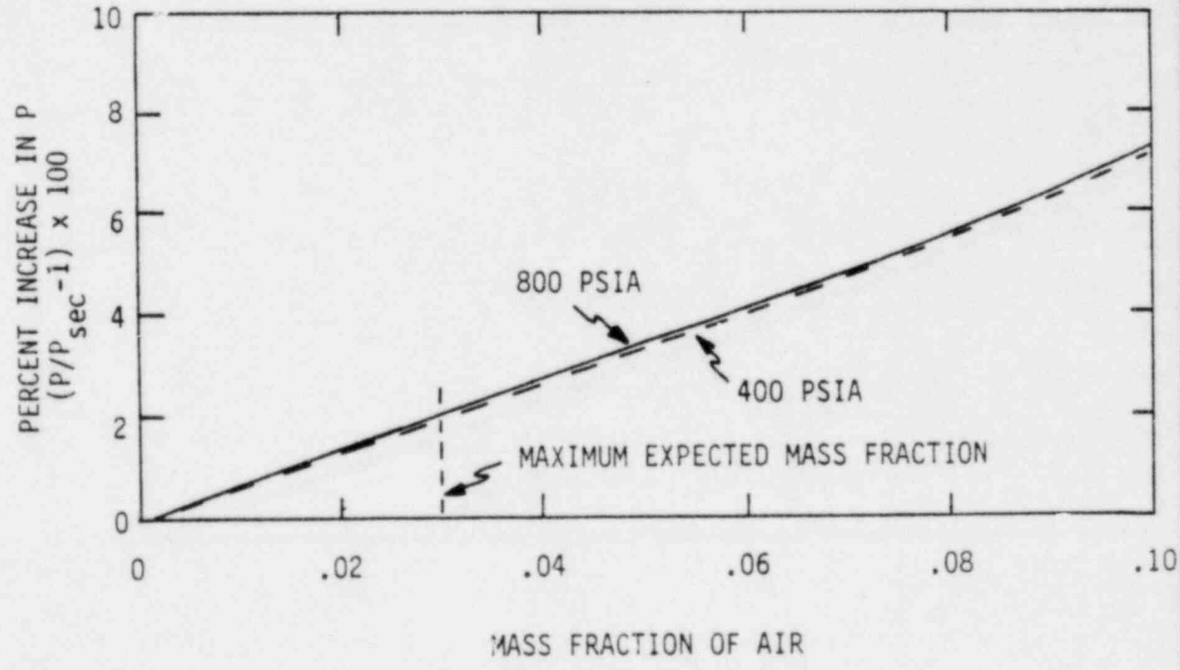

3.2 RESPONSE TO QUESTION 2 (MODELING OF ECCS INJECTION)

3.2.1 Statement of Question 2

NRC has asked that thermal nonequilibrium effects during Emergency Core Cooling System (ECCS) injection be considered. In particular, the NRC has asked that the effect of thermal nonequilibrium during Safety Injection Tank (SIT) activation be determined, the impact of ECCS nodal connections [ ] and nonequilibrium be assessed, and the basis for the nonequilibrium model be identified.

3.2.2 Detailed Response to Question 2

The question is addressed by comparing the cladding temperature response predicted by the Evaluation Model (E-M) with that predicted by alternate models for ECCS injection. The effect of nonequilibrium injection on SIT behavior is addressed to verify the definition of the limiting small break. Next, the effect of nonequilibrium treatment as well as [ ] injection of the high pressure safety injection pump flow is evaluated with a Realistic Model.

3.2.2.1 Nonequilibrium SIT Injection Analysis

The effect of thermal-nonequilibrium treatment of SIT injection was studied for a small break LOCA. These calculations were designed to identify the effect of nonequilibrium modeling of ECCS injection on SIT flow rates. Additionally, they were to identify the effect of nonequilibrium on the definition of the limiting small break, whose area is such that the pressure transient stays just above the SIT pressure setpoint. The calculations were done for a typical C-E PWR with 200 psig safety injection tanks, with ECCS injection [ ]

An assumption of thermal equilibrium during SIT discharge can have the effect of distorting the system dynamics, as the injected subcooled water instantaneously condenses enough steam to maintain saturation conditions. The resulting rapid depressurization produces an excessively high SIT injection flow which rapidly re-covers the core. Large amounts of steam are thus produced by quenching of the fuel rods, increasing the system pressure and quickly ending the SIT discharge. The equilibrium assumption can thus lead to SIT injection in the form of a short, intense burst of water, rather than the expected prolonged, gradual discharge.

In order to evaluate the impact of this behavior and the effect of using a nonequilibrium model during SIT discharge, the limiting small break (0.1 ft^2 break in the cold leg as determined with the equilibrium E-M) and a larger break (0.15 ft^2 break in the cold leg) were analyzed. The SITs do not come on for the 0.1 ft^2 break and do come on for the 0.15 ft^2 break. The 0.15 ft^2 break was analyzed twice, once using the nonequilibrium model starting at the time of SIT activation, and a second time with equilibrium modeling during SIT discharge.

Nonequilibrium modeling of SIT injection raises the cladding temperature by 42°F compared to equilibrium modeling, Table 3.2-1. The maximum cladding temperature for the equilibrium case with SITs occurs at SIT activation, when a large burst of water from the SITs, brought on by the rapid system depressurization caused by equilibrium (100%) condensation, causes the temperature to turn. For the nonequilibrium case, the depressurization is slower during SIT discharge due to the more gradual steam condensation. Thus, the SITs discharge more slowly and allow the cladding temperature to continue increasing for a relatively short time interval after SIT activation. Overall, the more gradual and prolonged SIT injection obtained with the nonequilibrium model produces only a moderate effect on cladding temperature.

The 0.1 ft^2 break does not reach a pressure low enough to activate the SITs. Its maximum cladding temperature, Table 3.2-1, exceeds that of the 0.15 ft^2 break where the SITs are activated regardless of the SIT injection model, equilibrium or nonequilibrium. Based on this result, it is concluded that the

limiting small break remains the one for which the pressure decreases to a value slightly higher than the SIT setpoint pressure. Hence nonequilibrium modeling of SIT injection does not change the definition of the limiting small break.

Experience has shown that a similar concept of the limiting small break also holds for reactor systems with 600 psig safety injection tanks. Therefore, the conclusion that nonequilibrium SIT injection does not change the limiting break definition is expected to apply to 600 psig SIT systems as well.

The results of this study have been used to set the boundaries for the following study of models for HPSI injection because they demonstrate that the 0.1 ft^2 cold leg break, for which the pressure remains just too high to activate the SITs, is the limiting break. Consequently, the remainder of the study on injection location and the effect of nonequilibrium on HPSI injection has been restricted to the limiting small break area.

3.2.2.2 The Realistic Model

A Realistic Model, developed to represent nonequilibrium [ ] ECCS injection, is described. Its use required revisions and additions of component models, as well as changes to the system nodalization of the E-M. The Realistic Model uses an extended version of the CEFLASH-4AS code. It is based on the Evaluation Model version of the code (Reference 3.2-1). The Realistic Model encompasses modifications to several component models and features the following major improvements:

a) a thermal nonequilibrium model,
b) [ ] ECCS injection,
c) a realistic core heat transfer model, described in response to Question 5,

d) various component model modifications that are required for consistency with a nonequilibrium treatment.

The thermal-nonequilibrium hydraulic model represents the coexistence of subcooled water and saturated steam in the same node by means of four conservation equations. An equation for the conservation of liquid mass in each node is solved along with the equations for conservation of total nodal mass, nodal energy, and path momentum. Details of the nonequilibrium model are presented in Section 3.2.4.

Heat and mass transfer between steam and the subcooled liquid is provided by means of a steam condensation model. It depends on the temperature difference between the phases (due to subcooling of the liquid), the interfacial heat transfer area, and correlations for the interphase heat transfer coefficients. Three modes of steam condensation are recognized, as illustrated in Figure 3.2-1. [

] A detailed description of the steam condensation model is presented in Section 3.2.4.

The inner vessel subcooled layer is a region of subcooled water that occupies a portion of the reactor vessel's lower plenum, and may occasionally extend into the lower core. As the subcooled water is heated in the inner vessel, the subcooled layer is continuously replenished by fresh ECCS injection. For minimal-condensation nonequilibrium conditions, the subcooled layer may achieve a considerable height for a substantial period of time. This suppresses production of bubbles in the inner vessel, thereby affecting the inner vessel two-phase mixture level. The Realistic Model provides an improved (relative to

the E-M) representation of the inner vessel subcooled layer which can handle the substantial subcooling that occurs in the downcomer in minimal-condensation nonequilibrium calculations.

A revised core heat transfer model, based on the ORNL Bundle Uncovery Tests and described in Section 3.5 (response to Question 5), is used in the Realistic Model. It describes the two-phase mixture level and the core-to-steam heat transfer coefficient, based on level swell data and heat transfer data recently obtained by ORNL at the Thermal Hydraulic Test Facility (References 3.2-2 and 3.2-3).

Figure 3.2-2 shows the system nodalization used in the E-M analysis of a typical C-E NSSS. A corresponding system nodalization used in the Realistic Model is shown in Figure 3.2-3. It differs from the E-M nodalization in three respects.

[

]

3.2.2.3 Nonequilibrium[ ]ECCS Injection

The small break LOCA behavior of a typical C-E PWR was analyzed with nonequilibrium,[ ]modeling of ECCS injection to determine the effect of HPSI injection. The analysis was done for the limiting case, a 0.1 ft^2 cold leg break and 200 psig safety injection tanks. The nodalization and component models comprising the Realistic Model, described in Section 3.2.2.2, were used. The decay heat (120% ANS), break flow and other models remained the same as in the E-M. This was done to allow comparisons between the Evaluation Model equilibrium[ ]ECCS injection representation and the nonequilibrium[ ]ECCS injection. First, a parametric study of condensation effects ranging from zero condensation (complete thermal nonequilibrium) to maximum condensation (equilibrium) was performed to understand the effect of condensation on the nonequilibrium model. Then the nonequilibrium case with the highest cladding temperature was compared to E-M results to demonstrate the conservatism of the Evaluation Model.

The results of the parametric study of condensation effects are represented by six cases analyzed with various degrees of condensation. The cases are listed in Table 3.2-2 in the order of increasing condensation, from zero to the maximum.

Figure 3.2-4 presents the calculated peak cladding temperatures (PCTs) for the six cases. The abscissa represents the average rate of steam condensation in the cold legs and downcomer up to the time of maximum core uncovery, normalized

by the average rate of equilibrium condensation. All condensation effects discussed in Section 3.2.4 are lumped together, including boiling due to downcomer wall heat. The boiling rate becomes significant at intermediate condensation rates, as in case 4, and rises with increasing cold-leg condensation. The ordinate is the PCT found with the PARCH code as discussed in Section 3.5.

As Figure 3.2-4 indicates, the highest PCTs are produced at zero condensation (case 1) and maximum condensation (case 6), while all intermediate condensation rates result in lower temperatures. In all cases, the calculated PCTs are well below 1940°F, the temperature predicted by the E-M for equilibrium[ ]injection. The behavior of PCT as a function of condensation rate, shown in Figure 3.2-4, is due to the competing effects of bubble production in the inner vessel and the break flow, both of which increase with the condensation rate. These competing effects are illustrated in Figures 3.2-5 and 3.2-6.

Figure 3.2-5 shows the height of the inner vessel's subcooled liquid layer as a function of normalized condensation rate, at 982 seconds into the transient. (This time was chosen because it is within $\pm$23 seconds of the time of maximum core uncovery for all of the cases shown). Increasing the steam condensation rate in the cold legs and downcomer reduces the height of the inner vessel subcooled layer. The latent heat from the condensing steam preheats the ECCS injection water as it passes through the system toward the lower plenum of the inner vessel, thereby reducing the ECCS water's subcooling. This has the beneficial effect of enhancing production of steam bubbles in the inner vessel, which swells the two-phase mixture level and reduces the PCT.

Figure 3.2-6 demonstrates the other competing effect due to the break flow rate. The figure shows the liquid portion of the total mass lost through the

break up to the time of maximum break uncovery (about 350 seconds when the coolant inventory in the broken cold leg reaches steady state), and again at the time of maximum core uncovery (982 seconds) as a function of normalized condensation rate. The mass loss increases significantly in the high condensation cases. The more rapid condensation depressurizes the upper annulus and reduces the rate of recession of the downcomer's two-phase mixture, prolonging the period of time in which downcomer water and ECCS water from the intact cold legs are fed to the break. At zero condensation, case 1, the suppression of bubble condensation in the downcomer produces a similar effect by increasing the downcomer's two-phase mixture level.

The competition between the effect of the inner vessel subcooled layer height and the break flow rate during break uncovery explains the behavior of PCT with condensation. At normalized condensation rates up to about 0.75, the dominant effect is that of the subcooled layer, resulting in a decreasing PCT as condensation increases. Beyond normalized condensation rates of 0.75, the subcooled layer is eliminated by steam condensation and has no further effect. The break flow effect becomes dominant at these condensation rates and produces the increase of PCT. Case 4, with a normalized condensation rate of 0.75 has no subcooled layer in the inner vessel and has a moderate break flow rate during break uncovery, resulting in the lowest calculated peak cladding temperature.

Of the six cases presented here, only the equilibrium calculation (case 6) results in SIT actuation. This occurs two and a half minutes after the cladding temperature has peaked and therefore has no effect on PCT. In the other cases, 1 through 5, the minimum cold leg pressure exceeds the safety injection tanks' pressure plus elevation head by 15, 22, 13, 6 and 0.4 psi, respectively. Thus, in the sense that they come close, but do not quite result in SIT discharge which reduces the PCT, all six cases adequately fit the classical definition of "worst break".

The PCTs calculated by the Realistic Model with nonequilibrium [ ]

injection are thus demonstrated to be well below the temperature predicted by the E-M for equilibrium[ ]injection. The highest PCT, produced by the no-condensation case 1, is about 180°F below the E-M temperature. Since some condensation is expected to take place in the cold legs and downcomer during ECCS injection, the conservatism of the E-M is considerably greater than 180°F in PCT, as indicated in Figure 3.2-4.

3.2.3 Summary and Conclusions for Question 2

The effect of nonequilibrium modeling on SIT injection has been determined for a typical C-E PWR with 200 ,sig SITs. A comparison of equilibrium and nonequilibrium modeling of SIT injection[ ]was made. In general, nonequilibrium modeling of SIT injection increases the cladding temperature relative to equilibrium modeling. However, the limiting 0.1 ft^2 break for which the pressure remains too high for SIT tank actuation, has a higher cladding temperature than the larger break, 0.15 ft^2, for which the SIT is actuated. Use of nonequilibrium modeling of SIT injection does not affect this result. Hence, the limiting break remains one in which the SIT is not actuated. A similar conclusion is made for reactor systems with 600 psig SITs.

The combined effect of[
]nonequilibrium modeling has been evaluated for the limiting break size, 0.1 ft^2 in a typical C-E plant. A Realistic Model that accomodates nonequilibrium effects and steam condensation and incorporates the core heat transfer model described in Section 3.5, was used in the analysis. The Realistic Model employs a condensation calculation consisting of component models that are based on published correlations developed from experimental data. A parametric study on condensation rate shows that a nonequilibrium model with no condensation produces the maximum PCT. The PCT calculated with the Evaluation Model exceeds that calculated with the Realistic Model by at least 180°F. Hence, use of the Evaluation Model maximizes the calculated cladding temperature.

3.2.4 Nonequilibrium Component Model Description

The details of several component models of the Realistic Model are presented in this section.

3.2.4.1 Description of Four-Equation Nonequilibrium Model

Conservation Equations CEFLASH-4AS solves the mixture mass, mixture energy, and mixture momentum conservation equations described in Reference 3.2-1 (Equations (II.A-4), (II.B-9), and (II.C-36), respectively).

The nonequilibrium model for ECC injection described here allows subcooled water and saturated steam to coexist in a node, as shown in Figure 3.2-7. This capability is implemented in the code by solving the equation for conservation of nodal liquid mass M_ℓ, in addition to the equation for conservation of total nodal mass M:

$$\frac{dM}{dt} = \sum W \qquad (3.2\text{-}1)$$

$$\frac{dM_\ell}{dt} = \sum (1-x)\, W + W_{cond} \qquad (3.2\text{-}2)$$

where x is the flow path quality, W is the total mass flow rate, W_{cond} is the steam condensation rate, and the summation is carried out for all paths connected to the node. The mixture energy and momentum equations are unchanged.

Integration of the four conservation equations defines the flowpath mass flow rates, nodal liquid mass, nodal steam mass, and nodal mixture energy. [

]

Calculation of the Steam Mass Flow Fraction and Flowpath Enthalpy CEFLASH-4AS calculates the flow path quality using[ ] (Reference 3.2-1). [ ] Note that the energy convected across the path allows definition of an average flowpath enthalpy H as:

$$H = (1 - x)\, H_{\ell} + xH_g \qquad (3.2\text{-}3)$$

where H_{ℓ} and H_g are the subcooled and saturated steam enthalpies, respectively

Calculation of Leak Flow The leak flow correlations coded in CEFLASH-4AS calculate the choked flow for equilibrium conditions in terms of the leak node pressure and leak path enthalpy. For simplicity and in order to use the same critical flow correlations for nonequilibrium calculations, the leak flow is calculated from the critical flow correlations at the equivalent enthalpy H^e,

$$H^e = (1 - x)\, H_f + xH_g \qquad (3.2\text{-}4)$$

where x is the leak path quality and H_f is the saturated liquid enthalpy. The leak flow enthalpy is calculated as in equation (3.2-3).

Solution of State Variables for a Nonequilibrium Node Integration of the conservation equations defines the nodal liquid mass, nodal steam mass, and nodal mixture energy. [

[

(3.2-5)

]

[

(3.2-6)

(3.2-7)

(3.2-8)

(3.2-9)

(3.2-10)

(3.2-11)

]

3.2.4.2 Steam Condensation

Three modes of steam condensation are represented in the Realistic Model - -

[

] The three modes of

condensation and variations on each mode are illustrated in Figure 3.2-1. [

]

Droplet Condensation This category includes subcooled water[

]the overall droplet heat transfer coefficient, hA. The corresponding condensation rate J is:

$$J = \left[\quad\right] \frac{(hA)_j (T_{sat} - T_j)}{H_{fg}} \qquad (3.2\text{-}12)$$

where h, A and T_j are, respectively, the heat transfer coefficient, interfacial area and fluid temperature of the subcooled liquid[ ]T_{sat} is the saturation temperature of the node, and H_{fg} is the latent heat of vaporization.

The interfacial area for droplets[ ]is found by dispersing the flow as uniform radius spherical droplets[

] The heat transfer coefficient for dispersed droplet flow is found from a constant Nusselt number of 8.067 (Reference 3.2-4). [

]

Bubble Condensation Steam bubbles[ ]are modeled as collapsing at a rate that is determined by their interfacial heat transfer. The model follows that used for RELAP4/MOD7, where the bubble surface area A_B is based on uniform-sized spheres whose radius is found from a critical Weber number of 8 (References 3.2-5 and 3.2-6). The interfacial heat transfer coefficient h_B is the same as that used for bubbly flow in RELAP4/MOD7 (Reference 3.2-5). Then the bubble condensation rate is found as:

$$J(t) = \frac{hA\,[T_{sat} - T_{\ell}(t)]}{H_{fg}} \qquad (3.2\text{-}13)$$

where $T_{\ell}(t)$ is the temperature of the subcooled liquid. Here the interdependence of the condensation rate and the subcooled liquid (sink) temperature are indicated by their dependence on time t[ ] Fluid properties and overall heat transfer coefficients are assumed constant over the time step.

Bubble production due to wall heat is treated as[

]

[

]

[

]

3.2.5 References for Question 2

3.2-1 "CEFLASH-4A, A FORTRAN-IV Digital Computer Program for Reactor Blowdown Analysis", CENPD-133P, August 1974 (Proprietary).

"CEFLASH-4AS, A Computer Program for the Reactor Blowdown Analysis of the Small Break Loss of Coolant Accident", CENPD-133, Supplement 1P, August 1974 (Proprietary).

"CEFLASH-4AS, A Computer Program for the Reactor Blowdown Analysis of the Small Break Loss of Coolant Accident", CENPD-133, Supplement 3-P, January 1977 (Proprietary).

3.2-2 T. Anklam, "Two-Phase Mixture Level Swell for Water and Steam Under High Pressure, Low Heat Flux Conditions in Rod Bundles", to be published

3.2-3 T. M. Anklam, "Low Flow, High Presure, Forced Convection and Radiation to Steam in Rod Bundle Geometry", to be published.

3.2-4 E. D. Hughes, et al, An Evaluation of State-of-the-Art Two-Velocity, Two-Phase Flow Models and Their Applicability to Nuclear Reactor Transient Analysis, EPRI NP-143, February 1976.

3.2-5 "RELAP4/MOD7 Nonequilibrium ECC Mixing Model", H. Chow, CHOW-1-79, June 19, 1979 (EG&G internal document).

3.2-6 G. B. Wallis, "One-dimensional Two-phase Flow", McGraw-Hill Book Company (1969).

3.2-7 [ ]

Table 3.2-1

Effect of Nonequilibrium on SIT Discharge

Break Size (ft^2)	SIT Actuated	SIT Model	Cladding Temperature* (°F)	(°F)
0.1	No	-	1419	Base
0.15	Yes	Equilibrium	1282	-137
0.15	Yes	Nonequilibrium	1324	-95

*Axial maximum cladding temperature for average rod

Table 3.2-2

Description of Cases for Nonequilibrium Parametric Study

Case	Description
1.	Complete thermal nonequilibrium. All condensation is suppressed, [ ]
2.	Minimal condensation. [ ]
3.	Limited condensation. [ ]
4.	Realistic condensation parameters. [ ]
5.	Enhanced condensation. [ ]
6.	Equilibrium.

FIGURE 3.2-1

MODES OF STEAM CONDENSATION

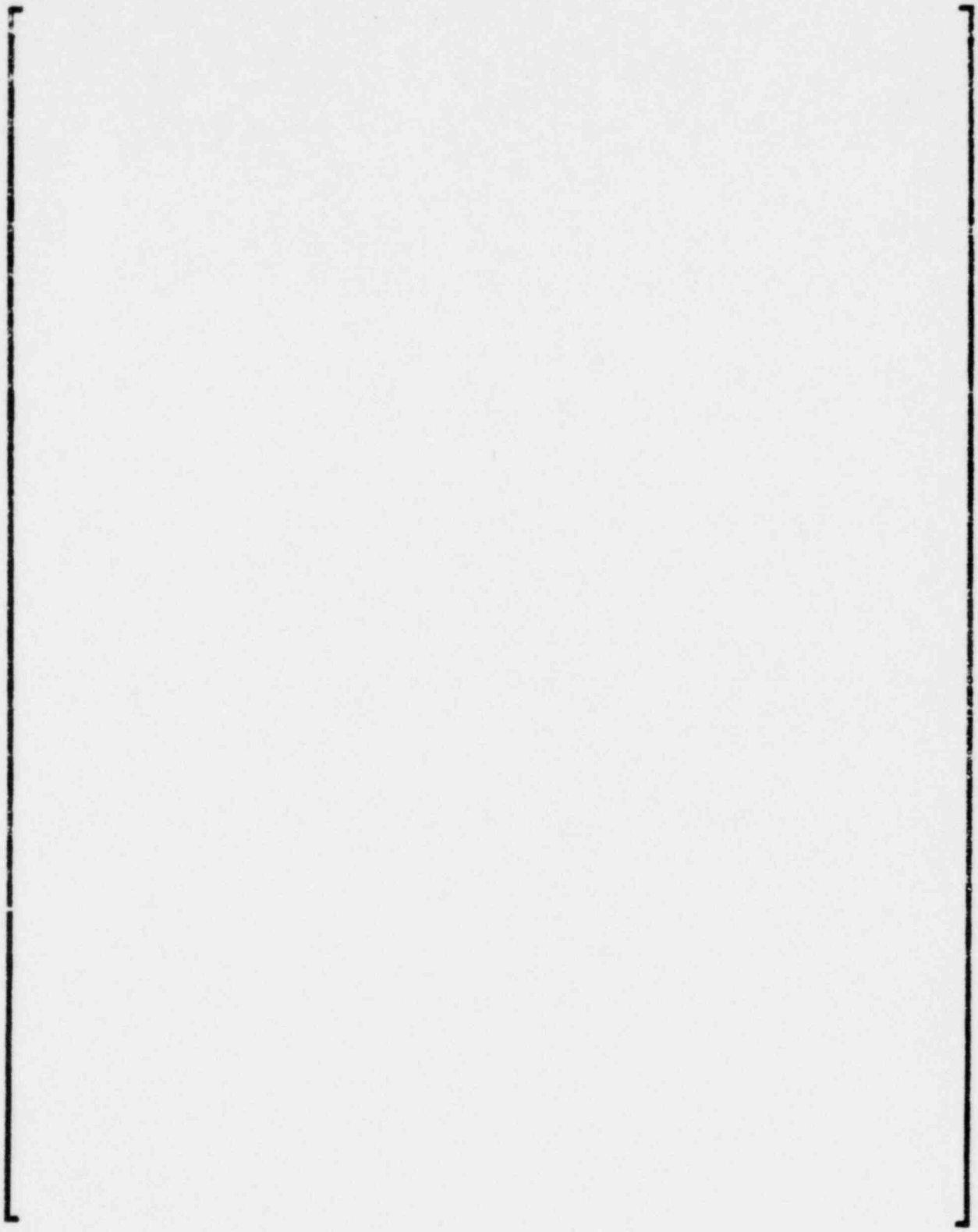

FIGURE 3.2-2

EVALUATION MODEL NODALIZATION

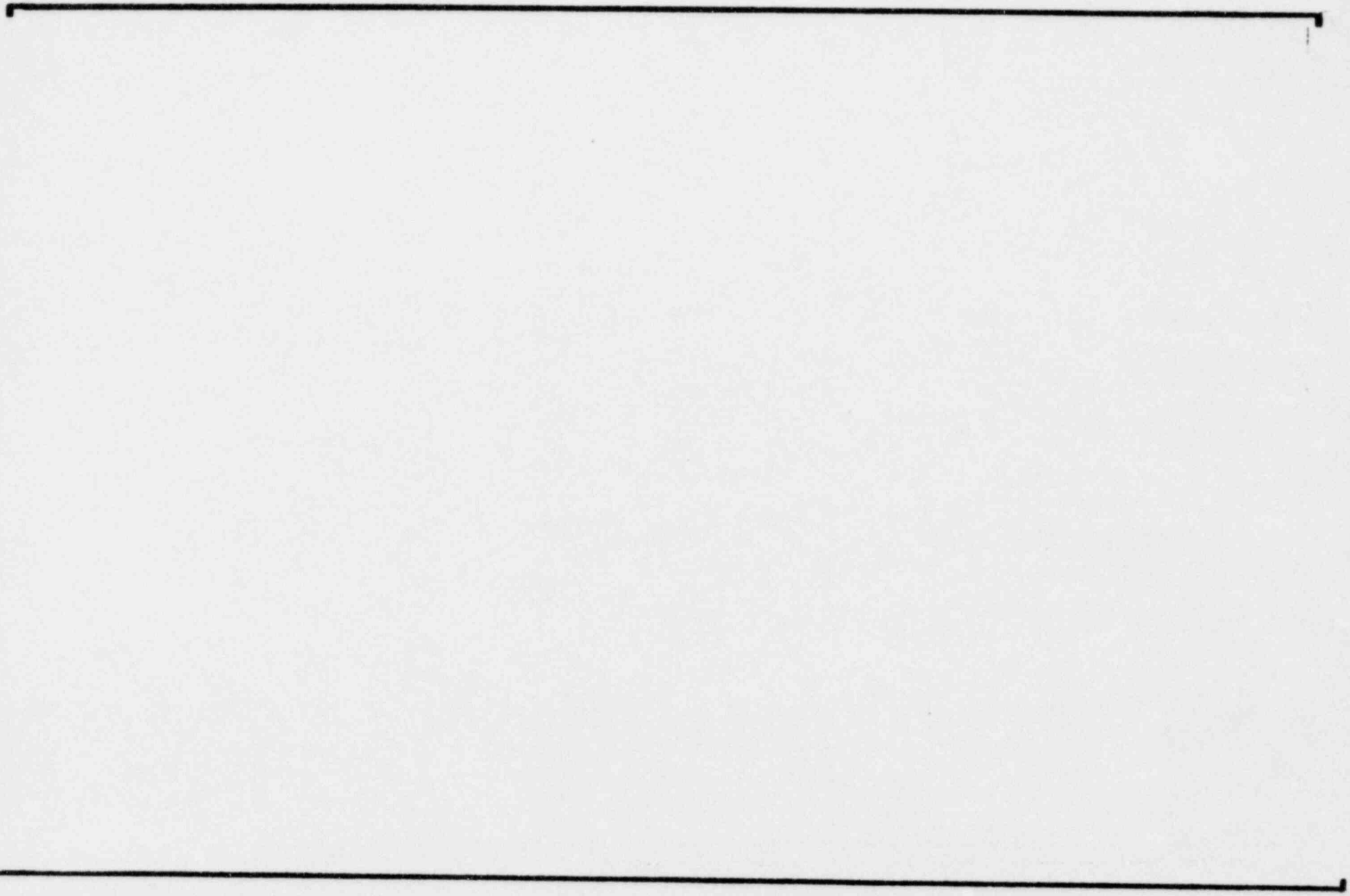

FIGURE 3.2-3

REALISTIC MODEL NODALIZATION

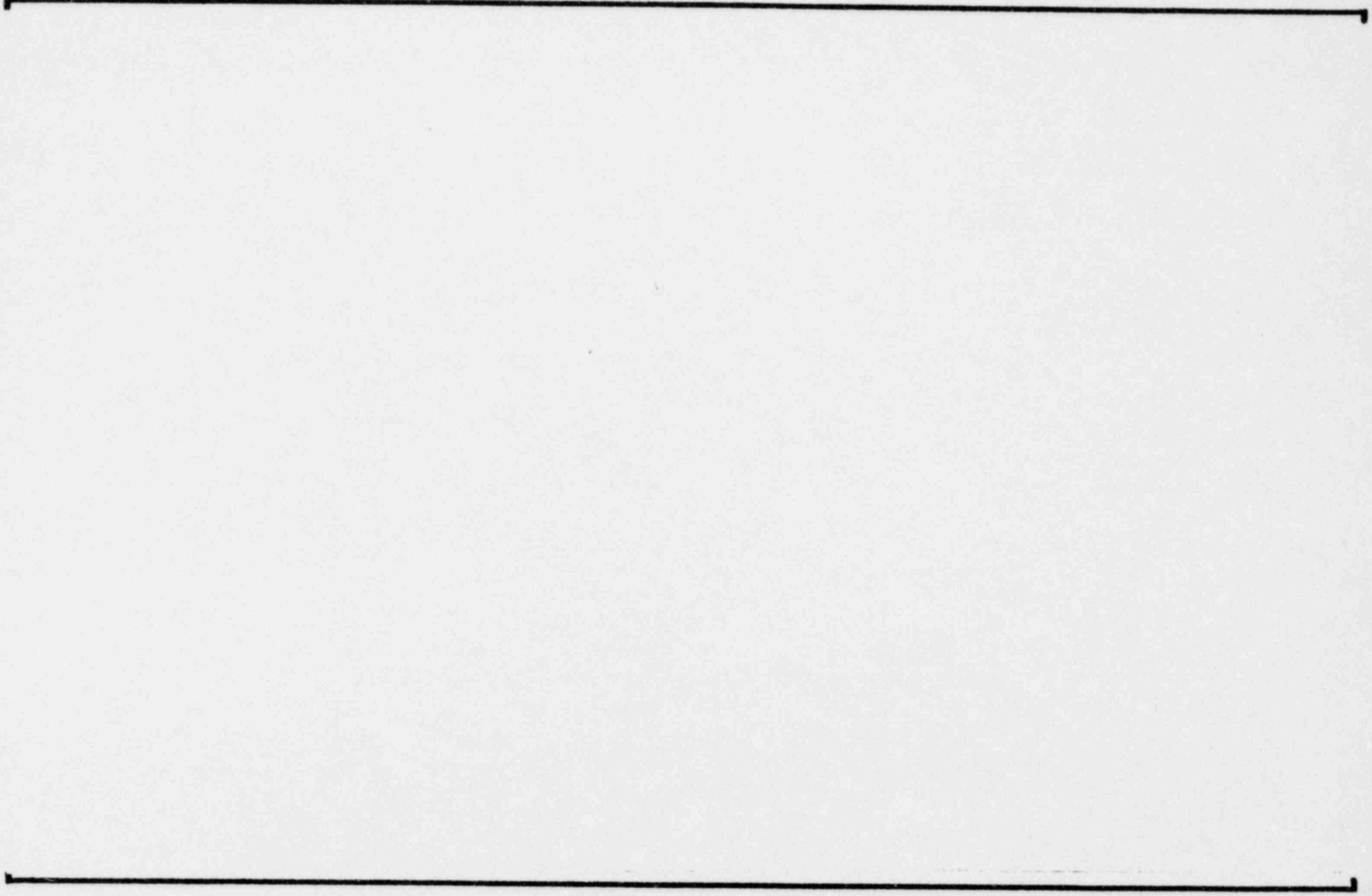

FIGURE 3.2-4

EFFECT OF CONDENSATION ON
PEAK CLADDING TEMPERATURE

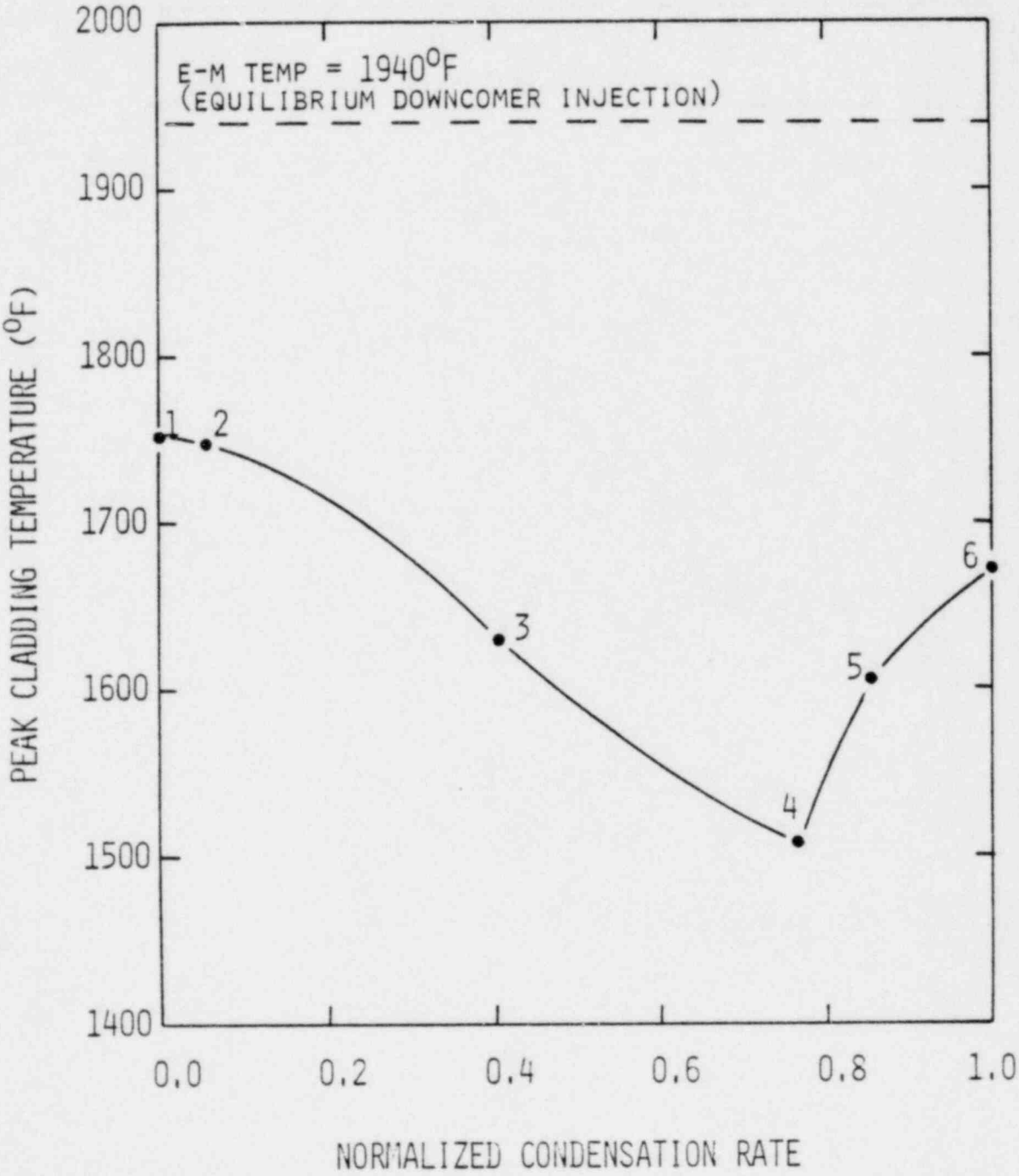

FIGURE 3.2-5

HEIGHT OF THE INNER VESSEL SUBCOOLED LAYER
(AT MAXIMUM CORE UNCOVERY TIME)

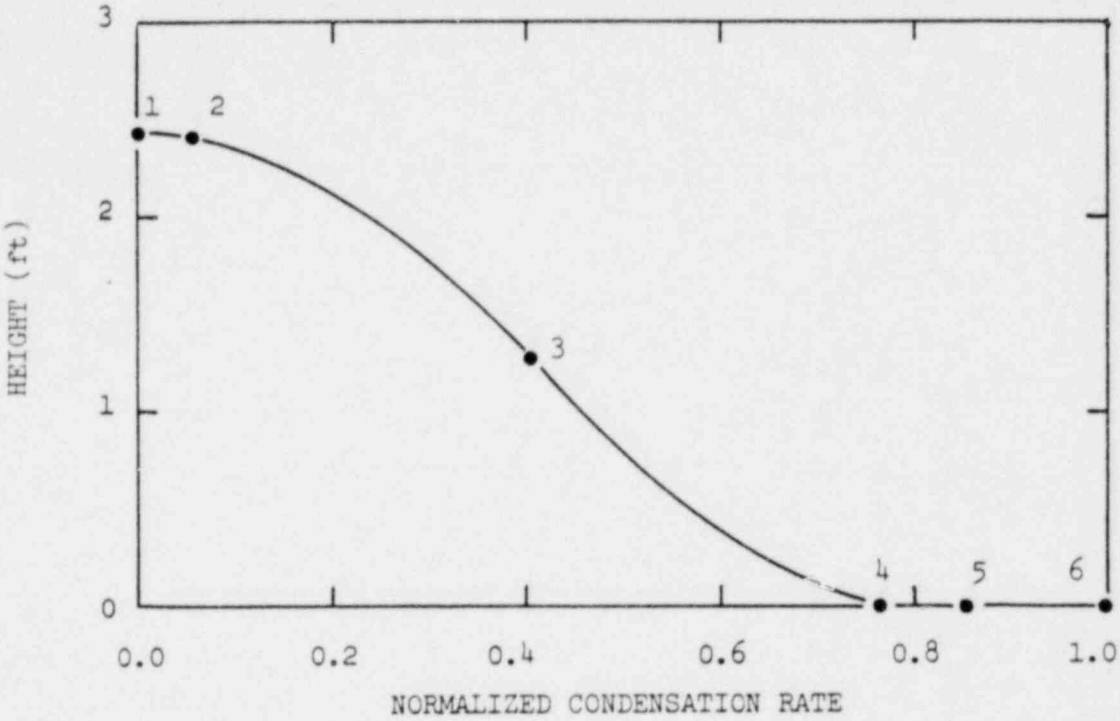

FIGURE 3.2-6

INTEGRATED LIQUID BREAK MASS LOSS UP TO TIMES OF MAXIMUM
BREAK UNCOVERY AND MAXIMUM CORE UNCOVERY

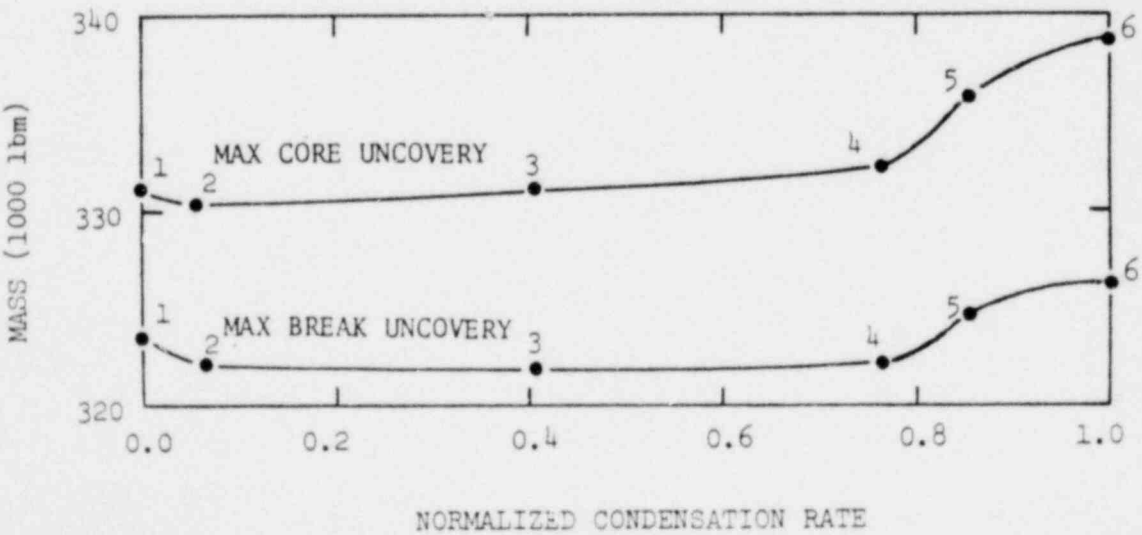

FIGURE 3.2-7

FOUR EQUATION NON-EQUILIBRIUM NODAL MODEL

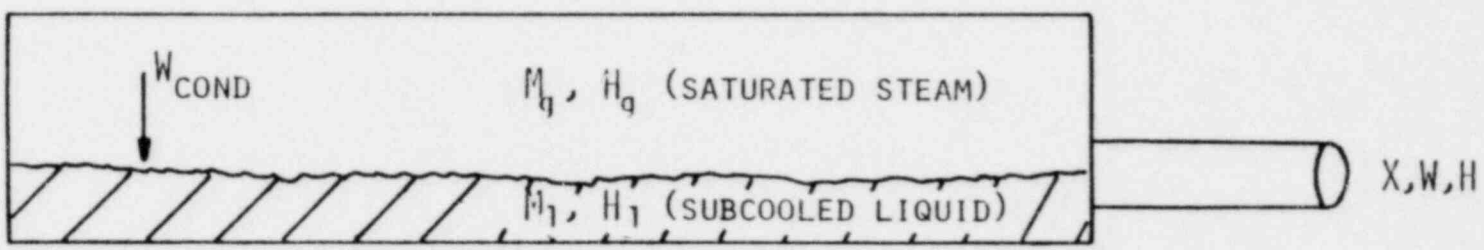

3.3 RESPONSE TO QUESTION 3 (MODEL VERIFICATION)

3.3.1 Statement of Question 3

Verify small break LOCA model by comparison of integral system test data from LOFT tests L3-1 and L3-6 as well as from Semiscale test S-07-10D to post-test predictions of these tests.

3.3.2 Detailed Response to Question 3

Test analyses of LOFT tests L3-1 and L3-6 were provided to the NRC on February 28, 1980 and April 1, 1981. References 3.3-1 and 3.3-2 describe the detailed C-E analyses of LOFT tests L3-1 and L3-6, respectively. Test analyses of Semiscale test S-07-10D were initiated but were terminated in May, 1981 when the NRC dropped the requirement to include this test (Reference 3.3-3). The results of the post-test analyses of LOFT tests L3-1 and L3-6 are summarized below.

LOFT Test L3-1

LOFT test L3-1 simulated a 0.09 ft^2 single-ended pump discharge break of a large PWR. The primary coolant pumps were tripped early in the transient. The post-test analysis was performed using a version of the CEFLASH-4AS computer code that contains several options that are not available in the licensing version. These options were created in order to perform non-licensing analyses such as predictions of LOFT and Semiscale small break tests, RCS pump studies, etc. The modifications to the pre-test analysis of L3-1 were:

- The break area was increased by 25 percent to account for a leaky valve in the warm-up line connected between the intact hot leg and a point downstream of the break orifice.

- A bypass flowpath between the broken hot and cold legs was added to account for the leaky valves in the reflood assist bypass system.

- An isothermal, rather than adiabatic, expansion of nitrogen was assumed for the accumulator cover gas to more realistically account for observed behavior.

Figure 3.3-1 shows the excellent agreement of the calculated and measured primary system pressure and reactor vessel two-phase mixture height.

LOFT Test L3-6

LOFT Test L3-6 also simulated a .09 ft^2 break in the cold leg of a large PWR. The L3-6 test differed from the L3-1 test in the following ways:

- The primary coolant pumps were powered throughout the test.

- The break was located in the side of the intact cold leg rather than on the end of the broken cold leg.

- Only the high pressure safety injection system was active. The accumulator was valved out throughout the test.

- The ECC injection location was changed from the intact cold leg to the annulus.

The post-test analysis was performed using a version of the CEFLASH-4AS computer code that contains several options that are not available in the licensing version. These options were created in order to perform non-licensing analysis such as that described here. In addition to these options, improvements have been made to the code to reduce execution time. These improvements, however, did not affect calculated results.

The major modifications to the pre-test analysis of L3-6 were:

- A leak in the steam generator steam valve was added in order to account for the steam valve leak.

- The initial mass inventory in the steam generator secondary side was increased by 35%, to agree with the actual initial conditions.

- The rate of heat generated by the primary coolant pumps and added to the fluid was made proportional to the rate of mass being pumped.

- The primary coolant pump injection (PCPI) flow, which in the blind analysis had been directed into the pump discharge cold leg, was split and redirected into the two loop seal risers. This permitted the pumps to "see" the PCPI liquid, more closely approximating the actual direct injection into the pump housing.

In addition, several model modifications were implemented as part of the post-test analysis, having been necessitated by several instances of localized anomalous behavior which were observed in the blind analysis results. The major model changes are described below.

- The two downcomer nodes, which in the blind analysis had been handled with a mixed homogeneous/heterogeneous algorithm, were remodeled as homogeneous-mixture nodes. This change was made in response to an observation in the blind analysis that the heterogeneous mixture in the upper half downcomer node was draining into the lower half downcomer node in a non-physical manner.

- The wall heat representation in homogeneous-mixture nodes was revised. Wall heat, the thermal interaction between coolant and internal metal structures, had been modeled in

the blind analysis as proportional to the mixture level in each individual node. Homogeneous-mixture nodes, however, were treated as being always full as long as the mixture quality was less than unity, resulting in overpredicted wall heat rates. While wall heat plays a small role for all full-scale PWRs and for most components of the LOFT facility, the LOFT downcomer presented an exception. The abnormally massive walls of the LOFT downcomer acted as a nearly infinite heat source and did not approach thermal equilibrium with the primary coolant within the transient time of the LOCE. Thus, the homogeneous-mixture downcomer model erroneously introduced a tremendous amount of additional wall heat into the system, a modeling aberration unique to the LOFT facility. A simple modeling change was therefore implemented for all homogeneous-mixture nodes, in which the wall heat rate was made proportional to the theoretical, fully-collapsed liquid level of the mixture. While this in itself tended to underpredict the wall heat, it created a fairly reasonable description of wall-fluid thermal interactions when combined with the conduction-limited (infinite convective heat transfer coefficient) wall heat transfer model of CEFLASH-4AS.

- The flow path connecting the downcomer node to the inactive loop cold leg node was split into two parallel paths between the same two nodes. This change was implemented in order to properly model the flow between the downcomer and the inactive cold leg -- another LOFT peculiarity.

Figure 3.3-2 compares the predicted and measured primary coolant system pressures. The agreement of analysis with data is excellent during most of the transient. The underprediction of pressure, which showed up at 1400 seconds, peaked at 90 psi at 1600 seconds, and gradually vanished thereafter.

LOFT Test L3-6 demonstrated the maintenance of adequate core cooling during a loss of coolant event in which the pumps were powered, even when a major portion of the primary fluid had been lost. After the primary coolant pumps are finally tripped, however, the ability of the system to provide the core with adequate cooling depends, in part, on the primary coolant mass inventory remaining in the system at the time of pump trip.

The L3-6 post-test analysis predicted a final mass inventory at the end of Test L3-6 (2371 sec) of 3138 lbm. This appears to be quite high when compared with the final inventory of 1496 lbm which was reported by EG&G. In order to trace the causes of this difference, the system mass balance was examined in detail. In the L3-6 experiment, mass entered and exited the system at three points -- high pressure injection (HPI), primary coolant pump injection (PCPI) and break flow. Of these, the HPI and PCPI flows were predicted correctly, since the former was a function of pressure which was predicted accurately (Figure 3.3-2), and the latter was delivered at a constant rate by a positive displacement pump. Thus, only the break flow need be considered for a mass inventory comparison.

The break flow during LOFT Test L3-6 exhibited two distinct regimes -- subcooled break flow during the first ~50 seconds and two-phase thereafter. (Because of the PCPI, the break flow never went to pure steam). Since break flow measurements were not available for the first 50 seconds of the test, the subcooled break flow was reconstructed by using the Henry-Fauske critical flow correlation with a discharge coefficient of 0.97. Measured pressures and temperatures in the break piping upstream of the orifice were used in evaluating the critical flow. The result of this calculation is presented in Table 3.3-1 and was corroborated by a similar calculation performed by EG&G. As the table shows, the post-test analysis, which used the homogeneous equilibrium model for critical flow with a discharge coefficient of 0.85, underpredicted the subcooled break flow.

During the period following transition to two-phase flow, the post-test analysis matched very well with the measured break flow data, as shown in Figure 3.3-3. Indeed, Table 3.3-1 shows that the post-test analysis under-

predicted total break flow by only 5.0% during that period. Thus, for the overall transient, the sum of the post-test analysis underpredictions of break flow appears to account for only half of the difference in mass inventory reported above.

The key to this inconsistency lies within the measured and calculated data reported by EG&G. Table 3.3-2 summarizes the mass balances of the post-test analysis prediction and the actual experiment. The table shows the actual final inventory, as calculated from the published data to be 2203 lbm, and the post-test analysis overprediction to be considerably less severe than reported above. Figure 3.3-4 shows the transient of the actual mass inventory, as well as the post-test analysis prediction.

There appears to be, then, an internal inconsistency between the L3-6 final mass inventory calculated by C-E and EG&G from the data (2203 lbm) and the mass inventory reported by EG&G (1496 lbm). At present, this difference has not been resolved.

Additional calculations were made to determine the possible effect on the system's final mass inventory if further model changes were made to improve the match between calculated pressure and experimental data beyond about 1200 seconds. This would prevent total uncovery of the reactor vessel outlet nozzle and voiding of the active loop, which would increase the break flow. These calculations showed that the resultant improvements in break and HPSI flows would decrease the final inventory to ~2050 lbm. This encouraging result appears to account for the difference between the actual final mass inventory and the one calculated by CEFLASH-4AS.

3.3.3 Summary and Conclusions for Question 3

The L3-1 post-test analysis was performed using information obtained from analysis of the L3-1 data. When these effects were properly represented by the CEFLASH-4AS representation of LOFT, the comparison between the experimental data and predicted parameters was excellent.

The L3-6 post-test analysis was performed using information obtained from analysis of the L3-6 data in order to identify parameters of the LOFT system behavior when the pumps are running. The post-test analysis did an outstanding job of predicting the primary coolant system pressure and the break flow. The PCS mass inventory was overpredicted, but the difference could not be precisely quantified because of an internal inconsistency in the data.

3.3.4 References For Question 3

3.3-1 "Combustion Engineering Analysis of LOFT Test L3-1", February, 1980.

3.3-2 "Analysis of LOFT Test L3-6 Performed by Combustion Engineering, Inc.", April, 1981.

3.3-3 Letter, Dr. J. K. Gasper (CEOG) to Dr. B. Sheron (NRC), "Post-Test Analysis of Semiscale Test S-07-10D", May, 1981.

Table 3.3-1

L3-6 Post-Test Analysis

Predicted and Actual Integrated Break Flows

(in lbm and % of initial mass inventory)

Time Period	Post-Test Analysis		Actual Test*		Difference Analysis-Test	
	lbm	%	lbm	%	lbm	%
0-50 sec	1,043	8.5	1,351	11	-308	-2.5
50-2371 sec	11,142	91.5	11,747	96.5	-605	-5
0-2371 sec	12,185	100	13,098	107.5	-913	-7.5

*From critical flow correlation during 0-50 sec, and LOFT Test L3-6 break flow data during 50-2371 sec.

Table 3.3-2

L3-6 Post-Test Analysis

Predicted and Actual Mass Balances at Time of Pump Trip

(in lbm and % of initial mass inventory)

	Post-Test Analysis		Calculated From Data		Reported by EG&G	
	lbm	%	lbm	%	lbm	%
Initial Inventory	12,200	100	12,161	100	12,161	100
Total HPSI	2,613	22	2,630	22(1)	2,630	22
Total PCPI	510	4	510	4(2)	510	4
Total Break	12,185	100	13,098	108(3)		
Final Inventory	3,138	26	2,203	18	1,496	12

(1) Integrated measured flow rate.

(2) 2371 sec. times constant flow rate.

(3) Table 3-4.

Figure 3.3-1

LOFT L3-1 Post-Test Analysis Inner Vessel Two-Phase Mixture Level and Inner Vessel Pressure

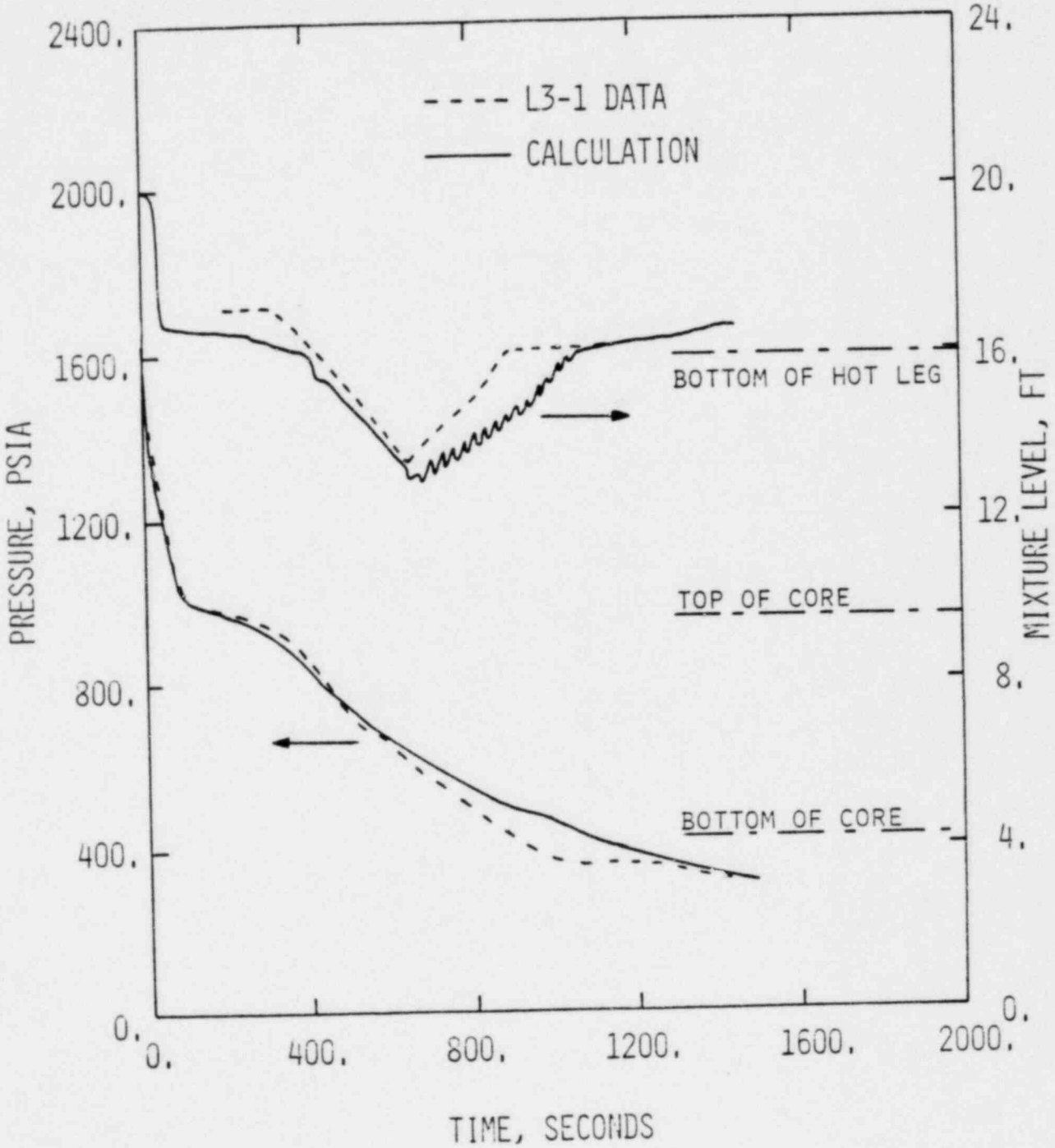

Figure 3.3-2

LOFT L3-6 Post-Test Analysis

Primary System Pressure

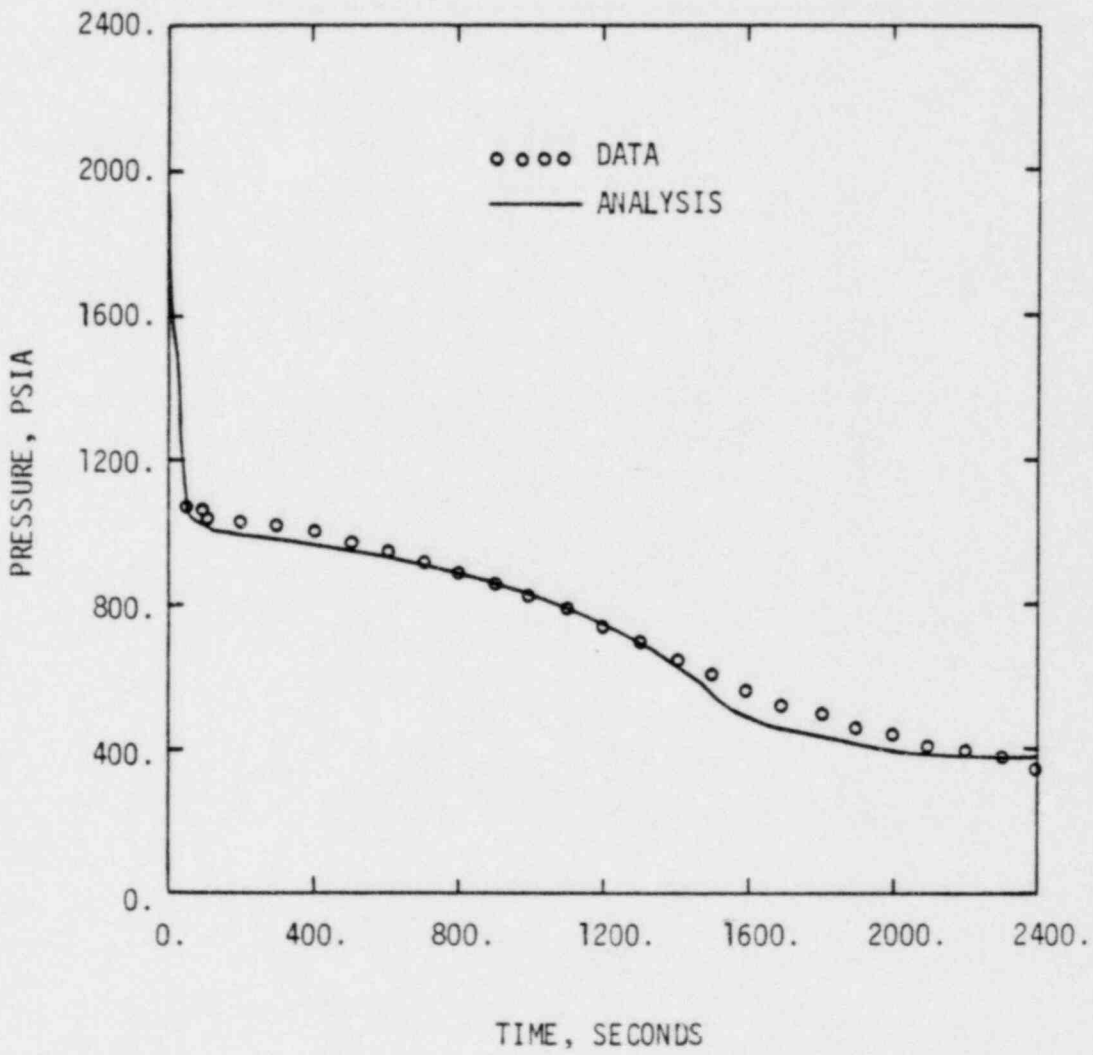

Figure 3.3-3

LOFT L3-6 Post-Test Analysis

Break Flow

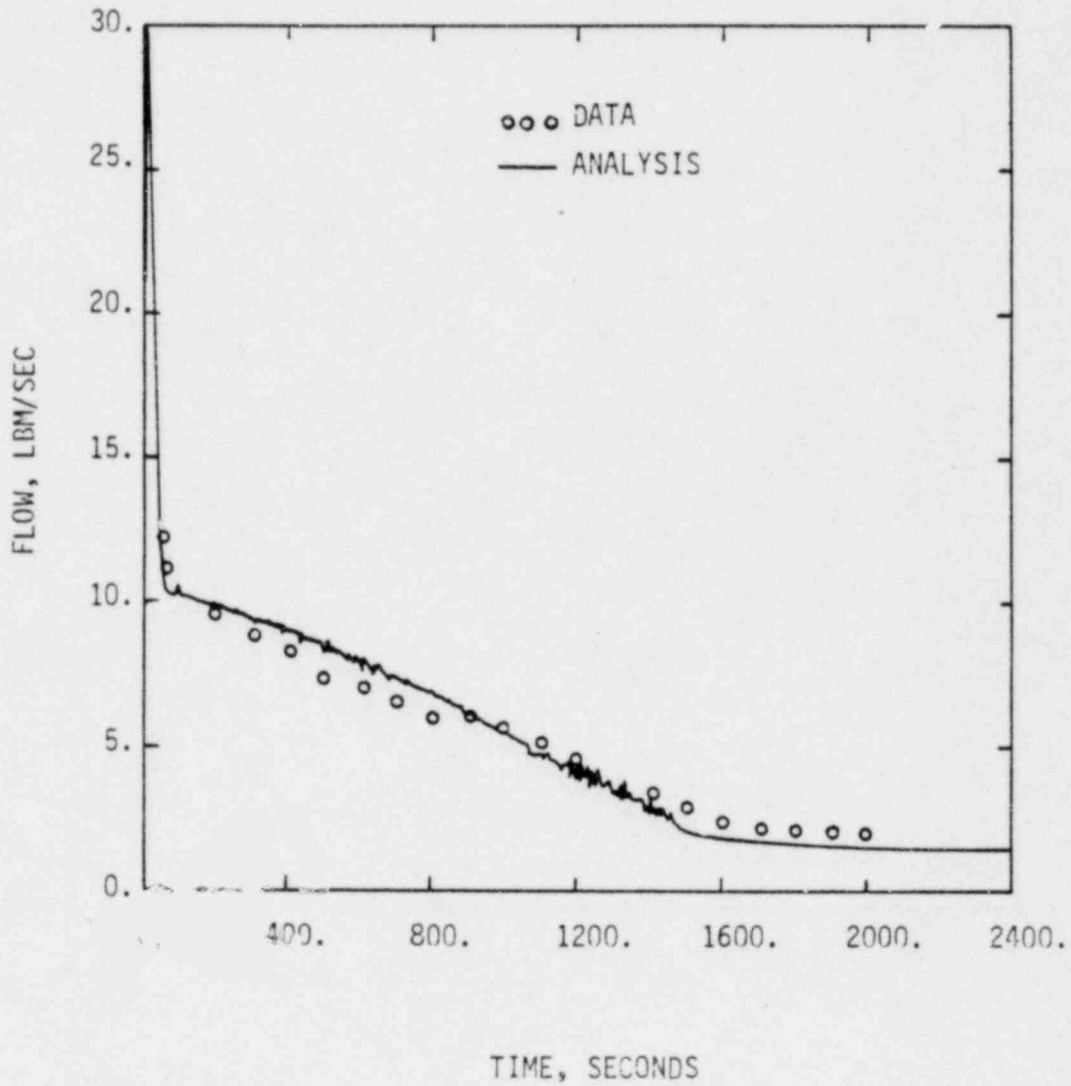

Figure 3.3-4

LOFT L3-6 Post-Test Analysis

Primary System Mass Inventory

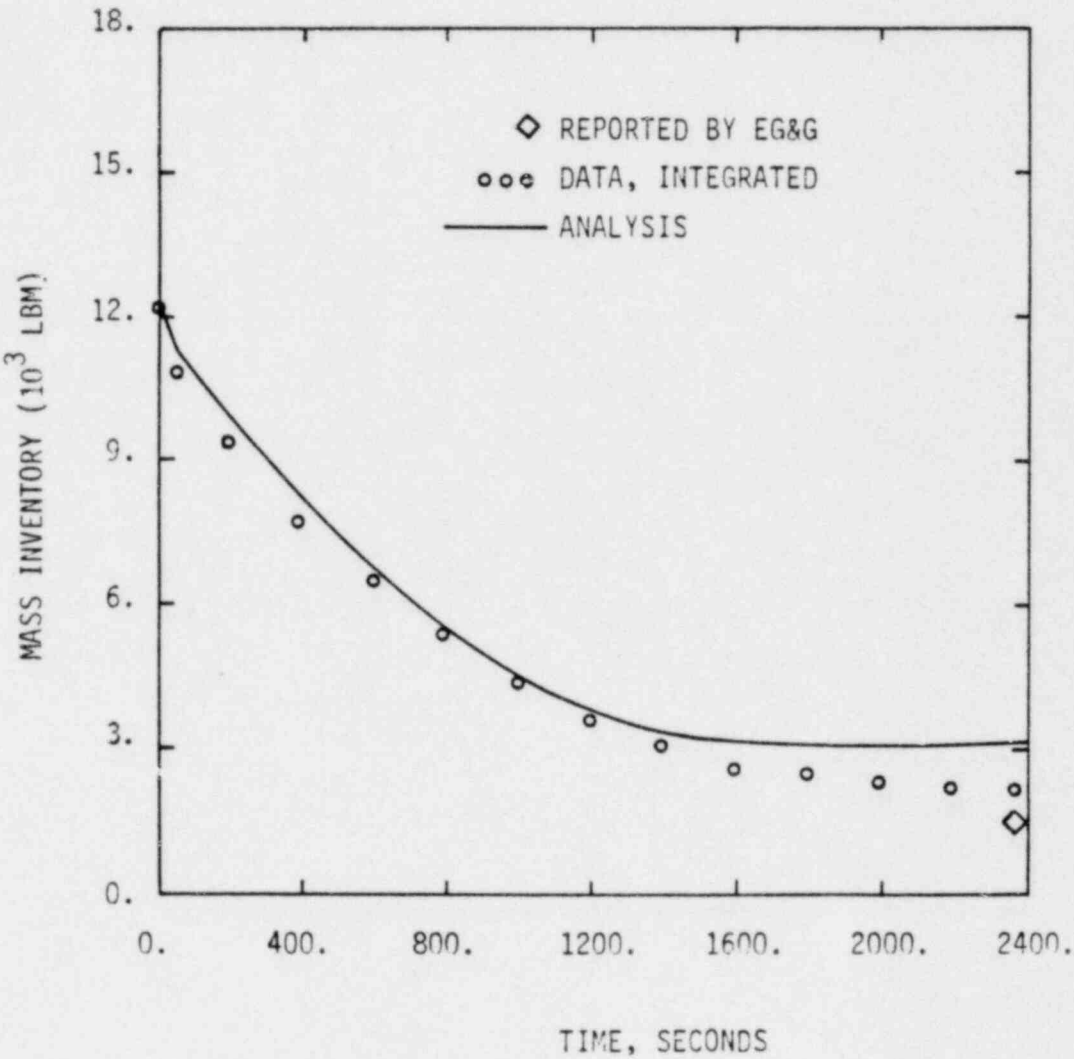

3.4 RESPONSE TO QUESTION 4 (FLOW REGIME EFFECT ON PRESSURE DROP)

3.4.1 Statement of Question 4

Verify that the model used to predict pressure drop in CEFLASH-4AS is conservative. In particular, the sensitivity of pressure drop across the steam generator to various flow regimes must be assessed. Calculations have been performed by the NRC that suggest that the selection of a particular flow regime, for the purpose of calculating steam generator pressure drop, can have a significant effect on the calculated height of the two-phase mixture in the reactor vessel.

3.4.2 Detailed Response to Question 4

During [ ] a SBLOCA, the pressure drop across the steam generator is primarily due to [ ] Figure 3.4-1 shows a typical situation [ ] The model also predicts that the hot leg contains a stratified two-phase mixture below a steam region as shown in Figure 3.4-1. [ ] This behavior has been observed in integral systems tests such as LOFT test L3-5. For limiting small break calculations, C-E calculates that core uncovery occurs [ ] as shown in Figure 3.4-2.

In order to determine the sensitivity of the reactor vessel two-phase mixture to assumed flow regimes in the steam generator, C-E performed the analyses described in Table 3.4-1. All analyses were performed using a typical limiting 0.1 ft^2 break for the sensitivity studies. The flow regimes investigated in the steam generator [ ] were heterogeneous (separated) and homogeneous. The flow regimes investigated in the flow paths were bubbly, slug and annular two-phase flow. In addition, the effects of imposing [ ] were investigated.

RESULTS

C-E Evaluation Model

The flow rates between the hot legs and the steam generators are determined by the solution of the momentum equation. The momentum equation used in CEFLASH-4AS is

$$\left(\frac{L}{A}\right)\frac{d\bar{w}}{dt} = -\Delta P + \bar{\rho}\, g\, \Delta Z - \frac{k_g\, |\bar{w}|\, \bar{w}}{2\,\bar{\rho}\, A^2}$$

$$- f\left(\frac{L}{D}\right)\frac{\bar{w}\,|\bar{w}|\,\phi_f^2}{2\,\rho_f\, A^2} + \text{momentum flux terms} \qquad (3.4\text{-}1)$$

where,

$$f = 0.184\,(Re_f)^{-0.2}$$

The flow resistance due to friction is determined by multiplying the resistance obtained if the flow were all single phase liquid by Thom's two-phase multiplier, which is pressure and quality dependent.

The C-E model also assumes that the steam generator and hot leg nodes, as well as all other nodes, contain a heterogeneous mixture. The base case was run using the C-E model without modifications.

The results for the base case are shown in Figure 3.4-3. [

]

Homogeneous Steam Generator Node

The only nodal flow regime options available in CEFLASH-4AS are separated (heterogeneous) and homogeneous. In the homogeneous option the fluid is assumed to be uniformly distributed in the node. Modeling the steam

generator in this way is not realistic but it will have two effects on the transient. First, [ ] the steam generator will not experience the transition from a two-phase mixture to steam as the level drops [ ] Instead, the density [ ] will gradually decrease as the node drains. As a result, more of the liquid in [ ] the steam generator will be transported [ ] when homogeneous modeling is used. This has the effect of putting more liquid on the [ ] and could increase the break flow rate and delay the time when steam starts to flow out of the break.

The second effect concerns the calculated [ ]

[ ]

(3.4-2)

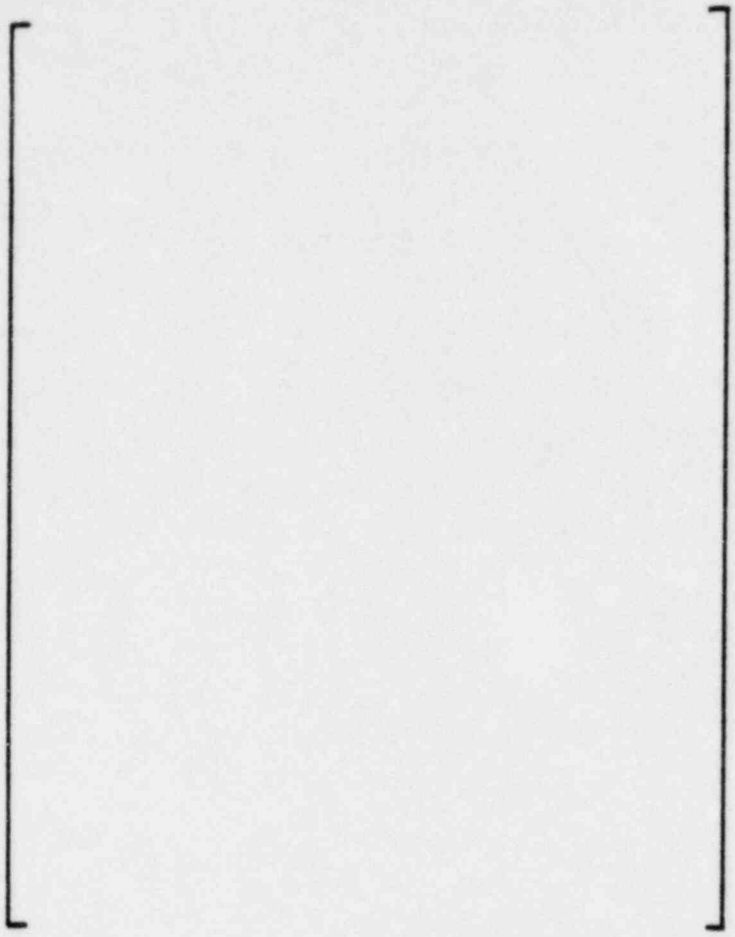

As shown in Figure 3.4-4, the combined effect of modeling[ ]the steam generator as a homogeneous node is to decrease the reactor vessel level in the upper plenum, compared to the base case, for part of the transient. However, there is no significant difference in core uncovery.

[ ]Flow[ ]By[ ]Correlation

[

(3.4-3)

]

[

]

In order to investigate this effect, equation (3.4-3) was used in CEFLASH-4AS [ ] Figure 3.4-5 compares the resulting reactor vessel mixture level to the level obtained without [ ] As shown, the core uncovers at a later time when [ ] is used. The rate of core uncovery and maximum uncovery are about the same for the two cases. The reason for the difference in the time of core uncovery can be related to [

]

Bubbly Flow

In order to investigate the effects of different flow regimes, various models were put into CEFLASH-4AS for calculating the frictional pressure drop in the steam generator. For bubbly flow the model recommended in Reference 3.4-1 is:

$$f \simeq .02$$
$$\phi_f^2 = \frac{\rho_f}{\bar{\rho}} \qquad (3.4\text{-}4)$$

This model basically assumes that the fluid is homogeneous.

Figure 3.4-6 compares the reactor vessel level obtained using this model for the frictional pressure drop to the results using the Thom model. As shown, Thom's model results in earlier core uncovery but the same axial extent of core uncovery. The reason for this is that equation 3.4-4 results in slightly higher frictional pressure drop than predicted by Thom's model. This [ ] delays the time that the two-phase mixture in the reactor vessel falls below the hot leg.

Slug Flow.

For slug flow the frictional pressure drop model recommended in Reference 3.4-1 for the frictional pressure drop is:

$$f \simeq .02$$

$$\phi_f^2 = 1 + C.\alpha \left(\frac{4D}{L_b} - 1\right) \qquad (3.4\text{-}5)$$

where

C_1 = shape parameter for the bubble ($\sim$.9)
L_b = the length of the bubble ($\sim$2D)

Figure 3.4-7 compares the resulting reactor vessel mixture level to that obtained using the Thom model. As was the case for the bubbly flow model, Thom's model results in earlier core uncovery.

Annular Flow

For annular flow the model recommended in Reference 3.4-1 for the frictional pressure drop is:

$$f \simeq .02$$

$$\phi_f^2 = \left(\frac{\rho_f}{\rho}\right)^2 \qquad (3.4\text{-}6)$$

This model goes to the correct limit when the fluid in the path is completely liquid but it does not go to the correct limit when the path becomes entirely filled with steam. In order to model the transition from a low quality fluid to steam, equation 3.4-6 was modified as follows

$$\phi_f^2 = \left(\frac{\rho_f}{\rho}\right)^{2-\chi} \qquad (3.4\text{-}7)$$

where χ is the flow path quality. Equation (3.4-7) results in a large two-phase multiplier for low quality and goes to the proper limit when the flow path quality goes to unity.

Figure 3.4-8 compares to resulting reactor vessel mixture level to that obtained using the Thom correlation. As was the case for bubbly and slug flow, the Thom correlation results in earlier core uncovery. There is almost no difference in the maximum axial extent of core uncovery.

3.4.3 Summary and Conclusions for Question 4

The effects of assumed flow regimes in the steam generator[ ]and flow paths were investigated. The flow regimes investigated in the steam generator [ ]were heterogeneous and homogeneous. The flow regimes investigated in the steam generator flow paths were bubbly, slug, and annular. In addition, the effects of imposing[ ] were investigated.

All of the effects investigated had a negligible impact on the predicted two-phase mixture level in the core for a typical limiting small break LOCA. Although the differences were slight, the C-E evaluation model (the Thom correlation) resulted in the most core uncovery.

3.4.4 REFERENCES FOR SECTION 3.4

3.4-1 G. Wallis, "One Dimensional Two-Phase Flow", McGraw-Hill Book Company (1969).

3.4-2 [

]

3.4.4 NOMENCLATURE FOR QUESTION 4

A	Flow area
$\frac{d\bar{w}}{dt}$	Rate of change of mass flow rate
D	Hydraulic diameter
g	Gravitational acceleration
k_g	Geometric loss coefficient
k_{down}	Loss coefficient in liquid flow path
k_{up}	Loss coefficient in steam flow path
$(\overline{L/A})$	Average length to area ratio along flowpath
(L/D)	Ratio of length to hydraulic diameter
Re_f	Reynolds number based on liquid flow
$\bar{w}$	Average mass flow rate
w_f	Liquid mass flow rate
w_g	Steam mass flow rate
Z_1	Elevation difference between bottom of steam generator node and bottom of hot leg node
Z_{HL}	Height of liquid in hot leg
α	Void fraction
ΔP	Pressure drop
ΔZ	Elevation difference
$\bar{\rho}$	Average flow path density
ρ_f	Density of liquid
ρ_g	Density of steam
ρ_{SG}	Density of two-phase mixture in steam generator

Table 3.4-1

Analyses Performed for the Flow Regime Effect on Pressure Drop Study

Node Flow Regime	Path Flow Regime
Heterogeneous	Thom's two-phase multiplier
Homogeneous	Thom's two-phase multiplier
Heterogeneous	[ ]
Heterogeneous	Bubbly Flow
Heterogeneous	Slug Flow
Heterogeneous	Annular Flow

Figure 3.4-1

Steam Generator [ ] During Small Break LOCA

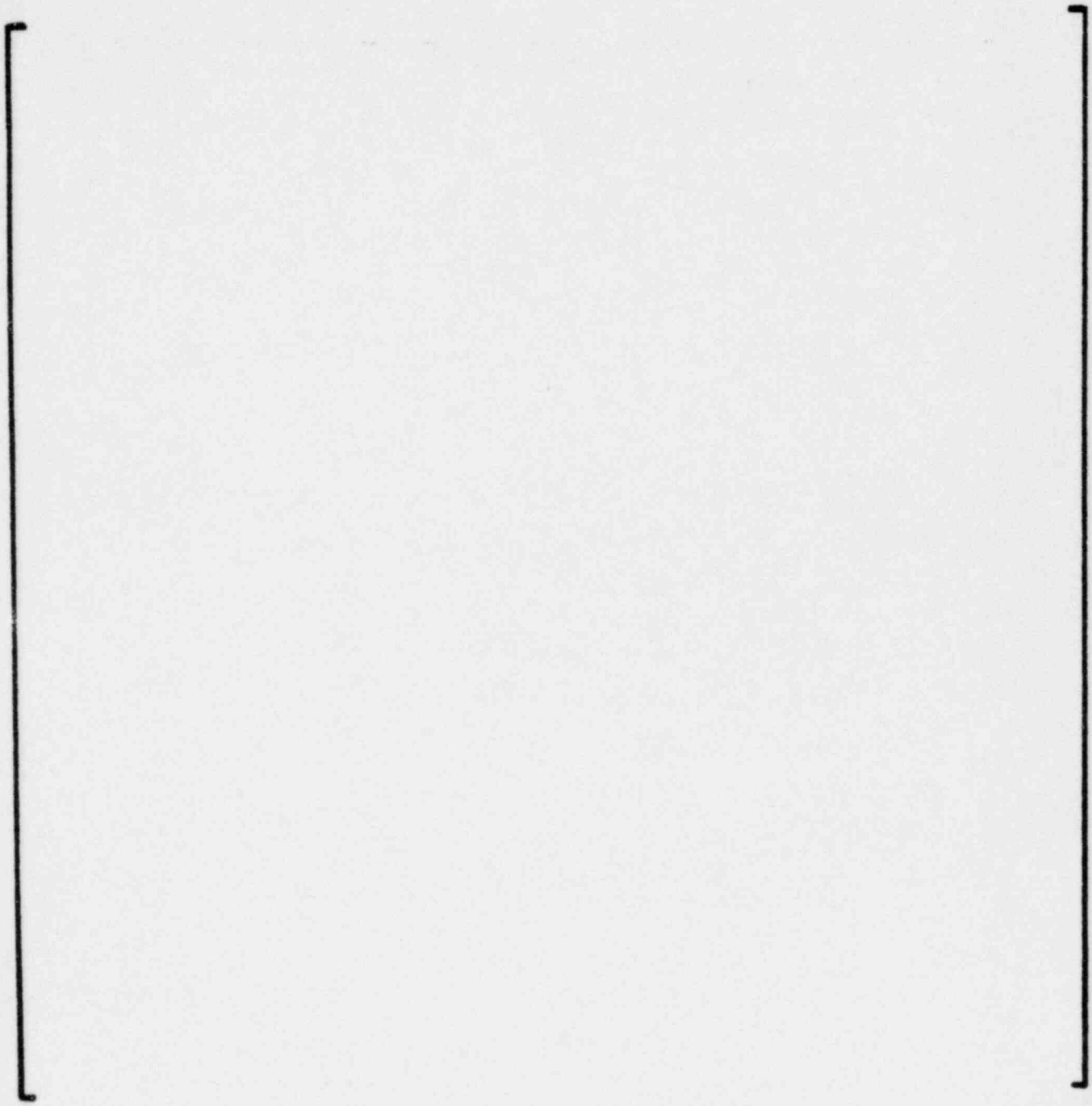

Figure 3.4-2

Fluid Distribution During Core Uncovery Phase

of Small Break LOCA

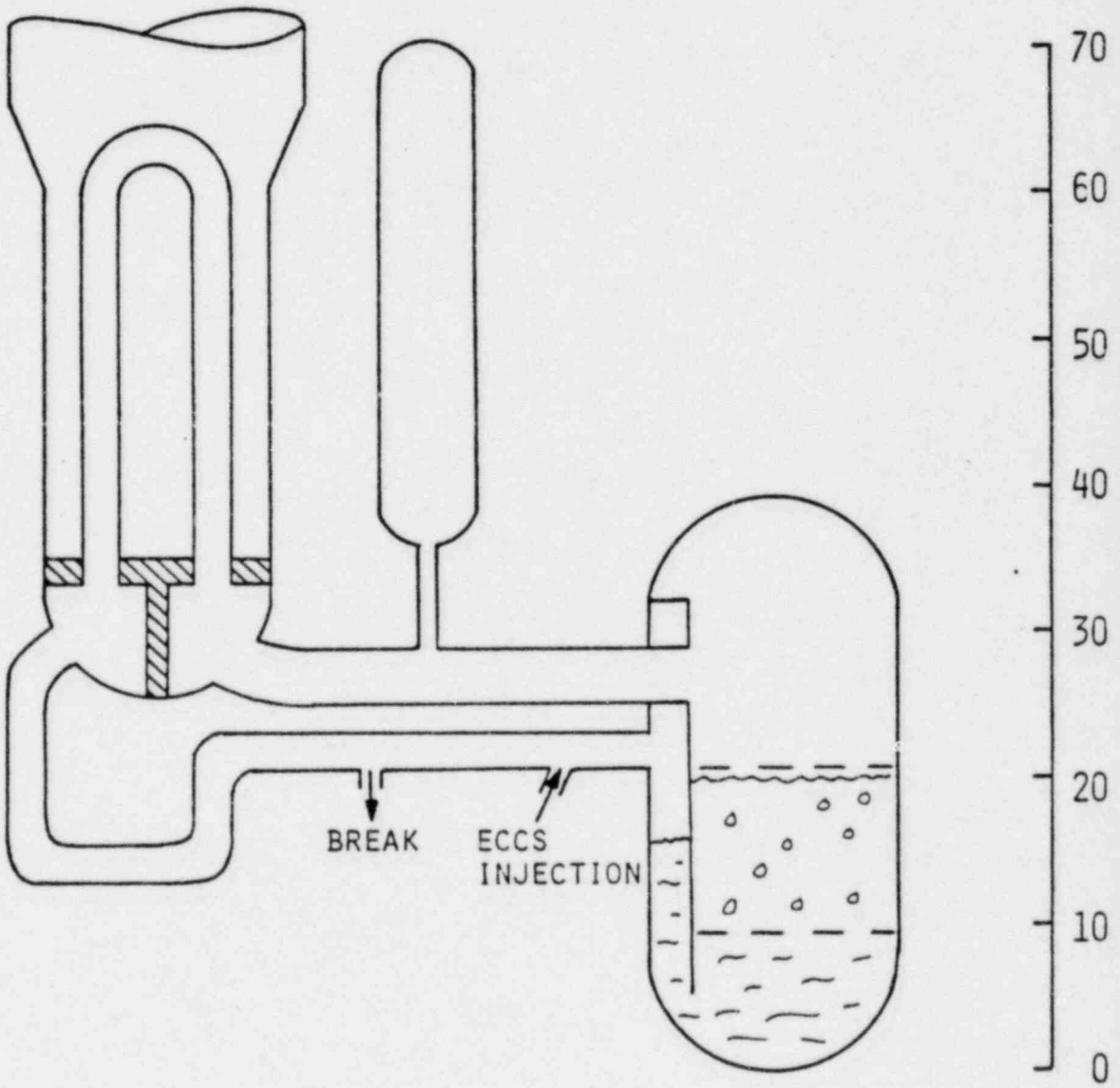

Figure 3.4-3

Core Mixture Level for Base Case

(0.1 FT^2 Break)

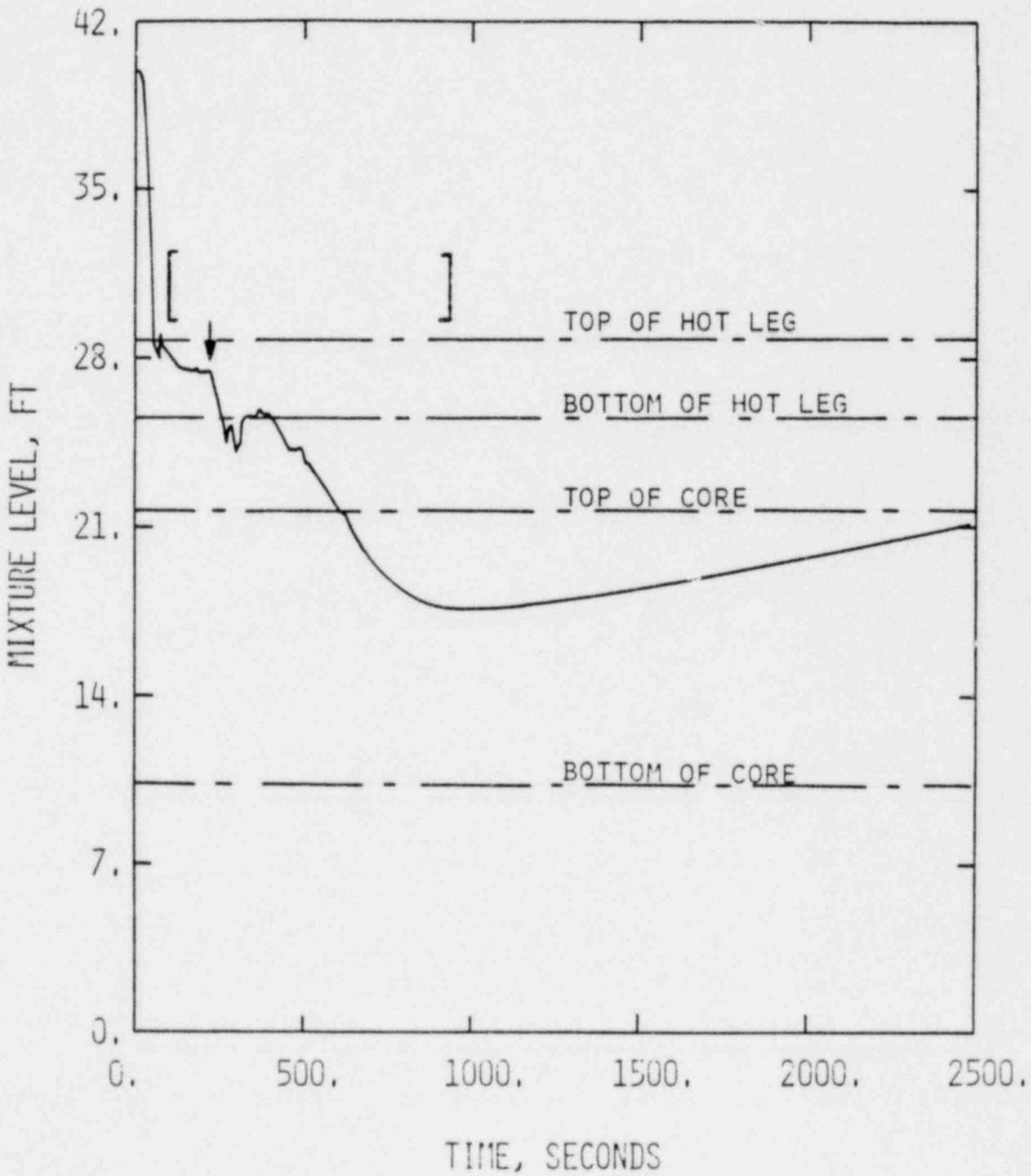

Figure 3.4-4

Effect of Modeling Steam Generator with

Homogeneous[ ]on Core Mixture Level

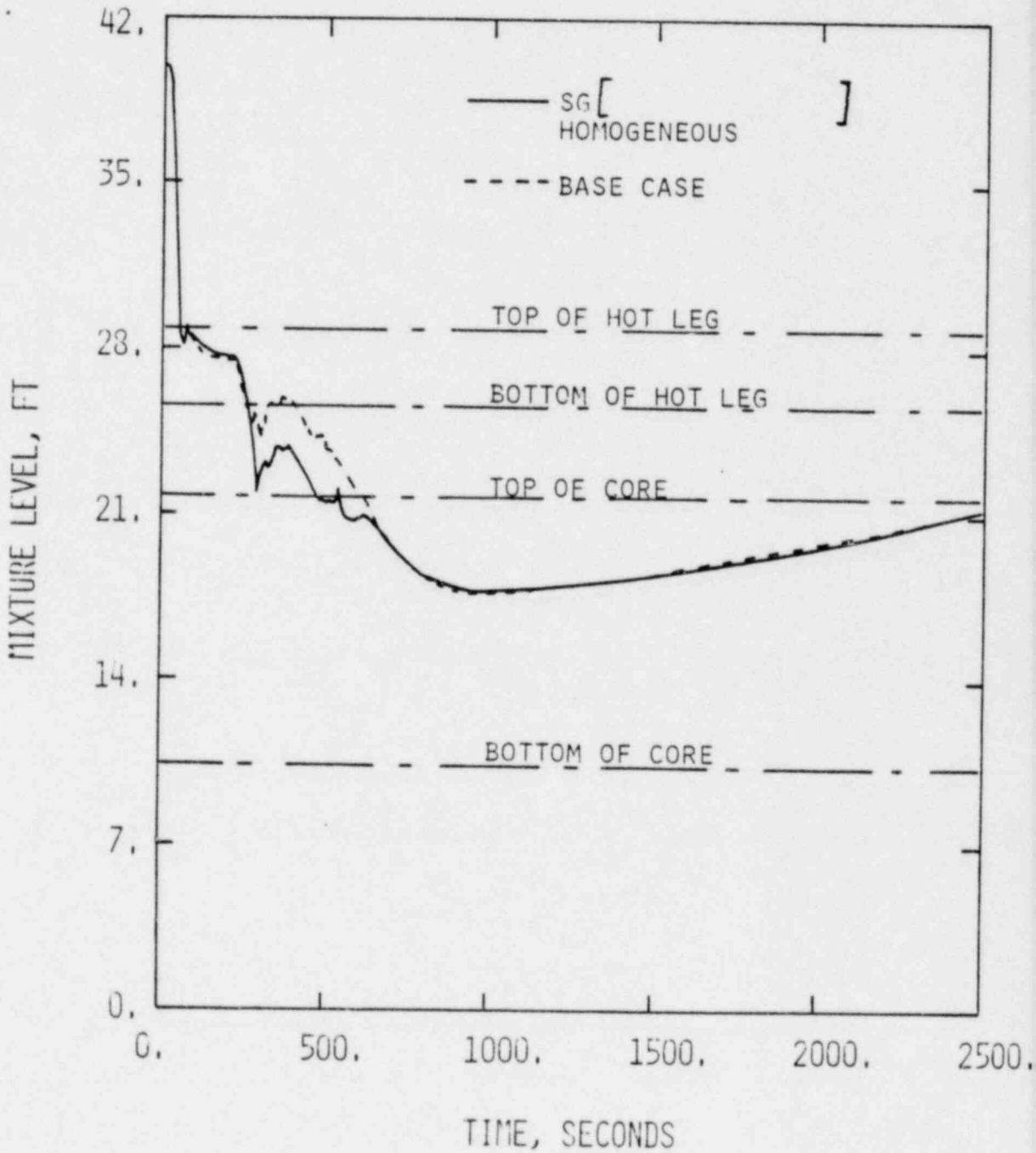

Figure 3.4-5

Effect of [ ] on Core Mixture Level

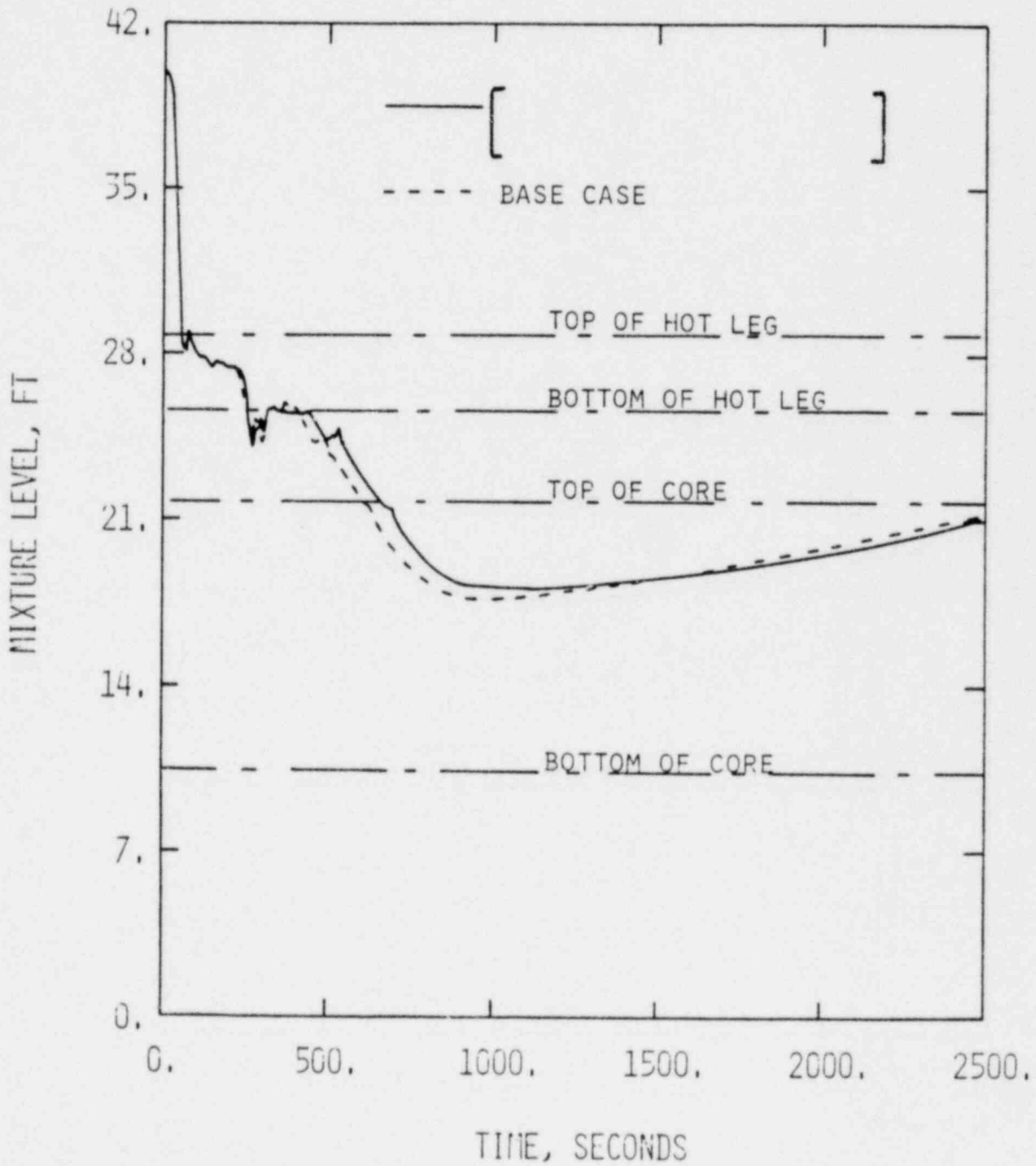

Figure 3.4-6

Effect of Modeling Bubbly Flow in

Steam Generator Flow Paths on Core Mixture Level

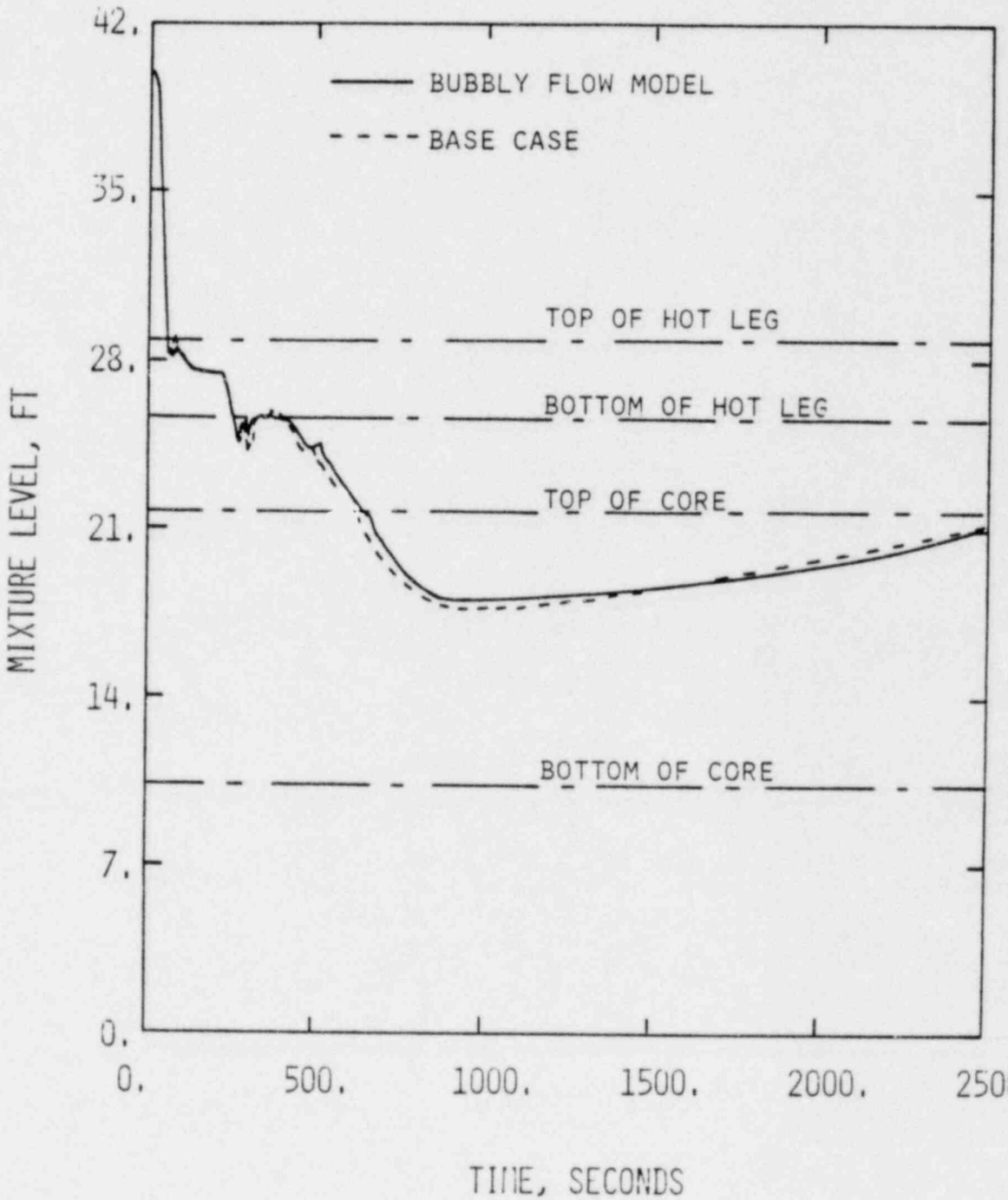

Figure 3.4-7

Effect of Modeling Slug Flow in

Steam Generator Flow Paths on Core Mixture Level

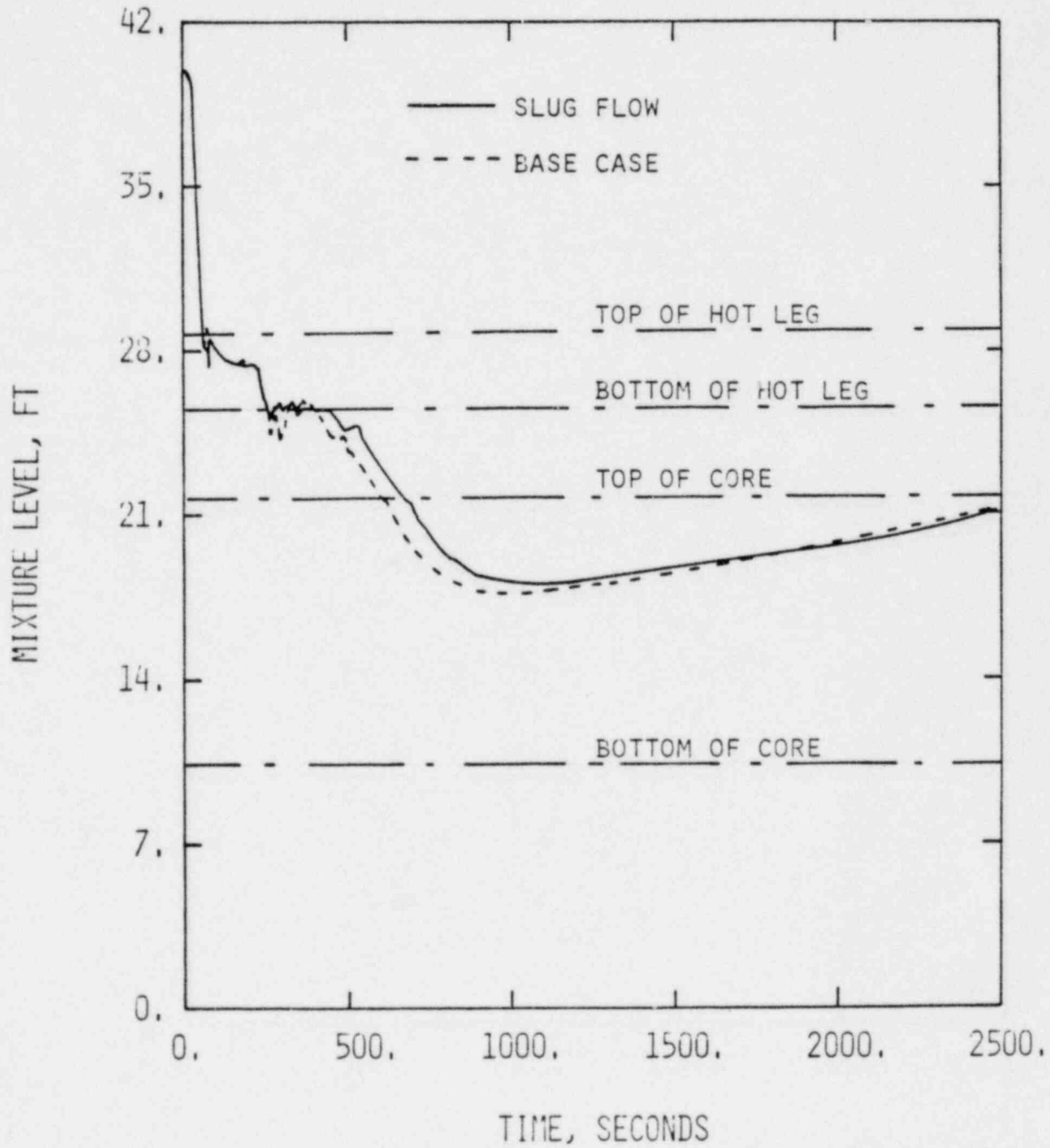

Figure 3.4-8

Effect of Modeling Annular Flow in Steam Generator Flow Paths on Core Mixture Level

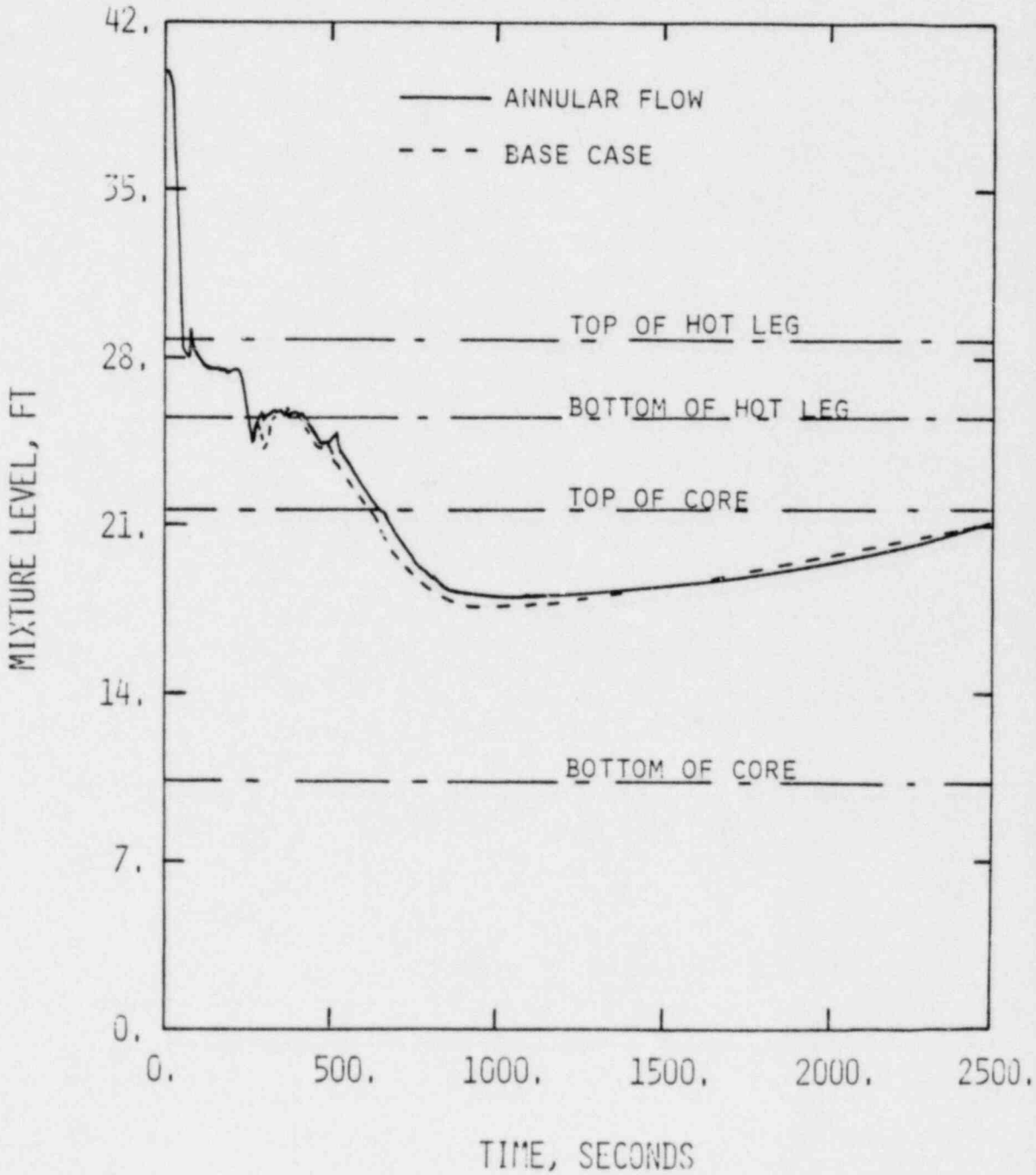

3.5 RESPONSE TO QUESTION 5 (CORE HEAT TRANSFER)

3.5.1 Statement of Question 5

The verification of the core heat transfer model to conditions encountered during small break transients must be documented. Of particular concern is the model used during partial core uncovery to determine the temperature of the uncovered cladding. The heat transfer model must be demonstrated to be conservative compared to applicable data, i.e., the ORNL Bundle Uncovery Tests.

3.5.2 Detailed Response to Question 5

The calculation of cladding temperature during the core uncovery phase of a small break LOCA depends strongly on two models. One of the models predicts the axial extent of the two-phase mixture region. The region above the two-phase mixture is cooled by the flow of steam generated in the two-phase region. Thus, the axial extent of the two-phase region should be conservatively predicted. The other model, used to calculate the cladding temperature, is the heat transfer coefficient model. The heat transfer model, used in the uncovered portion of the core, is particularly important because it is in this region that the cladding temperature can significantly exceed the saturation temperature.

The response to this question is divided into two parts. The first discusses the two-phase mixture swell model and the second discusses the heat transfer coefficient in the steam cooled region of the core.

Two-Phase Mixture Level

The level swell model determines the height of the two-phase mixture in the core during a small break LOCA. The height of the two-phase mixture determines both the steam flow rate available to cool the uncovered portion of the core and the axial extent of the uncovered portion of the core.

Level swell data has been obtained in rod bundle geometry from the Thermal Hydraulic Test Facility (THTF) at the Oak Ridge National Laboratory (ORNL). The ORNL level swell data, Reference 3.5-1, was used to evaluate C-E's level swell model.

The ORNL level swell results are presented in Table 3.5-1. Testing was conducted in the THTF, a 64 rod, high pressure, electrically heated test loop which was set up to produce conditions typical of the uncovered phase of a SBLOCA. The THTF rod bundle has uniform radial and axial power profiles and dimensions typical of nuclear fuel rods in 17 x 17 assemblies. The heater rods were instrumented with thermocouples at seven axial locations spaced ~2 ft apart. In addition, a low range differential pressure cell allowed measurement of the hydrostatic pressure drop across the test section.

Initial test conditions were established by pressurizing the system to the desired test pressure and setting the test section inlet flow to a predetermined value. Once initial conditions had been established, power was applied and the bundle was allowed to partially uncover. Eventually, the system would reach steady-state with the test section inlet flow equal to the boiloff rate and approximately 25% of the bundle uncovered. Steady state level swell data were acquired under these conditions.

Figure 3.5-1 shows the core uncovery phase of a SBLOCA. The region of interest is the two-phase region. In this region decay heat is removed from the rods by pool boiling. The height of the region depends on the amount of liquid present and the rate at which steam moves through the region. Heat transfer coefficients are quite large in this region and cladding temperatures are only a few degrees above the saturation temperature. The steam release rate from the surface of the region is approximately equal to the decay heat encompassed by the region divided by the enthalpy of vaporization.

The model for the relative motion between the phases used in CEFLASH-4AS is a drift velocity model. Drift velocity is defined in Reference 3.5-2 as the difference between the vapor phase velocity and the total volumetric flux.

$$V_D = u_g - (j_f + j_g) \qquad (3.5\text{-}1)$$

where

j_f = $u_f\ (1-\alpha)$
j_g = $u_g\ \alpha$
V_D = drift velocity
$u_{f,g}$ = actual liquid, vapor velocities
$j_{f,g}$ = superficial liquid, vapor velocities
α = vapor void fraction (volume vapor/volume mixture)

The drift velocity model used in CEFLASH-4AS (Reference 3.5-3) is independent of void fraction and varies only with pressure, as shown below.

$$\left[\qquad\qquad\right] \qquad (3.5\text{-}2)$$

where

V_D has units of ft/sec
P is the pressure in psia

The C-E model was evaluated by using it to predict the mixture level observed experimentally in the following way. The two phase mixture length ($L_{2\phi}$) can be found from the collapsed liquid length (L_c) and the average void fraction using the following relationship

$$L_{2\phi} = L_c/(1-\bar{\alpha}) \qquad (3.5\text{-}3)$$

The average void fraction can be computed by integrating along the boiling length as shown below

$$\bar{\alpha} = \frac{1}{L_{2\phi}} \int_0^{L_{2\phi}} \alpha \, d \, Z \qquad (3.5\text{-}4)$$

The local void fraction can be computed from the local volumetric flux (j_g) and the drift velocity (V_D) using equation (3.5-1)

$$\alpha = \frac{j_g}{V_D + (j_g + j_f)} \qquad (3.5\text{-}5)$$

Since the THTF has a uniform power profile in the axial and radial directions, the volumetric flux increases linearly from zero to a maximum value at the surface of the two-phase mixture. The surface volumetric steam flux is listed in Table 3.5-1.

$$j_g = j_g^s \, Z/L_{2\phi}$$

$$j_f \simeq 0$$

where

j_g^s = volumetric vapor flux at surface of the two-phase mixture

When the integration is carried out, the expression for the average void fraction is

$$\bar{\alpha}_{CE} = 1 - \frac{V_D}{j_g^s} \ln \left(1 + \frac{j_g^s}{V_D}\right) \qquad (3.5\text{-}6)$$

Figure 3.5-2 compares the results of this calculation to the data. Note that the C-E model underpredicts the two-phase level. This will result in a higher predicted cladding temperature than a model derived from the ORNL data.

Steam Heat Transfer Coefficient

During the core uncovery phase of a SBLOCA, the region above the two-phase mixture is filled with steam. The steam flow is given by its release rate from the two-phase surface below. Entrainment of liquid droplets into the steam region from the mixture below is not a significant core cooling mechanism, since in transients of interest (core uncovery and high cladding temperatures) the steam velocity does not exceed the entrainment velocity.

Cooling of the core in the uncovered region is accomplished by high pressure steam through the following two heat transfer mechanisms:

-- Forced convection to superheated steam.

-- Radiation to superheated steam and to colder metal surfaces.

The total heat flux at the outer surface of the fuel rod is, therefore,

$$q''_{tot} = h_{tot} (T_w - T_v) \qquad (3.5\text{-}7)$$

where

$$h_{tot} = h_{conv} + h_{rad} \qquad (3.5\text{-}8)$$

is the overall steam cooling heat transfer coefficient with convection and radiation components.

This response concerns the modeling methods that are used for core heat transfer in the steam region and their comparison to experimental data. The

forced convection model for h_{conv} and the radiation model for h_{rad} are discussed separately. The models' combined effects on calculated transients are then presented and compared to similar calculations using the C-E model.

Forced Convection

It is useful to first describe the model presently used at C-E in licensing calculations as well as other methods that are recognized as generally useful in correlating convective heat transfer data.

The C-E model (Reference 3.5-4) recognizes three heat transfer regimes in the steam region. For turbulent flow, the Dittus-Boelter correlation is used to evaluate the convective heat transfer coefficient,

$$h_{conv} = 0.023 \frac{k_v}{D} Re_v^{0.8} Pr_v^{0.4}, \quad Re_v > Re_v^{(T)} \tag{3.5-9}$$

where

$$Re_v = \frac{W_s D}{\mu_v A}. \tag{3.5-10}$$

The subscripts "v" indicate that all steam properties are evaluated at the bulk vapor temperature. In the laminar steam flow regime, the Sieder-Tate correlation is used,

$$h_{conv} = 1.86 \frac{k_v}{D} Re_v Pr_v \left(\frac{D}{L-\ell_{2\phi}}\right)^{1/3} \left(\frac{\mu_v}{\mu_w}\right)^{0.14}, \tag{3.5-11}$$

$$Re_v \leq Re_v^{(L)}.$$

Here again all steam properties are evaluated at the bulk vapor temperature, except for μ_w which is evaluated at the temperature of the clad surface. In the laminar-to-turbulent flow transition regime, the C-E model evaluates

the heat transfer coefficient by interpolating between equations (3.5-9) and (3.5-11),[

]

$$Nu_v = \frac{h_{conv} D}{k_v} .$$

The bounding transition flow Reynolds numbers are

$$Re_v^{(L)} = [\quad]$$
$$Re_v^{(T)} = [\quad] \qquad (3.5\text{-}12)$$

For heat transfer to steam with significant radial variations of fluid properties (temperature), there are generally two methods recognized in the literature as being useful in correlating convection data (Reference 3.5-5).

The first is the temperature ratio method, in which the correlations take the form,

$$(Nu)_{\substack{\text{radially}\\\text{varying}\\\text{properties}}} = (Nu)_{\substack{\text{radially}\\\text{uniform}\\\text{properties}}} \left(\frac{T_v}{a_1 T_v + a_2 T_w}\right)^{a_3} \qquad (3.5\text{-}13)$$

A particular, well-known temperature ratio correlation is the McEligot correlation,

$$h_{conv} = 0.021 \frac{k_v}{D} Re_v^{0.8} Pr_v^{0.4} \left(\frac{T_v}{T_w}\right)^{0.5} \qquad (3.5\text{-}14)$$

The second method for correlating convection heat transfer data with radially varying properties is the reference temperature method. In this method, the heat transfer coefficient is evaluated from a standard constant-property correlation, with the fluid properties evaluated at some reference temperature,

$$T_r = a_1 T_v + a_2 T_w \qquad (3.5\text{-}15)$$

which generally falls between the sink (bulk vapor temperature, T_v, and the source (rod) temperature, T_w. In this manner, a source temperature dependence is introduced for the fluid properties, accounting for the fact that the resistance to heat transfer in turbulent flow occurs primarily near the surface of the source.

Thus, the Dittus-Boelter correlation with the reference temperature method is

$$h_{conv} = 0.023 \frac{k_r}{D} Re_r^{0.8} Pr_r^{0.4} \qquad (3.5\text{-}16)$$

with C-E applying equation (3.5-16) with $T_r = T_v$ for turbulent flows.

Experimental heat transfer coefficients which were recently obtained at ORNL shed new light on the applicability of turbulent flow heat transfer correlations in variable-property ($T_w/T_v > 1.2$) cases (Reference 3.5-6). The test facility is a 64-rod, high pressure, electrically heated test loop designed to simulate conditions that are expected in typical SBLOCAs. For this test series,

Maximum $T_w > 2260^{o}F$
$3500 \leq Re_v \leq 10{,}000$
$380 \leq p \leq 1030$ psia
$8560 \leq$ surface heat flux $\leq 14{,}900$ Btu/ft^2-hr
$1.21 < T_w/T_v < 1.63$

Transition from the turbulent into the laminar flow regime was not observed to occur in the range of bulk vapor Reynolds numbers tested. Based on this

observation, the transition range assumed at C-E, equation (3.5-12), appears very conservative.

The convective test data indicates that the Dittus-Boelter correlation, equation (Reference 3.5-9), with steam properties evaluated at the bulk vapor temperature significantly overpredicts the heat transfer coefficient for rod-to-steam temperature ratios $T_w/T_v \geq 1.25$. This is shown in Figure 3.5-3 as a logarithmic plot of $Nu/Re_v^{0.8} Pr_v^{0.4}$ versus the temperature ratio T_w/T_v. The Reynolds number monotonically increases with the temperature ratio. Figure 3.5-3 clearly shows an increasing overprediction with increasing temperature ratio as the radial variations of fluid properties become increasingly important.

A similar trend of overprediction is observed for the reference-temperature form of the Dittus-Boelter correlation, equations (3.5-15) and (3.5-16), with $a_1 = a_2 = \frac{1}{2}$. The McEligot correlation, equation (3.5-14), provides a substantially improved correlation, but still overpredicts the high temperature ratio data.

A reference temperature correlation in which the fluid properties are evaluated at the rod surface temperature, $T_r = T_w$,

$$h_{conv} = 0.021 \frac{k_w}{D} Re_w^{0.8} Pr_w^{0.4} \qquad (3.5\text{-}17)$$

does provide a good match with the test data, as shown in Figure 3.5-4. Equation (3.5-17) is therefore representative of the ORNL data in the Reynolds number and temperature ratio ranges of the experiments.

In light of this new information, equation (3.5-17) has been implemented in the PARCH code, as a user option, for calculating the convective coefficient for heat transfer to steam in the turbulent flow regime. The Reynolds number evaluated at the clad surface temperature is calculated as

$$Re_w = \frac{W_s D}{\mu_w A} \cdot \frac{\rho_w}{\rho_v} \qquad (3.5\text{-}18)$$

Comparing this with equation (3.5-9), we find that

$$\frac{Re_w}{Re_v} = \frac{\nu_v}{\nu_w} .$$

Since the kinematic viscosity (ν) increases and the Prandtl number decreases as the temperature goes up, the revised convection correlation, equation (3.5-17), yields considerably lower heat transfer coefficients than equation (3.5-9).

Radiation

The second mode of core cooling in the uncovered portion of the core is thermal radiation from the rods to high-pressure, superheated steam and to the colder metal structures. The C-E licensing model does not account for core cooling by radiation*.

ORNL's analysis of the THTF heat transfer data shows that, under conditions typical of some SBLOCAs, thermal radiation accounts for 22 to 37% of the total heat transfer from uncovered fuel rods to their surroundings. Of that, radiation to colder metal structures accounts for 3.5 to 6.2% of the total heat transfer.

In order to assess the C-E heat transfer model, a rod-to-steam radiation model was incorporated into PARCH as a user option.

A radiation heat transfer coefficient is defined as the ratio of radiant heat flux to the rod-to-steam temperature difference,

$$h_{rad} = \frac{E\sigma\,(T_w^4 - T_v^4)}{T_w - T_v} \qquad (3.5\text{-}19)$$

$$= E\sigma\,(T_w+T_v)\,(T_w^2+T_v^2)$$

*PARCH does have a radiation model for calculating radial heat transfer across the gap in the fuel rod.

where the exchange coefficient, E, is given by

$$E = \frac{1}{\varepsilon_w^{-1} + \varepsilon_v^{-1} - 1} \qquad (3.5\text{-}20)$$

The emissivity of the outer surface of the zircaloy cladding, ε_w, is given empirically as a parabolic function of temperature (Reference 3.5-7).

The emissivity of high-pressure steam, ε_v, varies with the pressure and temperature of the vapor and was calculated by the Hottel empirical method (3.5-8) using the high pressure emissivity corrections of Ferriso (3.5-9).

Results

A series of runs was executed with the PARCH code, using the ORNL recommended core-to-steam heat transfer calculation. The purpose was to compare results using the ORNL model to existing results obtained using the C-E model.

Figure 3.5-5 and Table 3.5-2 present the peak cladding temperatures (PCTs) for a spectrum of cold leg breaks in the reactor coolant pump discharge leg of a typical C-E designed NSSS. The break sizes analyzed are 0.05, 0.1, 0.2 and 0.5 ft^2. PARCH input deck setups for these cases are based on an existing ECCS performance study that used the C-E Evaluation Model. The inputs of the earlier and present studies differ only in the code version and in the use of three input options that control the three components (radiation, convection and transition) of the best-estimate model.

The reasons for the differences in predicted peak clad temperature are as follows. The limiting break size is predicted by LOCA analysis models currently used at C-E, as a direct outgrowth of the relationship between system dynamics and the hydraulic behavior of the primary coolant system and ECCS. A LOCA transient that has severe hydraulics (delayed SIT injection and prolonged core uncovery) is allowed to become thermally severe (high fuel rod temperatures) by the conservative nature of the core heat transfer model. By ignoring radiation to steam, the heat transfer model under-calculates the core cooling ability of steam, and becomes more conservative at higher temperatures. This magnifies the influence of system hydraulics, which are a function of break size, by treating the hydraulically severe transients more conservatively than the less severe transients.

In the ORNL heat transfer model, steam is a better heat sink. In particular, radiation to steam becomes more effective as the temperature increases, thereby damping out the effects of system hydraulics. Therefore, in the ORNL analyses considered here, the PCT for the limiting break size is reduced more than the PCT for non-limiting breaks.

Figure 3.5-6 shows the clad surface and coolant temperatures along the length of the rod, for the 0.1 ft^2 break, at the time the PCT occurs. Also shown are the convective and total heat transfer coefficients, h_{conv} and h_{tot}, in the steam region. Corresponding curves from the C-E heat transfer model are shown in broken lines. Also indicated are the steam flow regimes for the ORNL model. (For the C-E model the steam flow is transitional throughout because of the higher transition point Reynolds number.) Due to improved rod-to-steam heat transfer, the ORNL model shows a slightly higher steam temperature and a considerably lower cladding temperature. It also exhibits a shift of the PCT location from the peak power location to the top of the rod.

The same information is shown in Figure 3.5-7 for the 0.5 ft^2 break. Here, too, the C-E model predicts transitional steam flow throughout. Since the two-phase level is depressed in this case, the steam flow rate is lower than it was for the 0.1 ft^2 break. This causes the ORNL model to show a considerable increase in steam temperature relative to the C-E model. Therefore, despite its higher heat transfer coefficient, the ORNL model predicts only a slight improvement in the rod-cooling ability of the steam. The PCT, therefore, remains at the peak power location.

3.5.3 Summary and Conclusions For Question 5

Two-Phase Mixture Level

Level swell data has been recently obtained in rod bundle geometry from the Thermal Hydraulic Test Facility (THTF) at the Oak Ridge National Laboratory (ORNL). A comparison of the C-E level swell model to the ORNL data led to the following conclusion.

-- The C-E model predicts a lower mixture level than any of the ORNL data. Modification of the C-E model to be more representative of the ORNL data would result in higher predicted two-phase mixture levels than are currently predicted. This would increase the steam flow rate available to cool the uncovered portion of the core and reduce the steam temperature at the hot spot. The combined effects would result in lower predicted clad temperatures.

Steam Heat Transfer Coefficient

Heat transfer data was recently obtained by ORNL with the THTF. The data, obtained in high pressure bundle uncovery tests under conditions typical of small breaks, led to the following conclusions regarding the C-E heat transfer model.

-- Rod-to-steam thermal radiation, which is not accounted for in PARCH, is an important core cooling mechanism. Radiation accounts for 22-37% of the total heat transfer to steam.

-- Steam flow through the rod bundle remains turbulent for Reynolds numbers as low as 3,500. This contrasts with the [ ] transition flow regime that is normally used in C-E analyses.

-- In severe, high-temperature transients, radiation is an important cooling mechanism, and the C-E model is therefore very conservative.

-- In the less severe, lower-temperature transients, radiation becomes less important relative to convection. The C-E model is more accurate in predicting cladding temperatures in these cases, but always stays on the conservative side.

3.5.4 References for Question 5

3.5-1 T. Anklam, "Two-Phase Mixture Level Swell For Water and Steam Under High Pressure, Low Heat Flux Conditions In Rod Bundles", To be published.

3.5-2 G. Wallis, "One Dimensional Two-Phase Flow", McGraw-Hill Book Company (1969).

3.5-3 "CEFLASH-4AS A Computer Program for Reactor Blowdown Analysis of the Small Break Loss of Coolant Accident", CENPD-133, Supplement 3-P, January, 1977 (Proprietary).

3.5-4 "PARCH, A FORTRAN-IV Digital Program to Evaluate Pool Boiling, Axial Rod and Coolant Heatup", C-E Report, CENPD-138, August 1974 (Proprietary).

Supplement 1, February 1975 (Proprietary).

Supplement 2, January 1977 (Proprietary).

3.5-5 T. M. Anklam, "ORNL Small Break LOCA Heat Transfer Tests", handouts to NRC.

3.5-6 T. M. Anklam, "Low Flow, High Pressure, Forced Convection and Radiation to Steam in Rod Bundle Geometry", to be published.

3.5-7 "High Temperature Properties of Zircaloy and UO_2 for Use in LOCA Evaluation Models", C-E Report, CENPD-136, July 1974.

3.5-8 H. C. Hottel and A. F. Sarofim, "Radiative Transfer", McGraw Hill Book Co., 1967.

3.5-9 C. C. Ferriso, C. B. Ludwig and F. P. Boynton, "Total Emissivity of Hot Water Vapor - I. High Pressure Limit", Int. J. Heat & Mass Transfer, Vol. 9, 1966.

3.5.5 Nomenclature For Question 5

Two Phase Mixture Level

j_f, j_g	Superficial velocity of liquid, vapor
L	Length
P	Static pressure
u_f, u_g	Velocity of liquid, vapor
V_D	Drift velocity
Z	Distance measured from the top of subcooled region
$\alpha, \bar{\alpha}$	Local, average void fraction

Subscripts

c	Collapsed liquid
f	Liquid
g	Vapor
2ϕ	Two-phase

Steam Heat Transfer Coefficient

A	Coolant channel area
a_1, a_2, a_3	Constants in temperature ratio and reference temperature correlations
C_p	Specific heat at constant pressure
D	Hydraulic diameter
E	Radiant heat exchange coefficient, equation (13)
h_{conv}	Convective heat transfer coefficient
h_{rad}	Radiant heat transfer coefficient, equation (12)
h_{tot}	Overall steam cooling heat transfer coefficient
k	Thermal conductivity
L	Length of fuel rod
$\ell_{2\phi}$	Height of two-phase mixture above bottom of core
Nu	Nusselt number, h_{conv} D/k

Pr	Prandtl number, $C_p \mu/k$
q"	Surface heat transfer rate per unit area
Re	Reynolds number, $W_s D/\mu A$
$Re_v^{(L)}$, $Re_v^{(T)}$	Transition point Reynolds numbers at the laminar and turbulent endpoints of the transitional regime
T	Temperature; T_v, vapor temperature; T_w, clad surface temperature; T_r, reference temperature
W_s	Steam mass flow rate
ε	Emissivity; ε_v, vapor emissivity; ε_w, clad surface emissivity
μ	Absolute viscosity
ν	Kinematic viscosity
ρ	Density
σ	Stefan-Boltzmann constant = 0.1714×10^{-8} Btu/hr-ft^2-$^oR^4$

Subscripts

r	Quantity evaluated at reference temperature, T_r
v	Quantity evaluated at bulk vapor temperature, T_v
w	Quantity evaluated at clad surface temperature, T_w

TABLE 3.5-1

THTF LEVEL SWELL DATA

Linear Power/Rod (kw/ft)	Pressure (psia)	Volumetric Vapor Flux (ft/sec)	Mixture Level* (ft)	Collapsed* Liquid Level (ft)	Average Void Fraction
.357	419	3.38	8.63	4.30	.502
.250	613	1.57	7.38	4.99	.324
.411	618	2.73	8.01	4.30	.465
.268	1018	.87	7.58	5.81	.237
.378	1009	1.39	6.99	4.79	.315
.421	387	3.76	7.28	3.41	.531

*Mixture level and collapsed level are measured relative to the top of the subcooled region.

TABLE 3.5-2

FUEL ROD PERFORMANCE - BREAK SIZE SPECTRUM STUDY

	C-E MODEL			ORNL HEAT TRANS. MODEL		
Break Size (ft^2)	PCT (^oF)	Hot Spot Elevation (% Core Height)	Peak Zirconium Oxidation (%)	PCT (^oF)	Hot Spot Elevation (% Core Height)	Peak Zirconium Oxidation (%)
0.05	1824	85	6.2	1468	100	0.58
0.1	1970	85	10.1	1576	100	0.85
0.2	1609	90	0.41	1478	90	0.21
0.5	1622	85	0.28	1582	85	0.23

Figure 3.5-1

Schematic of Nuclear Reactor Subchannel

During Uncovered Phase of SBLOCA

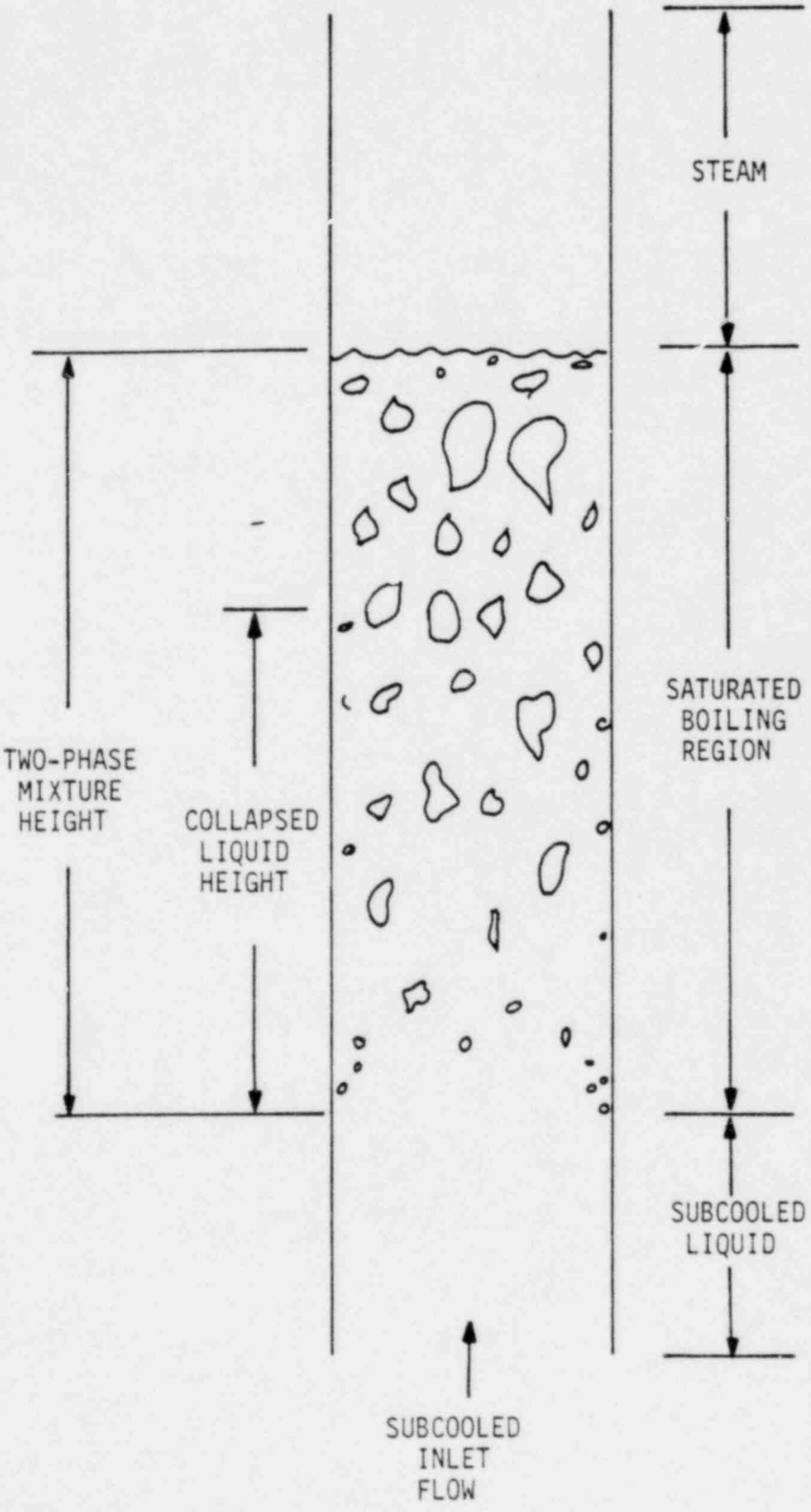

Figure 3.5-2

Comparison of the C-E Predictions

to the ORNL Level Swell Data

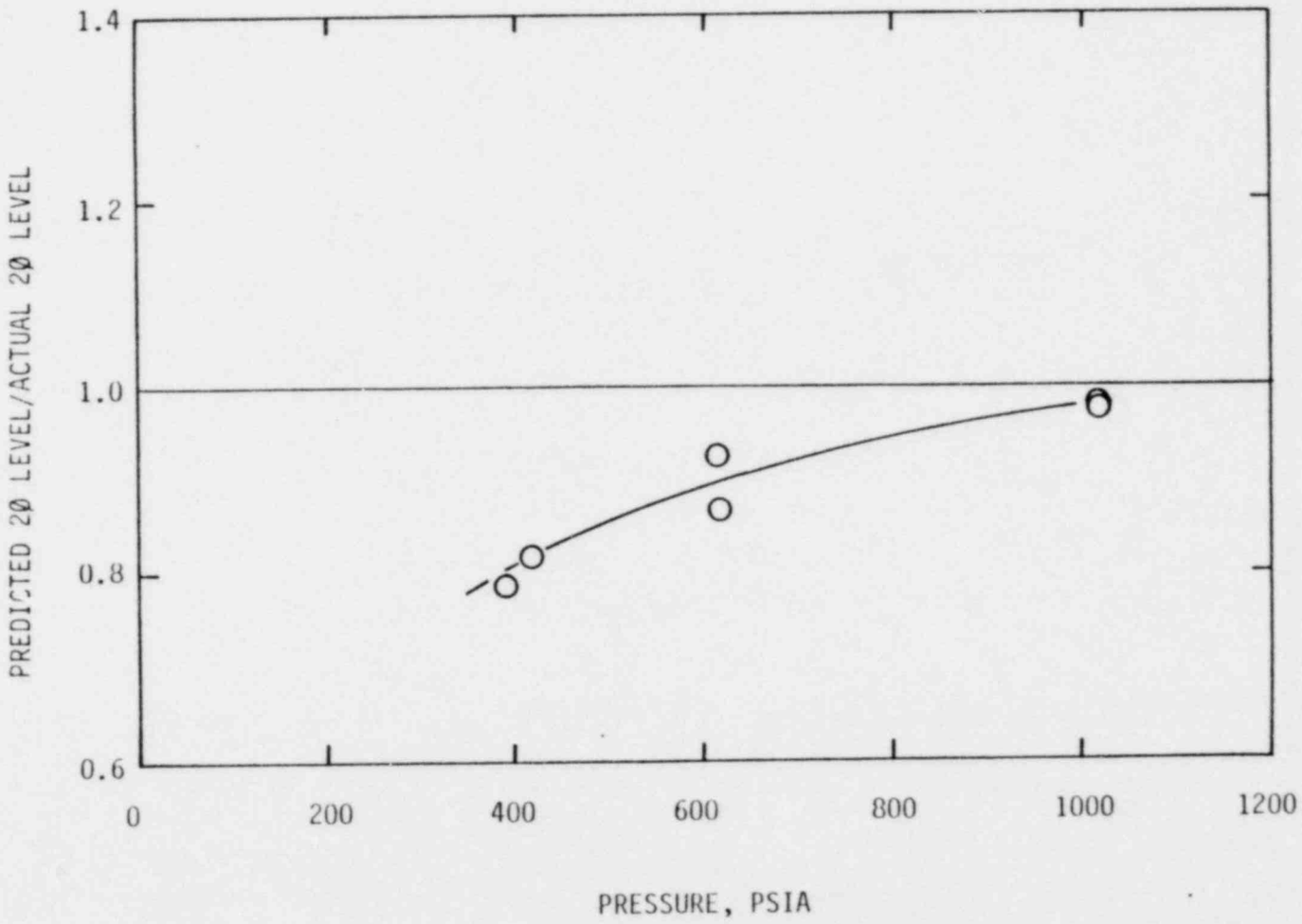

Figure 3.5-3

Comparison of Dittus-Boelter Correlation, Equation (3.5-9)

to ORNL Data (3.5-6)

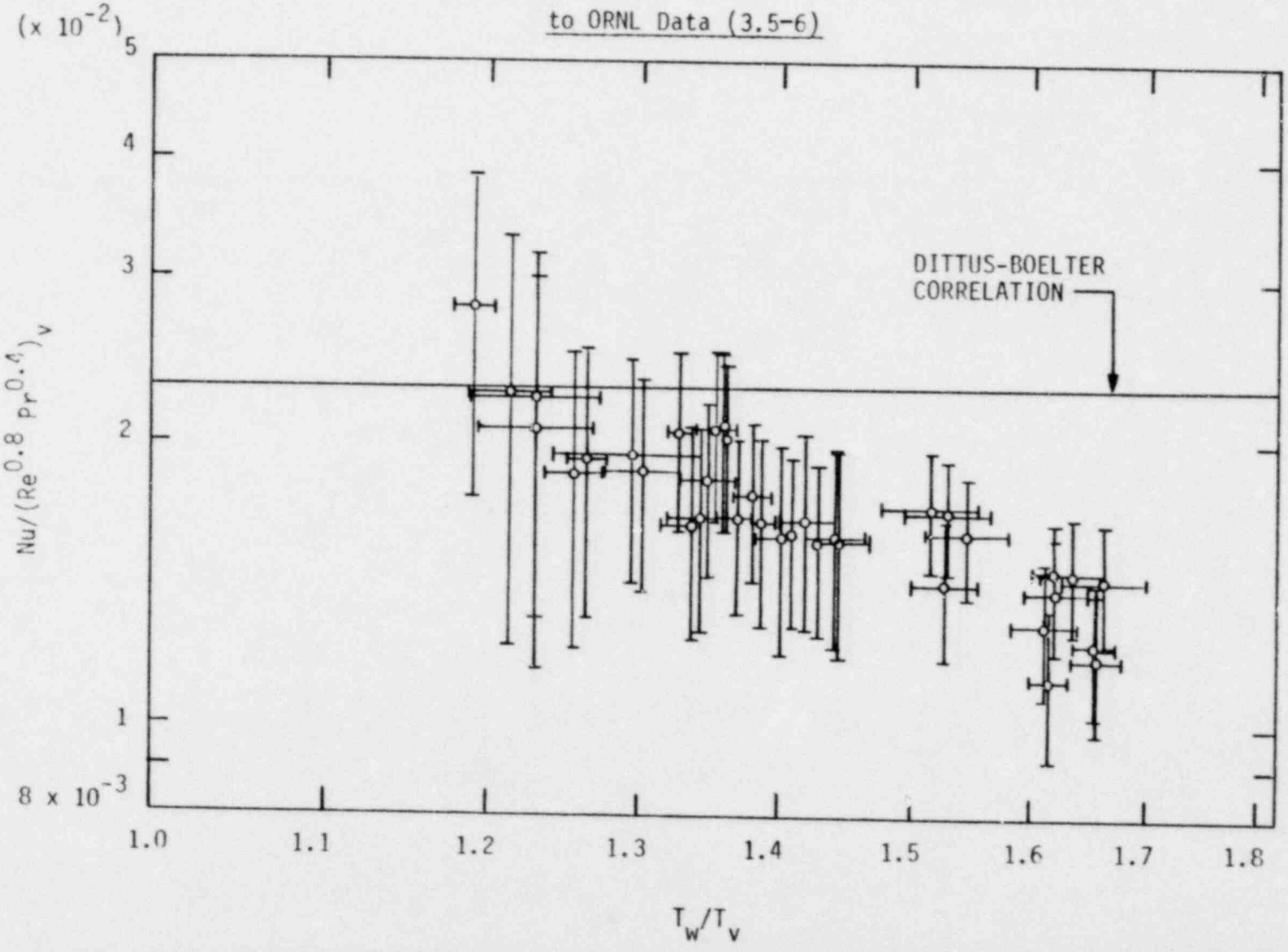

Figure 3.5-4

Comparison of Reference Temperature Dittus-Boelter Correlation, Equation (3.5-17), to ORNL Data (3.5-6)

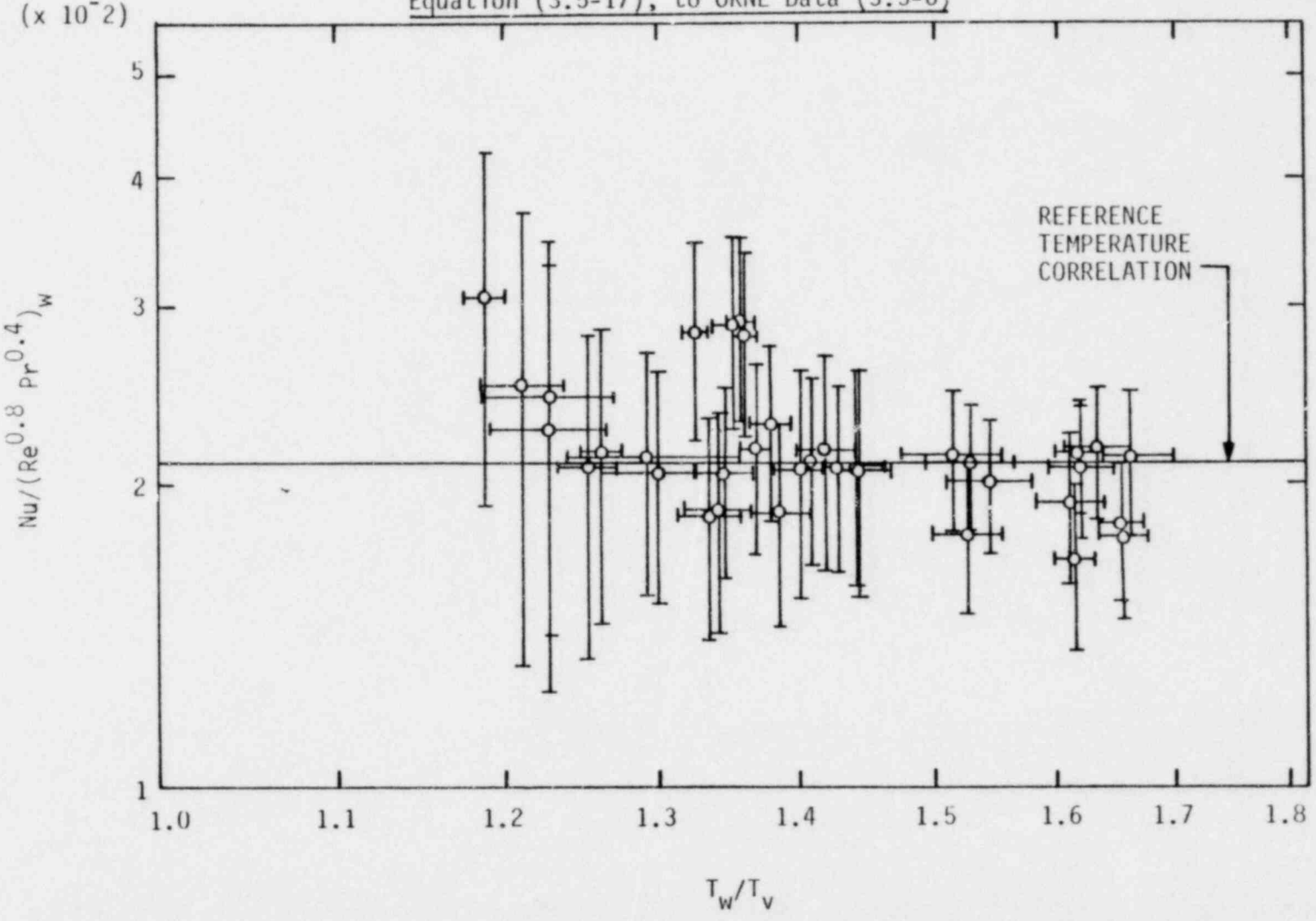

Figure 3.5-5

Peak Clad Temperature Vs. Break Size

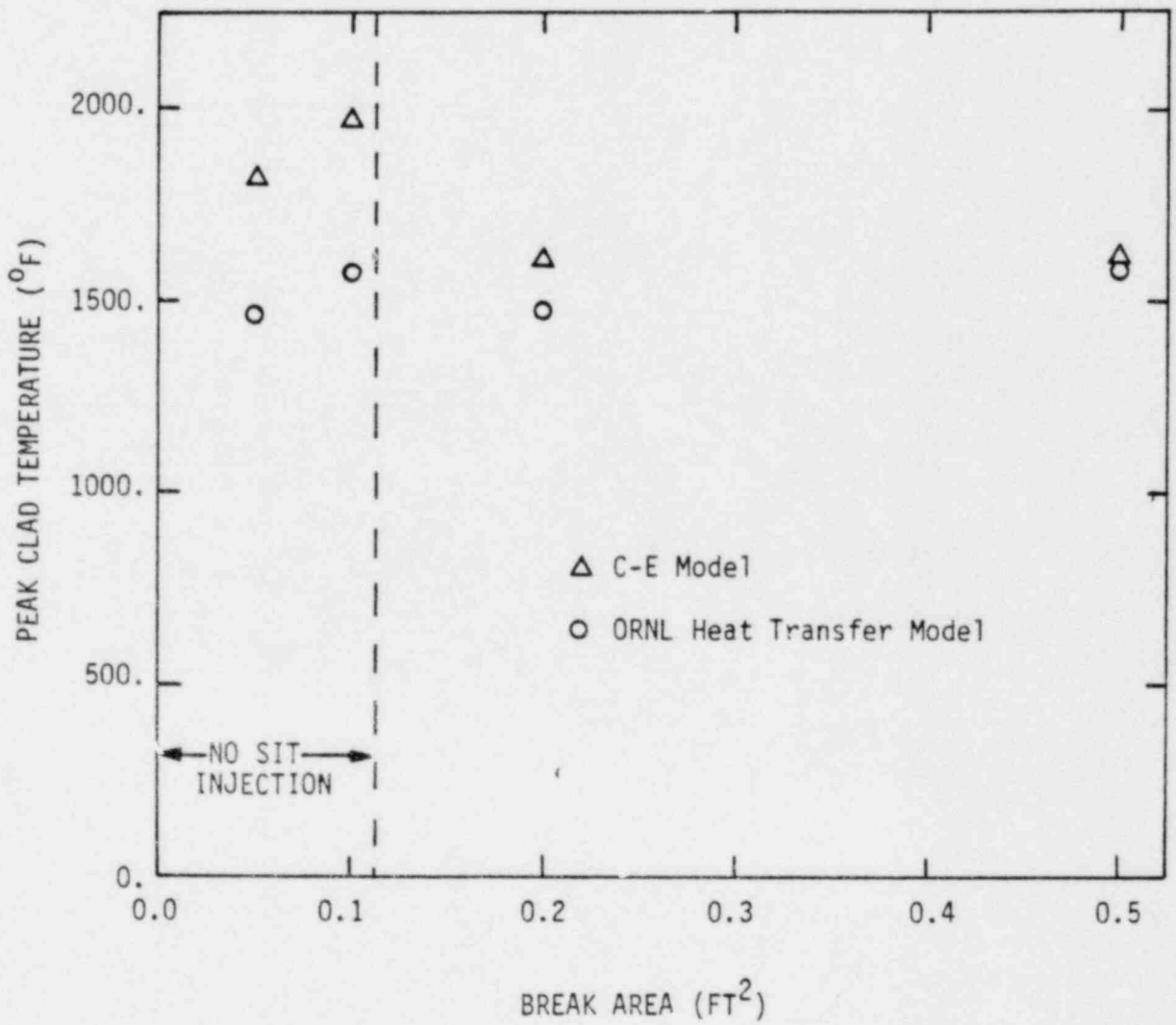

Figure 3.5-6

Clad and Coolant Temperatures and Heat Transfer Coefficients Vs. Axial Location, at the Instant PCT Occurs, for the 0.1 ft^2 Break

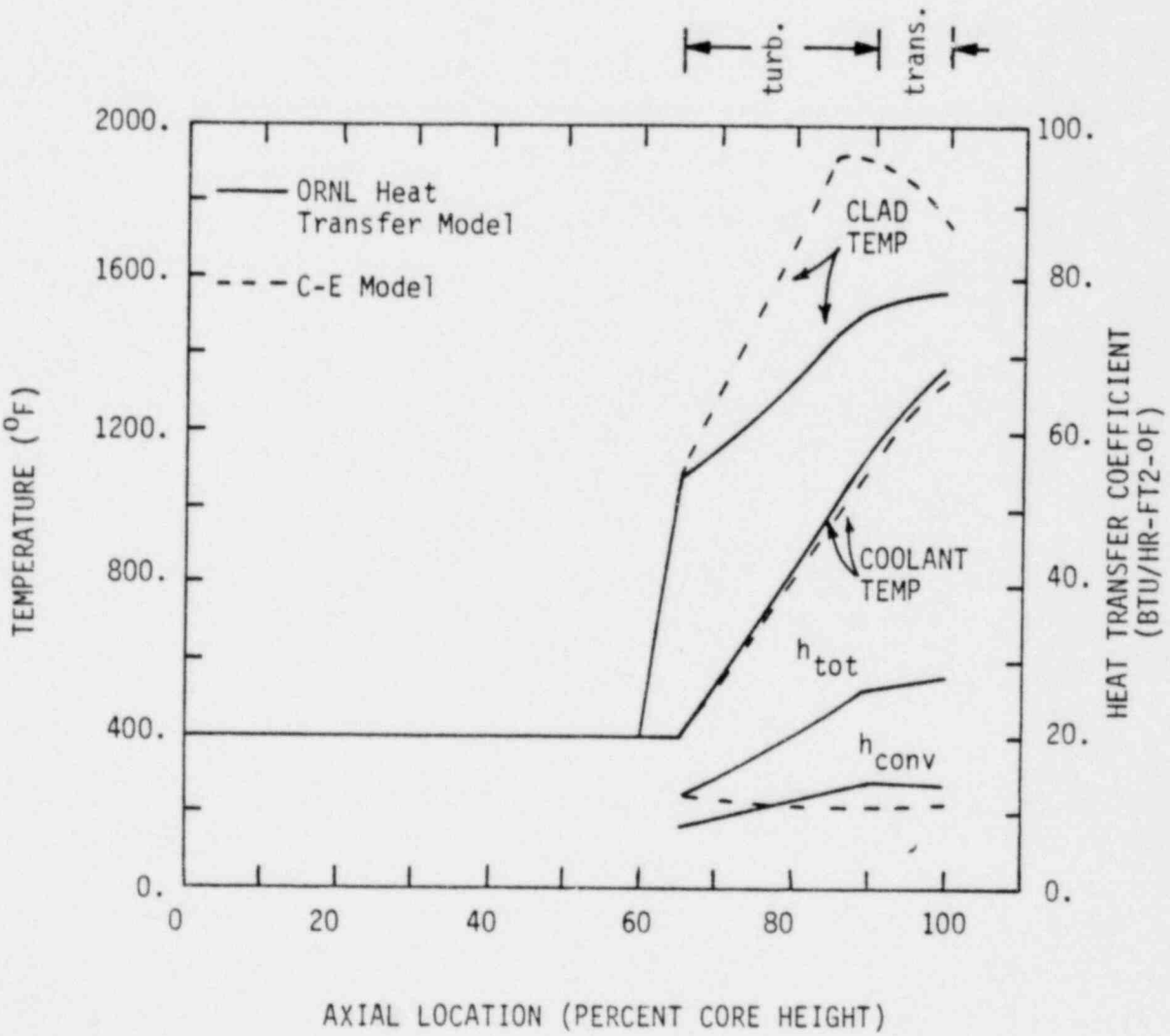

Figure 3.5-7

Clad and Coolant Temperatures and Heat Transfer Coefficients Vs. Axial Location, at the Instant PCT Occurs, for the 0.5 ft^2 Break

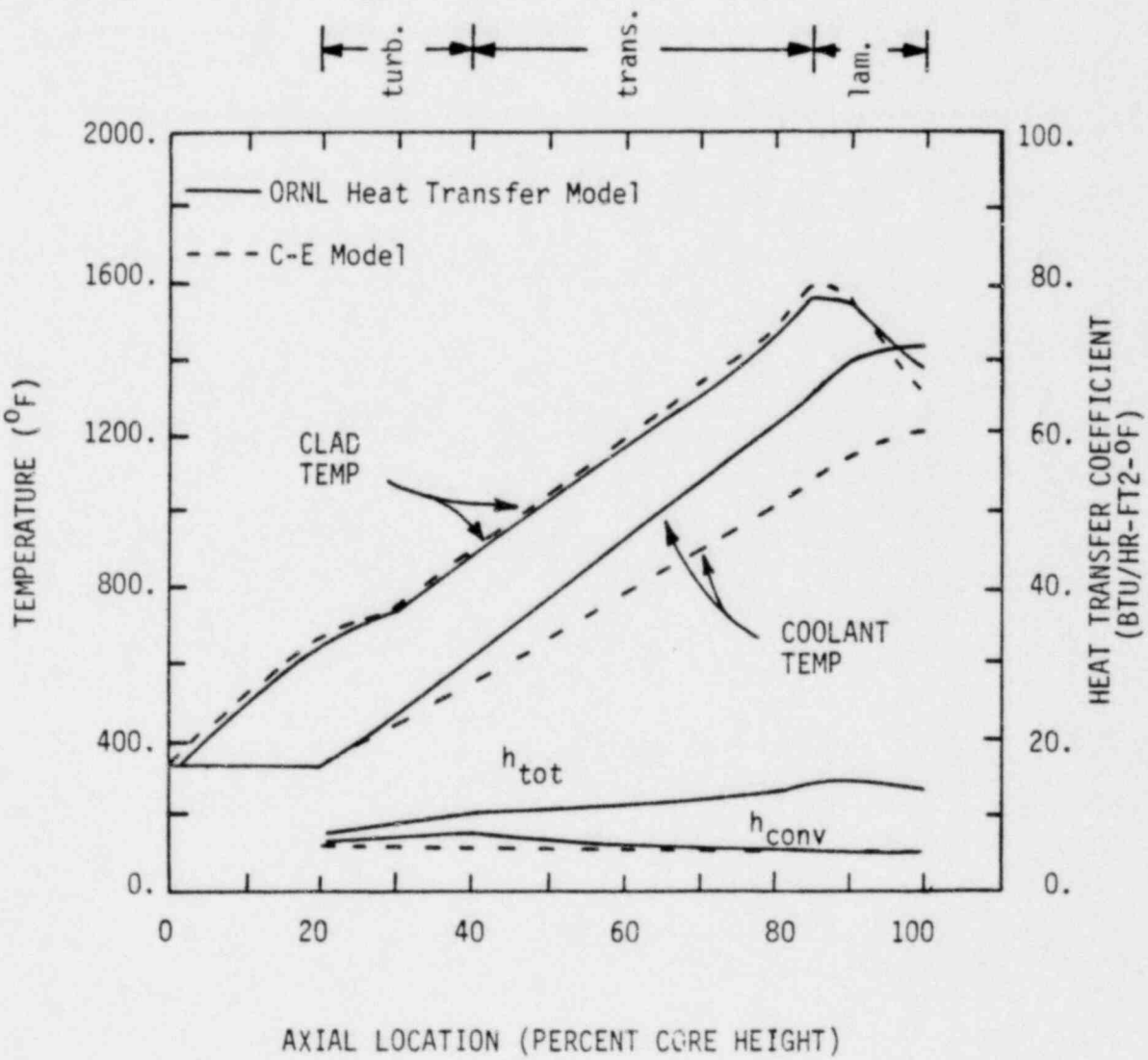

3.6 RESPONSE TO QUESTION 6 (METAL HEAT TRANSFER)

3.6.1 Statement of Question 6

Heat transfer from metal surfaces, i.e. piping, vessel walls, etc., constitutes a significant portion of the heat transferred to the primary side fluid during a small break LOCA. Since the heat transferred to the fluid affects the system depressurization rate, demonstrate that metal heat transfer is calculated conservatively.

3.6.2 Detailed Response to Question 6

Since the small break LOCA is characterized by relatively slow depressurization rates, heat deposition from the energy stored in the metal walls may have an influence on the transient responses. In particular, the time of actuation of the safety injection tanks is determined by the total energy deposited in the primary system fluid prior to the time of actuation. [ ] a correction is applied to [ ] the lumped parameter metal heat transfer model in CEFLASH-4AS. The lumped parameter model which is the same as that in previous FLASH codes underestimates the metal wall heat transfer if no correction is applied.

The formulation of the correction factor is described in detail in Reference 3.6-1. Use of it produces [ ] Values of the correction factor, which is dependent on break size, are shown in Figure 3.6-1. The values for a blowdown time of [ ]

The heat deposited into the coolant contained in the control volume is defined from the energy equation written for the node as:

$$\dot{U}_i = \sum_j W_{ij}\, h_{ij} + Q_i \qquad (3.6\text{-}1)$$

where

$$Q_i = \left[\qquad\qquad\right] \qquad (3.6\text{-}2)$$

$$T_{metal_i}\,(t + \Delta t) = T_{metal_i}\,(t) - \frac{Q_i\, \Delta t}{(mC_p)_i} \qquad (3.6\text{-}3)$$

and

$\dot{U}_i$ = change in internal energy for control volume i
W_{ij} = mass flow rate of path j connected to node i
h_{ij} = enthalpy of flow path j connected in node i
Q_i = wall heat deposition

[ ]

mC_p = wall specific heat
$Z_{2\emptyset_i}$ = two-phase level in node i
Z_{TOT} = total height of node i
T_{metal} = wall temperature
T_{fluid} = node coolant temperature
Δt = time increment

It may be noted that [ ]

[

]

[

]

In order to evaluate the sensitivity of predicted results to the magnitude of wall heat transfer, calculations were performed both with and without the correction factor applied.

The metal components in the reactor vessel and the vessel itself contribute most of the wall heat because the vessel retains two-phase fluid throughout the transient. The correction factors for the annulus and inner vessel are [ ] respectively. Thus, the annulus wall heat transfer is nearly [ ] but that from the inner vessel components is increased by [ ]

The effect of the wall heat transfer correction on the inner vessel two-phase volume and pressure is shown in Figures 3.6-2 and 3.6-3, respectively. The effect is clearly very small. The reason for this lack of sensitivity to increased wall heat transfer can be explained by considering the rates of energy input from the core and expelled out the break. The core heat input determines the long-term rate of two-phase level recession due to boiloff. The energy release rate at the break determines the rate of depressurization. The various rates of energy exchange are shown in Figure 3.6-4. The wall heat input rate either with or without correction is small compared to the other two rates. Furthermore, the difference in wall heat predicted by the two methods is small compared to the wall heat input with either method.

3.6.3 Summary and Conclusions for Question 6

The conclusion from this study is that wall heat transfer does not strongly influence the calculated results. However, even though the effect is small, the reference treatment described above maximizes the rate of wall heat input over the small break spectrum. Its use, therefore, clearly produces more adverse results than would be realistically expected.

3.6.4 References For Question 6

3.6-1 CENPD-132-P, "Calculation Methods for the Combustion Engineering Large Break LOCA Evaluation Model", Combustion Engineering Proprietary Report (August, 1974).

Figure 3.6-1

Correction Factor for Metal Wall Heat Transfer

Figure 3.6-2

Influence of Metal Wall Heat

on Inner Vessel Two-Phase Volume

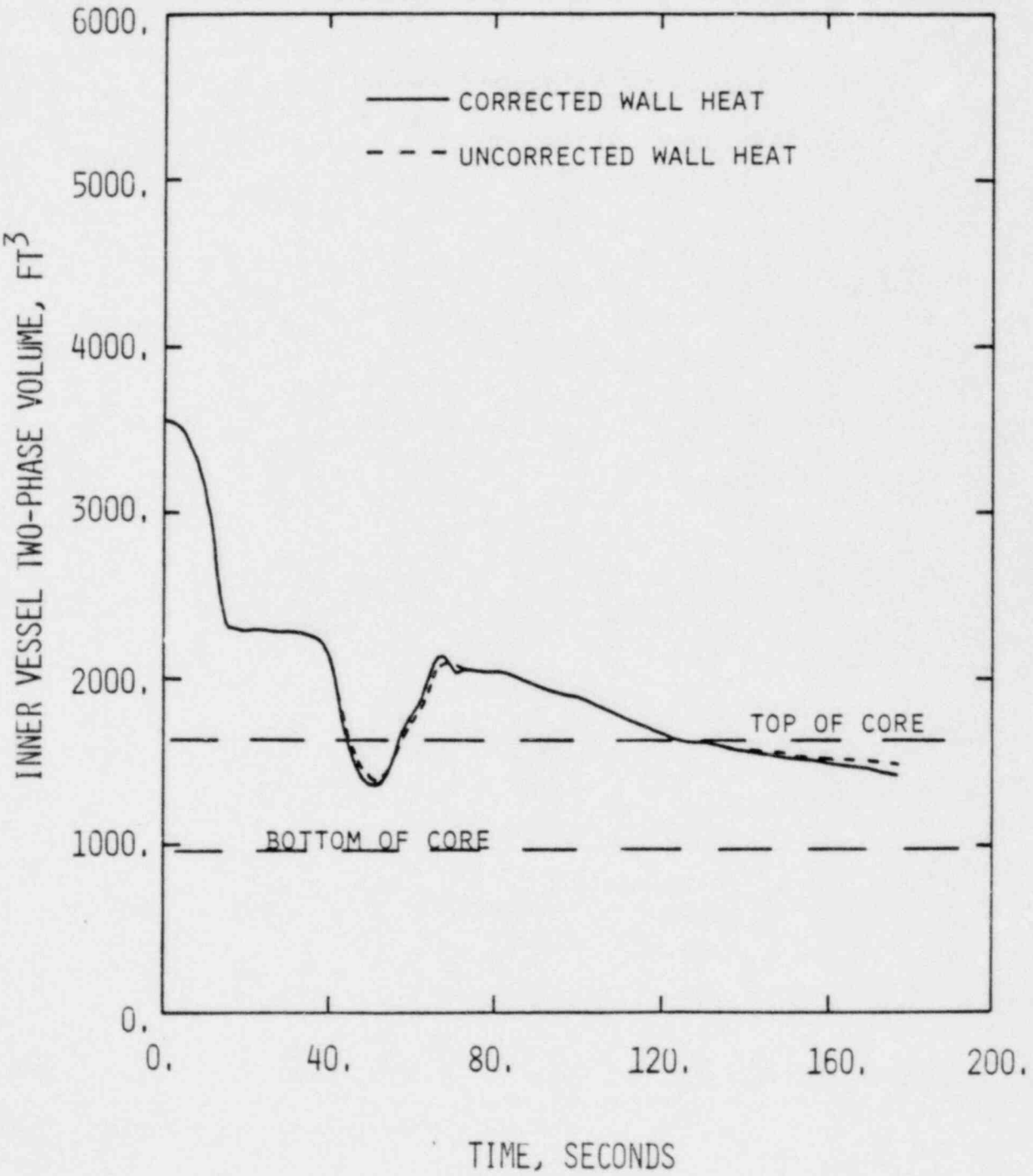

Figure 3.6-3

Influence of Metal Wall Heat

on Inner Vessel Pressure

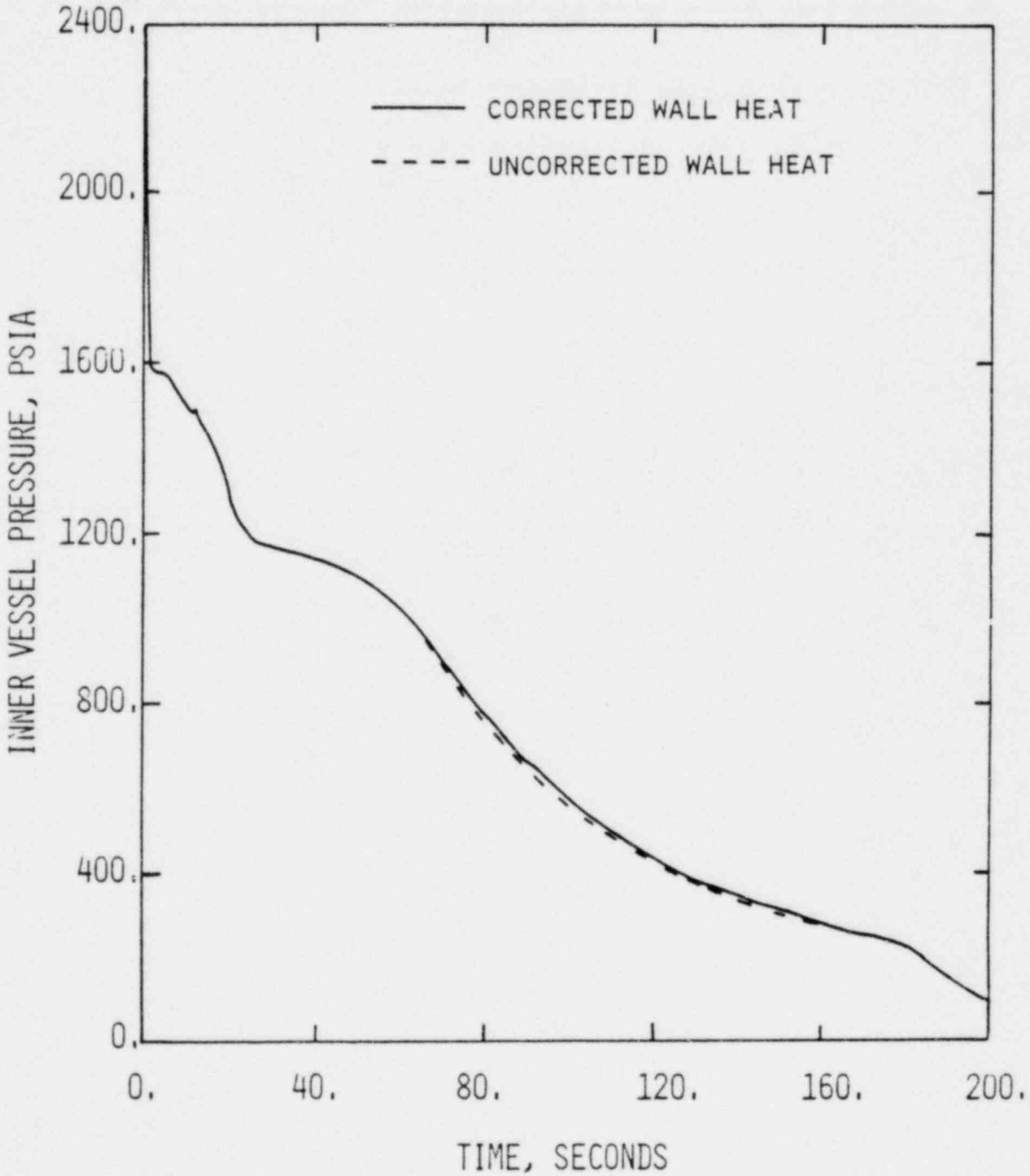

Figure 3.6-4

Comparison of Wall Heat Input to Core

Heat Input and Break Energy Efflux

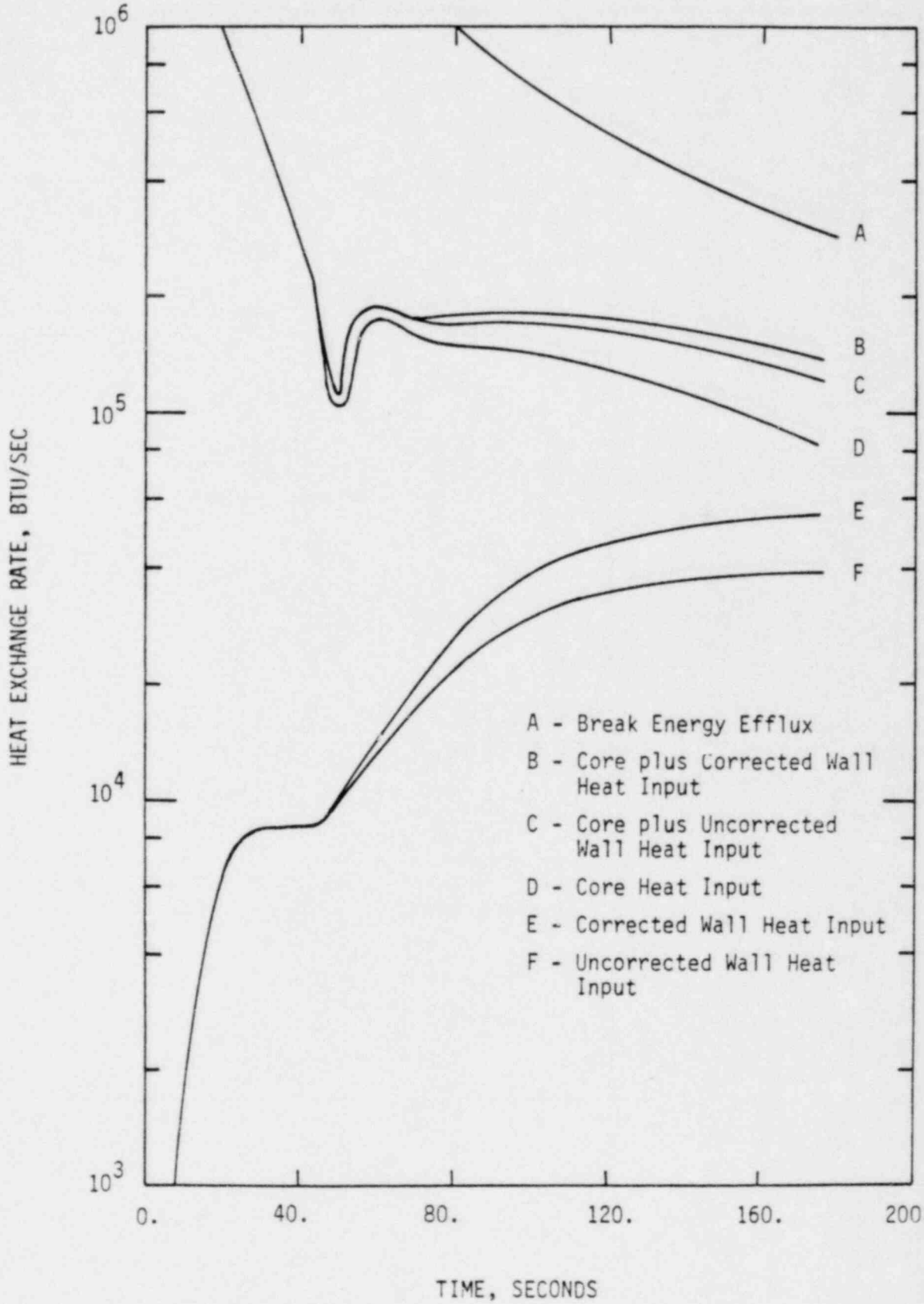

3.7 RESPONSE TO QUESTION 7 (BREAK FLOW MULTIPLIER)

3.7.1 Statement of Question 7

C-E's licensing model for calculating the break flow rate uses a single break flow multiplier for subcooled water, two-phase mixture and dry steam. This modeling approach is questioned and demonstration is required to show that the effects of variable break flow multipliers are bounded by analyzing a spectrum of break sizes.

3.7.2 Detailed Response to Question 7

C-E has submitted a response to this question in Reference 3.7-1. That response is summarized and amplified below.

The C-E model uses the following critical flow correlations to calculate discharge of subcooled water, two-phase mixture, and dry steam:

- Subcooled water: Modified Henry-Fauske Model (Reference 3.7-2)
- Two-phase mixture: Moody Model (Reference 3.7-3)
- Dry steam: Modified Murdock-Bauman Model (Reference 3.7-4)

The modifications to the two single-phase discharge models were made to provide [ ] for conditions of saturated water or steam. As described in Reference 3.7-5, these modifications affect calculated critical flow rates [ ] and therefore have a negligible effect upon small break LOCA calculational results. To account for the effects of break size and geometry, C-E considers a full spectrum of "effective" break flow areas (actual flow area times a discharge coefficient to account for geometry effects) in each small break LOCA analysis. Justification for C-E's choice of critical flow correlations and its use of an effective flow area to account for both size and geometry effects is given below.

The theoretical and experimental justification for C-E's choice of the Henry-Fauske and Murdock-Bauman models for single-phase water and steam discharge is given in Reference 3.7-5. Use of the Moody model for two-phase critical flow is a direct requirement of 10CFR50, Appendix K (Reference 3.7-6) and therefore does not necessarily represent C-E's choice of a best-estimate model. However, since the size of the break is not a clearly defined parameter in a small break LOCA analysis, any representative two-phase discharge model will be adequate to predict maximum core uncovery provided the spectrum of effective flow areas examined is broad enough to span the range of possible leak flow rates.

To provide additional verification of the appropriateness of the C-E model for small break LOCA calculations, C-E has examined additional experimental data and performed a study to determine the sensitivity of core thermal/hydraulic behavior to calculated break flow rate. In these studies, attention was focused primarily on the effect of varying the discharge coefficients for both subcooled and two-phase flow from breaks in the primary system piping.

To verify the applicability of the C-E break flow model to small primary coolant system pipe breaks, C-E has examined available data from several critical flow experiments and found that the data of Sozzi and Sutherland (Reference 3.7-7) is most appropriate for this application. This data was obtained under conditions of relatively constant pressure over a range of coolant enthalpies typically encountered during the subcooled and low-quality two-phase discharge periods of a small break LOCA. In addition, the effects of break geometry were considered through variation of both the size and the shape of the break nozzle. A small break can be postulated as resulting from either the shearing-off of a small pipe connected to the primary system, such as an instrument line, or a small hole in one of the primary system pipes themselves. Sozzi and Sutherland examined nozzles that are representative of both break geometries and found that, particularly for subcooled flow, geometry effects are very strong and no single critical flow model will be appropriate for both postulated break types.

A break resulting from the shearing-off of a small pipe was approximated by a rounded-edge nozzle or sharp orifice with a short length of tubing downstream equal in diameter to the nozzle throat. As shown in Figure 3.7-1, the measured critical mass flux through this particular nozzle configuration decreases steadily with increasing liquid enthalpy (decreasing subcooling) until the fluid stagnation conditions reach saturation, then decreases very sharply immediately after the transition to two-phase flow. Such behavior is typical of critical flow data obtained using converging-diverging nozzles, and therefore is reasonably well predicted by several existing flow models. Although Sozzi and Sutherland recommend the Homogeneous Equilibrium Model (HEM) (Reference 3.7-8) as a best-fit to the experimental data, Figure 3.7-1 shows that the C-E model predicts the data equally well using an effective flow area equal to the actual nozzle area times a discharge coefficient (C_D) of 0.75. For this particular break geometry, therefore, the experimental data support C-E's approach of defining a single effective flow area for both subcooled and two-phase flow.

To evaluate the discharge flow through a small hole in a primary coolant pipe, the authors measured the critical flow rate through a sharp-edged orifice in a relatively thin wall. As shown in Figure 3.7-2, discharge through this nozzle configuration was dominated by non-equilibrium effects and the observed variation in critical mass flux with fluid stagnation enthalpy was quite different from that described in the previous paragraph.

Since the trend of this data would not be predicted by any available critical flow model, C-E chose to examine the effect of this strong geometry effect through a break flow sensitivity study in which the discharge coefficients (C_D) for subcooled flow and two-phase flow were varied. The results of this study, shown in Figure 3.7-3, indicate that both the depth and duration of core uncovery are insensitive to the subcooled discharge coefficient and the timing of core uncovery is delayed by reducing the two-phase discharge coefficient. However, the depth of core uncovery is nearly the same for all cases.

In all cases, the core uncovered after the break flow had switched from a two-phase mixture to steam - a characteristic of limiting small break LOCA's. This study shows that the minimum mixture level in the core, for limiting

small breaks, is a function of the discharge coefficient during the time steam flows out the break. Since limiting small breaks are characterized by slow uncovery and recovery of the core, the peak clad temperature (PCT) is a function of the decay heat and the minimum mixture level in the core. Therefore, one would expect nearly the same PCT for all cases performed in this sensitivity study. Naturally, delaying the time the core level reaches its minimum will result in less decay heat and a slightly lower peak clad temperature. In fact, heat transfer calculations predicted the PCT for the nominal case to be 1624^{o}F and for the case with the two-phase discharge coefficient equal to 0.6 to be 1540^{o}F.

Therefore, a break spectrum analysis using the C-E model with constant discharge coefficients is expected to result in a higher PCT than an analysis using a best-estimate break flow model. This is because the C-E model (Moody) predicts a higher break flow than a best estimate model (HEM). As a result, the C-E model will predict the core to uncover sooner than a best estimate model, and the higher decay heat during core uncovery will result in a higher PCT.

3.7.3 Summary and Conclusions for Question 7

For the calculation of break flow, the choice of break flow multiplier, or discharge coefficient, during subcooled or two-phase discharge is particularly important. Sensitivity studies for the worst (highest clad temperature) small break have shown that the depth and duration of core uncovery are insensitive to variations of the subcooled discharge coefficient. However, a variation of the two-phase discharge coefficient primarily effects the timing of core uncovery. A two-phase discharge coefficient of 0.6 results in less break flow, later core uncovery and, due to reduced decay heat, in lower cladding temperatures than a coefficient of 1.0.

In the C-E Small Break LOCA Evaluation Model a discharge coefficient of 1.0 is used for subcooled and two-phase break flow. As mentioned above, the choice of the numerical value of the discharge coefficient for the subcooled break flow is of little consequence for the cladding temperature.

The choice of a discharge coefficient of 1.0 for two-phase flow, however, results in early core uncovery. Therefore, the discharge coefficient used in the C-E Evaluation Model maximizes the calculated cladding temperature.

3.7.4 References for Question 7

3.7-1 CEN-114-P (Amendment 1-P), "Review of Small Break Transients in Combustion Engineering Nuclear Steam Supply Systems", July, 1979 (Proprietary).

3.7-2 Henry, R. E. and Fauske, H. K., "The Two-Phase Critical Flow of One-Component Mixtures in Nozzles, Orifices, and Short Tubes", Journal of Heat Transfer, May, 1971.

3.7-3 Moody, F. J., "Maximum Flow Rate of a Single Component Two-Phase Mixture", Journal of Heat Transfer, February, 1965.

3.7-4 Murdock, J. W., and Bauman, J. M., "The Critical Flow Function for Superheated Steam", Trans. ASME, Series D, Vol. 86, 1964.

3.7-5 CENPD-132P, "Calculative Methods for the C-E Large Break LOCA Evaluation Model", August, 1974 (Proprietary).

3.7-6 Code of Federal Regulations 10CFR50, Appendix K, "ECCS Evaluation Models", Federal Register, Vol. 39, No. 3, January 4, 1974.

3.7-7 Sozzi, G. L. and Sutherland, W. A., "Critical Flow of Saturated and Subcooled Water at High Pressure", General Electric Col, NEDO-13418, July, 1975.

Figure 3.7-1

Comparison of Critical Flow Models

to Data of Sozzi and Sutherland

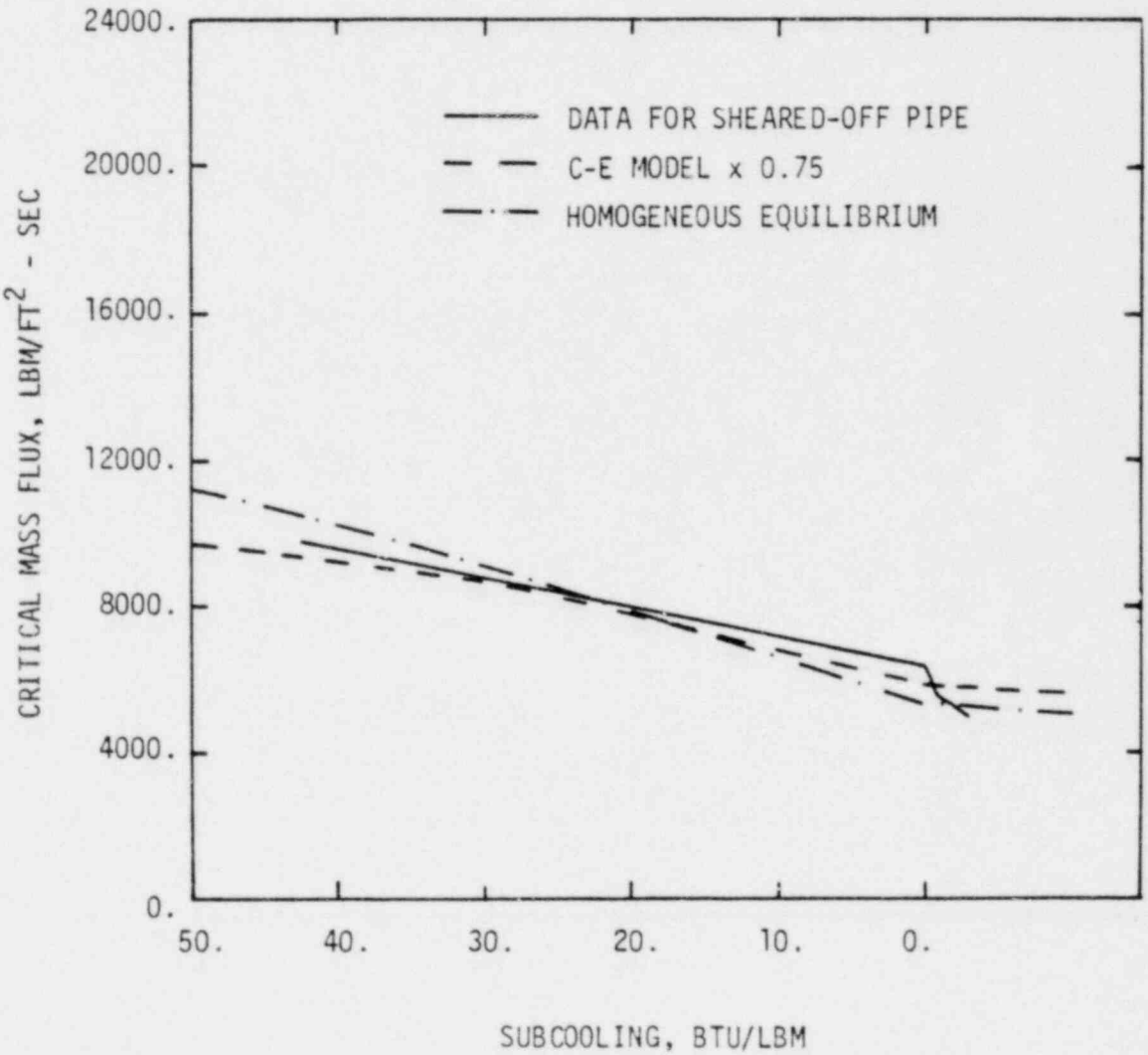

Figure 3.7-2

Subcooled Critical Flow for

Small Break LOCA Geometry

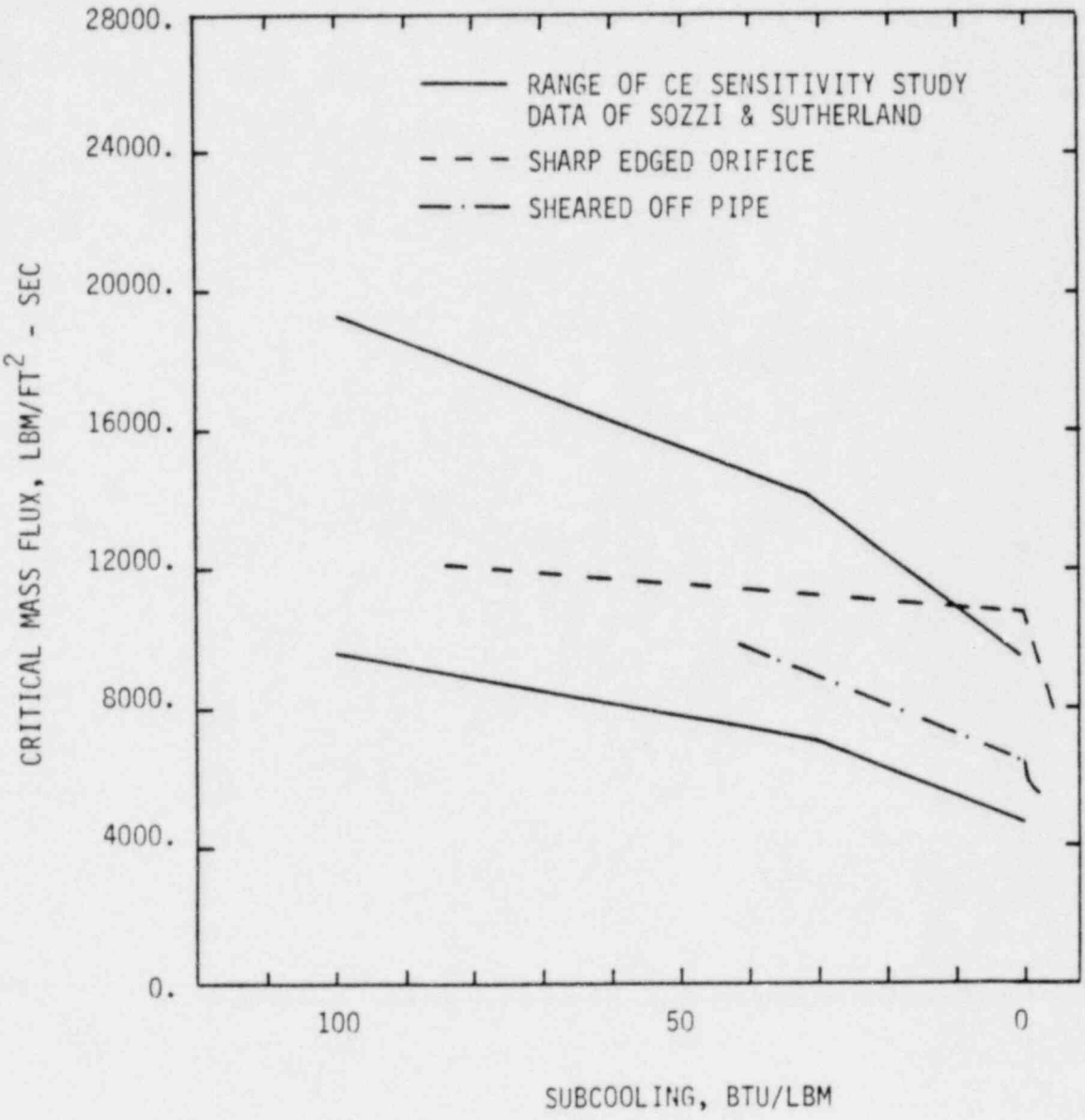

Figure 3.7-3

Subcooled C_D Sensitivity Study

Effect on Inner Vessel Mixture Level

(Break Area = 0.1 FT^2)

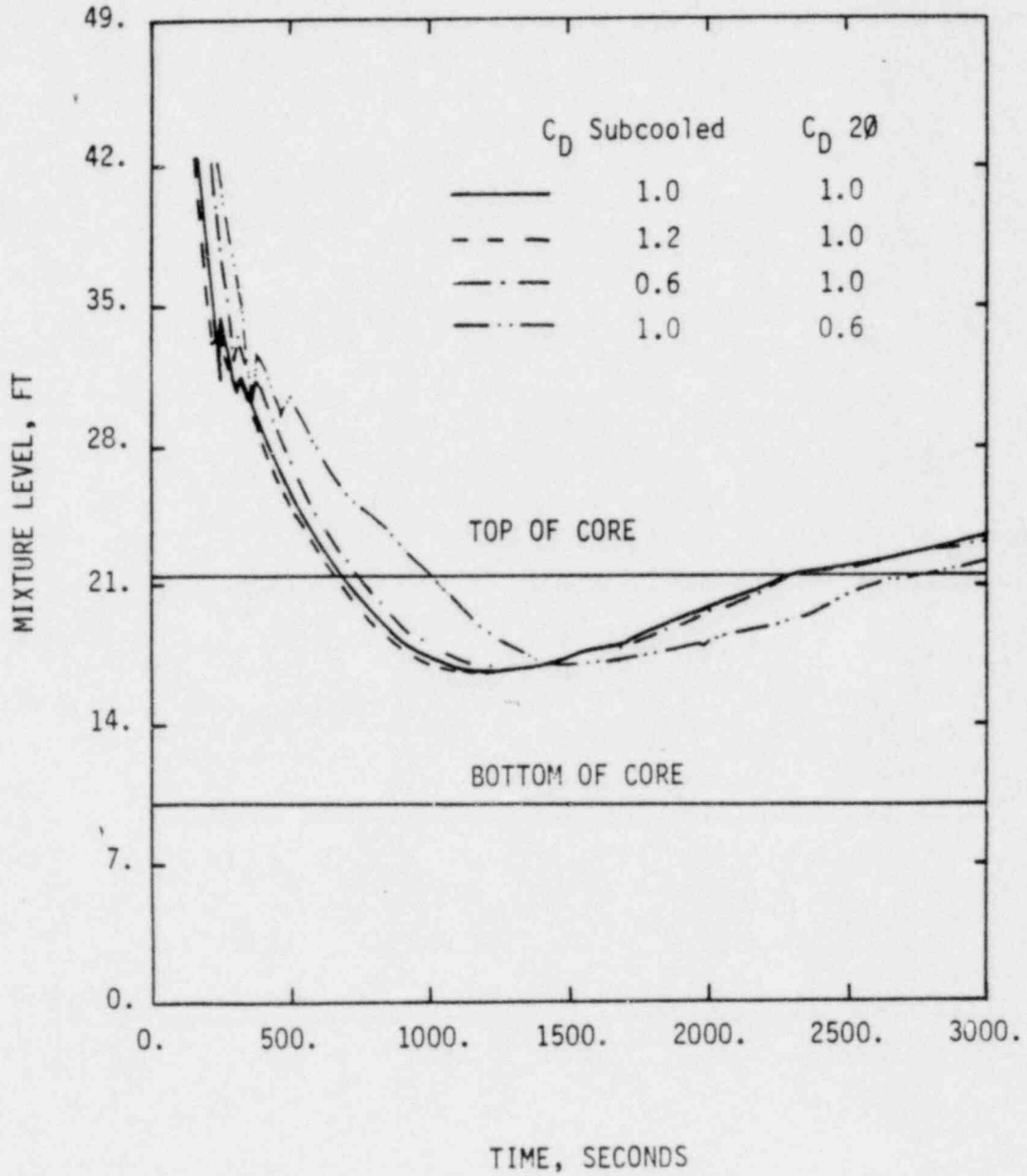

COMBUSTION ENGINEERING, INC.